

**2D ARBITRARY LAGRANGIAN-EULERIAN
(ALE) MODEL OF BLOOD FLOW
IN THE LEFT VENTRICLE OF THE HEART**

**ZATI HAKIM AZIZUL HASAN
WGA040092**

DISSERTATION SUBMITTED IN FULLFILLMENT
OF THE REQUIREMENTS FOR THE DEGREE OF
MASTER OF COMPUTER SCIENCE

**FACULTY OF COMPUTER SCIENCE AND
INFORMATION TECHNOLOGY
UNIVERSITY OF MALAYA**

DECEMBER 2006

“I declare that this dissertation entitled “Two Dimensional Arbitrary Lagrangian-Eulerian (ALE) Model of Blood Flow in the Left Ventricle of the Heart” is the result of my own research except where otherwise acknowledged. The dissertation has not been accepted for any degree and is not concurrently submitted in candidate of any degree to any other university or institution”.

Signature :
Name of Candidate : ZATI HAKIM AZIZUL HASAN
Metrics Number : WGA040092
Date : 06 DECEMBER 2006

UNIVERSITI MALAYA
ORIGINAL LITERARY WORK DECLARATION

Name of Candidate: **ZATI HAKIM AZIZUL HASAN** (I.C/Passport No:

Registration/Matric No: **WGA040092**

Name of Degree: **MASTERS OF COMPUTER SCIENCE**

Title of Project Paper/Research Report/Dissertation/Thesis ("this Work"):

**TWO DIMENSIONAL ARBITRARY LAGRANGIAN-EULERIAN (ALE) MODEL
OF BLOOD FLOW IN THE LEFT VENTRICLE OF THE HEART**

Field of Study: **IMAGE PROCESSING, ARTIFICIAL INTELLIGENCE**

I do solemnly and sincerely declare that:

- (1) I am the sole author/writer of this Work;
- (2) This Work is original;
- (3) Any use of any work in which copyright exists was done by way of fair dealing and for permitted purposes and any excerpt or extract from, or reference to or reproduction of any copyright work has been disclosed expressly and sufficiently and the title of the Work and its authorship have been acknowledged in this Work;
- (4) I do not have any actual knowledge nor do I ought reasonably to know that the making of this work constitutes an infringement of any copyright work;
- (5) I hereby assign all and every rights in the copyright to this Work to the University of Malaya ("UM"), who henceforth shall be owner of the copyright in this Work and that any reproduction or use in any form or by any means whatsoever is prohibited without the written consent of UM having been first had and obtained;
- (6) I am fully aware that if in the course of making this Work I have infringed any copyright whether intentionally or otherwise, I may be subject to legal action or any other action as may be determined by UM.

Candidate's Signature:

Date: 06 DECEMBER 2006

Subscribed and solemnly declared before,

Witness's Signature:

Date: 06 DECEMBER 2006

Name: PROF. IR. DR. SELVANATHAN NARANAISAMY
Designation: LECTURER

To my dearest Abah, Mak, brother, sisters and closest friends...

A C K N O W L E D G E M E N T

I am most grateful to Allah SWT, for blessing me health to carry on, strength to focus and never give up, and faith that keep me believing success is sweetest when it is well-earned. My deepest gratitude to the Almighty for inspiring and guiding this humble being.

I am deeply indebted to my supervisor Prof. Ir. Dr. Selvanathan Naranaisamy; a leading character whose abundance knowledge and passion has taught this way of productive research and by heart I have to admit without his driven persuasion and persistent motivation, this journey might have been a task too far and too grand for me.

I ought to extend my appreciation to Mr. Yung Yew Kuan from First High Tech Sdn. Bhd. for the supplement of the heart data, Mr. Anandan from Engineering for his guidance in finite element analysis, and to Mr. David Too from Active Media Sdn. Bhd. for the technical support. This research has been fully supported and funded by the Fellowship Scheme of University of Malaya of which I am sincerely grateful.

Special thanks to Dr. Rosli Salleh; for the permission to commence this research and dissertation at his laboratory, and to Mr. Sim Kim Hwa for all his assistance on the ministerial computer. My scientific colleagues; Unaizah Hanum, Shahrizal Fadlie, Salhana, Sara, Ahmad Haris and Syarifalillah, have without exception been most supportive. Credit to them for the ever endless energy and care all this while, will always reminisce to the constant banter and laughter; they are my family at work.

I owe much loving thanks to my parents; Mr. Azizul Hasan Shahabuddin and Mrs. Norsiah Idris, and siblings; Ainul Hizan, Zafarizal Aldrin, Ida Zafrina, and Uniza Nur, for their boundless trust, endless prayers, and kind understanding throughout my long time away for my studies. Thank you Abah, Mak, everybody, for letting me take this step ahead, and be rest assured that there has been no room for regrets in this decision. To my housemates and closest associates, thanks for keeping things real, my appreciation for the honesty and necessary supplementary activities. It is an incomparable pleasure to learn I have found my true friends in all of you and may we remain as good friends forever.

ABSTRACT

This research is a study of the dynamics of the heart valves and the blood using numerical computational technique. This numerical technique is known as the Arbitrary Lagrangian-Eulerian (ALE) and is introduced in a finite element environment. By means of a mesh movement method, the ALE uses separate sets of reference systems to study the fluid-structure interaction of the heart. The fluid domain is most conveniently described with respect to an Eulerian reference frame while a Lagrangian formulation is more appropriate for the structure domain. Due to the incompatibility factor of the two reference frames, coupling of the reference systems is carried out on an arbitrary computational grid which allows numerical modeling of the blood motion and the mechanical valves under physiological conditions defined by governing constitutive formulation. The use of graphical simulation in a time step fashion is an essential aid in obtaining realistic physical representation of the dynamic interaction. Results from the experimental simulations in comparison to physiological data have been encouraging. This geometrically simplified model albeit with much constraints has the capability to derive plausible velocity pattern of the flow in relation to the periodicity mechanics of the mitral and aortic valves in two cardiac cycles.

TABLE OF CONTENTS

DECLARATION.....	II
ORIGINAL LITERARY WORK DECLARATION	III
DEDICATION.....	IV
ACKNOWLEDGEMENT	V
ABSTRACT.....	VI
TABLE OF CONTENTS.....	VII
LIST OF FIGURES	X
LIST OF TABLES	XII
NOMENCLATURE.....	XIII
1 Introduction	15
1.1 Preface.....	16
1.2 Research Motivation	16
1.3 Research Objective.....	17
1.4 Research Background.....	18
1.5 Research Overview	20
1.6 Research Scope	21
1.7 Thesis Organization.....	22
1.8 Summary	24
2 Literature Review	25
2.1 Overview	26
2.2 The Heart Anatomy	26
2.2.1 The Left Heart.....	28
2.2.2 The Cardiac Mechanics.....	30
2.2.2.1 Systole.....	30
2.2.2.2 Diastole	31
2.2.3 The Windkessel Theory	32
2.3 Dynamics of the Blood Flow (Hemodynamics)	34
2.3.1 Velocity of Blood Flow	34
2.3.2 Relationships between Blood Flow, Pressure, and Resistance.....	35
2.3.3 Resistance to Blood Flow	36
2.3.4 Laminar Flow and the Reynold’s Number	37
2.3.5 Turbulent Flow	38
2.3.6 Newtonian Property	39
2.4 Computational Fluid Dynamics (CFD) and the Navier-Stokes Equations	40
2.4.1 CFD approach in Hemodynamics	40
2.4.2 The Navier-Stokes equation.....	41
2.4.2.1 The Navier-Stokes Equation and the Incompressible flow.....	41
2.4.2.2 The Navier-Stokes Equation and Time Dependency.....	43
2.5 The Arbitrary Lagrangian Eulerian (ALE) Modeling	43
2.5.1 The Lagrange Reference Frame	44
2.5.2 The Eulerian Reference Frame.....	45
2.5.3 Coupling of the Lagrangian-Eulerian Reference System	46
2.5.4 Controlling Equations in ALE	46
2.5.5 Function of the Navier-Stokes Equation in the ALE.....	47
2.5.6 Computational Grid Mapping	47
2.6 The Balance Laws Formulation	48
2.6.1 Fundamentals Theory of the Balance Laws	48
2.6.2 Quantities representing the Balance Laws	50
2.6.3 Localizing the Balance Law.....	51
2.6.4 Balance Laws Assumptions	53
2.6.5 Conservation of Mass	54
2.6.6 Conservation of momentum.....	55
2.6.7 Surface Traction and the Stress Tensor (Cauchy’s stress tensor).....	56

2.7	Understanding the Finite Element Method.....	57
2.7.1	The Mesh	57
2.7.2	The Finite Elements	58
2.7.2.1	A simple example: linear elements in 1D.....	58
2.7.3	The Lagrange Element.....	60
2.7.4	Curved Mesh Element.....	61
2.7.5	Weak Constraints.....	62
2.8	The Software FEMLAB	64
2.8.1	Advantages of the Software Package	64
2.8.2	Predefined Boundary Conditions in FEMLAB	64
2.8.2.1	Inflow / Outflow Velocity	65
2.8.2.2	Outflow or Pressure.....	65
2.8.2.3	Slip or Symmetry	66
2.8.2.4	No Slip	66
2.8.2.5	Normal Flow or Pressure.....	66
2.8.2.6	Neutral.....	67
2.9	Conclusion	68
3	Methodology.....	69
3.1	Overview	70
3.2	Geometrical Modeling.....	70
3.3	Acquisition of the Heart Data.....	71
3.3.1	Reverse Engineering Processes.....	71
3.3.1.1	Generation of Points Cloud data.....	72
3.3.1.2	Optimizing Scan Data	77
3.3.1.3	Sampling	78
3.3.1.4	Surface Wrapping.....	79
3.3.1.5	Filling up the holes.....	81
3.3.2	Data Measurements.....	83
3.4	Solid Modeling.....	85
3.4.1	2D Solid Modeling in FEMLAB.....	86
3.4.2	Modeling of Curves and Solid Objects	86
3.4.2.1	Curves / Boundary Modeling	87
3.4.2.2	Solid Modeling.....	92
3.4.2.3	Subdomains and the Split Operation	95
3.5	Modeling ALE on the Left Ventricle	97
3.5.1	Modeling Mesh Movement for the ALE.....	99
3.5.2	Coupling of Reference System for the Mesh Movements.....	102
3.5.3	PDE for the Mesh Movement	106
3.5.4	Schematic Representation of the Mesh Movement Method.....	109
3.5.5	Assumptions for the Mesh Movement Method.....	112
3.5.6	Setting the Boundaries Physics for the Mesh Movement.....	113
3.5.7	Setting the Mesh on the Left Ventricle Model	116
3.6	Solving the model	121
3.6.1	The time dependant solver	122
3.6.2	Settings for the time dependent solver	123
3.7	Postprocessing and Visualization.....	124
3.7.1	2D Postprocessing and Visualization.....	124
3.8	Conclusive Remarks.....	128
4	Results and Analysis.....	129
4.1	Overview	130
4.2	Experimental Results.....	130
4.2.1	Incompressible Laminar Flow	130
4.2.2	Incompressible Turbulent Flow	133
4.2.3	Incompressible Flow with Pressure	137
4.2.4	The Stress Tensor Test.....	140
4.2.5	The Poisson Test.....	143
4.2.6	The ALE Test	145
4.3	Simulation Results	148
4.3.1	Incompressible Blood Flow through the Left Ventricle Model.....	148
4.3.2	Simplified Valve	152
4.3.2.1	Deformation of the Mitral Leaflets.....	152
4.3.2.2	Deformation of the Aortic Leaflets.....	153
4.3.2.3	Velocity Profile in the Left Ventricle	154

4.3.2.4	Periodic Motion of the Leaflets	157
4.4	Conclusive Remarks	158
5	Discussion	159
5.1	Overview	160
5.2	The Left Ventricle Architecture Limitation	161
5.3	Discussion on the ALE Modeling	162
5.3.1	Analyzing the Finite Element Convergence and Accuracy	162
5.3.2	The Mesh Generation	163
5.3.3	Usage of Weak Constraints	163
5.3.4	Coupling of Variables	164
5.3.5	Artificial Stabilization Techniques	164
5.4	Hardware Limitations	165
5.5	Assumptions on the Left Ventricle Model	165
5.6	Evaluating the blood flow in the left ventricle model	166
5.6.1	Evaluating the Aortic Outflow	168
5.6.2	Evaluating the Mitral Inflow	169
5.7	Contribution Highlights	170
5.8	Suggestions for future work	171
6	Conclusion	173
6.1	Assessment	174
	REFERENCES	176
	APPENDIX A	181
	APPENDIX B	182

LIST OF FIGURES

Figure 2.1: Gross Anatomy of the Heart (Atlas of Echocardiography 1999)	27
Figure 2.2: The sequence of blood flow in the circulation (Price and Wilson 1992)	28
Figure 2.3: Anatomy of the human heart, aortic valve and mitral valve (Price and Wilson 1992)	29
Figure 2.4: Pressure, flow and volume events during the cardiac cycle (Yellin 1995)	32
Figure 2.5: Simple representation of the aorta in the Windkessel Theory.....	33
Figure 2.6: Some Pulse Waves in the Beating Heart.....	34
Figure 2.7: Sample Body of Material Undergoing Deformation.....	49
Figure 3.1: Generations of points cloud data of the outer layer of the left	73
Figure 3.2: Generation of points cloud data of the inner layer of the left.....	74
Figure 3.3: More views on the outer side of the left ventricle. (a) Top half of the outer left ventricle and (b) bottom half of the outer left ventricle	75
Figure 3.4: Generation of point clouds data on the left ventricle valves. (a) the aortic cylinder, (b) the mitral cylinder, (c) aortic semilunar valve and (d) mitral bicuspid valve.....	76
Figure 3.5: Results of noise reduction on the heart's surface curvature at (a) minimum noise reduction, (b) medium noise reduction and (c) maximum noise reduction.....	78
Figure 3.6: Results from curvature sampling on the surface model at (a) 30% curvature sample, (b) 65% curvature sample and (c) 100% curvature sample.....	79
Figure 3.7: Results from polygonal surface reconstruction at (a) 10mm point distance, (b) 5mm point distance and (c) 2mm point distance	80
Figure 3.8: Results from surface wrapping on the left ventricle data. (a) Surface wrapping at 10mm point distance, (b) surface wrapping at 5mm point distance and (c) surface wrapping at 2mm point distance point distant	81
Figure 3.9: The left ventricle surface model. (a) model front view and (b) model top view	82
Figure 3.10: Regions of interest considered for the left ventricle measurements. (a) length and diameter measurements and (b) the crease angle calculation	84
Figure 3.11: Hierarchical Inheritance Structure of the 2D Geometry Classes.....	87
Figure 3.12: Example of functions used in the curves modeling.....	89
Figure 3.13: Boundary modeling of the left ventricle model with five different closed domains created separately.....	90
Figure 3.14: The curves modeling of the aortic cylinder.....	91
Figure 3.15: Solid Modeling of the Left Ventricle Model.....	94
Figure 3.16: The solid modeling of the aortic valve.....	95
Figure 3.17: (a) Conceptual design of the subdomains using boundary modeling and (b) coercion of the boundary subdomains into solid.....	96
Figure 3.18: Relation between moving configurations and motions	104
Figure 3.19: Schematic Presentation of the ALE Method	111
Figure 3.20: Interior and Exterior Boundary of a Domain	114
Figure 3.21: Boundaries Marked with Number	114
Figure 3.22: Closer Examination of the Valve Boundaries	115
Figure 3.23: Varied Settings Available for the Mesh; Coarsest to Finest	119
Figure 3.24: Several Different Mesh Settings for the Model	120
Figure 3.25: Meshing of the Left Ventricle Model.....	121
Figure 3.26: The Surface, Contour and Arrow Plot for the 2D Visualization and Postprocessing.....	125
Figure 3.27: The Streamline Plot.....	126
Figure 3.28: 10% Deformation of the Surface, Contour and Arrow Plot for the 2D Visualization and Postprocessing.....	127
Figure 4.1: Laminar Flow in a Tube.....	131
Figure 4.2: Laminar Flow Pass a Curved Domain	131
Figure 4.3: Incompressible Flow with Occurrence of Turbulent.....	134
Figure 4.4: Occurrence of Turbulent in the Flow	134
Figure 4.5: Backstep Flow with $V_{mean} = 0.1$	136
Figure 4.6: Backstep Flow with $V_{mean} = 1.0$	136
Figure 4.7: Backstep Flow with $V_{mean} = 0.5$	136
Figure 4.8: Flow with Pressure.....	138
Figure 4.9: Pressure Flow with Resistance.....	139
Figure 4.10: Incompressible Flow Pass Periodic Boundaries.....	141

Figure 4.11: Flow Pass Tight Channel	143
Figure 4.12: Results from the Poisson Test.	144
Figure 4.13: Mesh Movement in a Prescribed Moving Boundary.....	146
Figure 4.14: Mesh Movement in a Free Moving Boundary	147
Figure 4.15: Velocity Profile in the Systolic and Diastolic Phase of the Left Ventricle Two Dimensional Simulation	149
Figure 4.16: Blood Flow through the Left Ventricle Chamber during Early Systolic Phase	151
Figure 4.17: Closing Movement of the Mitral Leaflets during the Left Ventricle Contraction.....	152
Figure 4.18: Closing Movement of the Aortic Valve Leaflets during the Left Ventricle Filling.	153
Figure 4.19: Velocity time profile of the mean velocity (cm/s) through the mitral valve and between the leaflet boundaries.	156
Figure 4.20: Velocity time profile of the mean velocity (cm/s) across the aortic outflow and into the aortic cylinder.....	156
Figure 4.21: Periodic Flow due to the Periodic Motion of the Mitral and Aortic Valve Leaflets	157
Figure 5.1: Blood flow pattern in (a) the Aortic Outflow and (b) the Mitral Inflow	167
Figure 5.2: Flow Events in the Cardiac Cycle from Yellin (1995).....	167
Figure A.1: 3D Rendition of the Left Ventricle (Front View).....	181
Figure A.2: The rendered Left Ventricle showing (a) the aortic tricuspid leaflets and (b) the mitral tricuspid leaflets	181
Figure B.3: The measurement studies the length of the aortic cylinder, diameter of the cylinder opening and diameter of the semilunar valve at the orifice. (a) Length of the aortic cylinder is computed to be 21.706mm. (b) Diameter of the cylindrical opening is computed to be 17.000mm. (c) At the base, the diameter of the semilunar valve is computed as 10.180mm.	182
Figure B.4: The measurement studies the length of the mitral cylinder, diameter of the cylindrical opening and diameter of the mitral valve at the orifice. (a) Length of the mitral cylinder is computed to be 20.842mm. (b) Diameter of the cylindrical opening is calculated to be 18.367mm. (c) Diameter of the mitral valve at the orifice is calculated to be 14.845mm.	182
Figure B.5: The measurement studies the vertical length of the chamber and three curvature diameters that are significant to the shape of the body. (a) The length of the body from the base to the ventricle's apex is computed to be 45.644mm. (b) Diameter of the body near the base of the valves is calculated to be 38.917mm. (c) Diameter of the body in the middle part of the chamber is computed to be 36.351mm. (d) Diameter of the body near the ventricle's apex is calculated to be 29.388mm.....	183

LIST OF TABLES

Table 3-1: Number of points sampled for each structure scanned.....	77
Table 3-2: Field Variables Representing Properties the mesh Displacement.....	100
Table 3-3: Field Variable Representing the Mesh Velocity	101
Table 3-4: Boundary Settings for the Mesh Movement	115
Table 3-5: Mesh Parameters Settings for the Geometry.....	117
Table 3-6: Settings for the Time Dependant Solver	123

NOMENCLATURE

2D	Two – Dimensional
3D	Three – Dimensional
ALE	Arbitrary Lagrangian – Eulerian
CAD	Computer Aided Design
CFD	Computational Fluid Dynamics
CO	Composite Object
CT	Computed Tomography
DOF	Degree of Freedom
FEM	Finite Element Method
FEMLAB	Finite Element Method Laboratory
FSI	Fluid - Structure Interaction
N-S	the Navier-Stokes equation
NURBS	Non-uniform rational B-spline
PDE	Partial Differential Equation
ODE	Ordinary Differential Equation
RE	Reverse Engineering
RA	Right Atrium
RV	Right Ventricle
LA	Left Atrium
LV	Left Ventricle
CA	Cardiac Output
SV	Stroke Volume
V	Blood velocity
A	Cross-sectional area
d	Displacement vector
E	Young's modulus of elasticity
F	Force vector
K	Stiffness matrix
k	Specific permeability vector
L	Length
M	Mass matrix
p	Pressure
Q	Volumetric flow rate
R	Resistance
R _p	Total peripheral resistance
Re	Reynolds number
t	Time
U	Displacement vector
u	Displacement
v	Fluid velocity vector
X	Solution vector
κ	Fluid bulk modulus of elasticity
λ	Relaxation factor
μ	Fluid viscosity

ν	Poisson ratio
ρ	Density
ρ_m	Compressible fluid density
τ	Stress tensor
ϕ	Porosity
d	Displacement
f	Fluid
s	Solid
τ	Stress
η	Viscosity of blood
N_R	Reynold's number
K_x	Body force in x – direction
K_y	Body force in y – direction
Ω_f	Mesh Velocity
Ω_s	Mesh Displacement
ξ	Spatial Motion
χ	Physical Motion
ϕ	Arbitrary set of quantities
$j\phi$	Sum of fluxes
$\sigma\phi$	Sum of body forces

Chapter 1

Introduction

**The important thing is not to stop questioning.
Curiosity has its own reason for existing.**

Albert Einstein

1.1 Preface

The goal of this chapter is to provide a preface to the research undertaken. In sequential order, the introduction begins by defining the objective of the research which is followed by a brief description on the research background and the research overview. The chapter is continued with revision on the research scope and an extension to the motivation that drives the development process through to completion. An outline of the organization of thesis and a short summary conclude the chapter.

1.2 Research Motivation

Accurate measurement of blood flow is usually invasive and very difficult to make in spite its important role to clinical or physiological diagnosis. Therefore, an alternative method capable of determining the flow of the cardiac output, non-invasively, will be beneficial to the study and prediction of the general flow pattern, particularly in the left part of the heart. In recent studies, computational methods are widely applied for vascular diagnosis by considering blood flow in alternative treatments for a particular cardiac case. An example of this is the measurement of blood velocity through the ventricle using advanced computational simulation which decreases the use of any cardiac catheterization, resulting in improvement to the evaluations of patients with a potential circulatory disorder. For this reason, it has been an objective of this research to come out with a simple simulation implementation that realistically depicts a two-dimensional description of the general flow pattern in the left ventricle of the heart. It is hoped that with such direction, the 2D virtual model would support the concern to development of non-invasive method to visualize blood flow and would open rooms for better qualitative and quantitative clinical diagnosis.

1.3 Research Objective

The objective of this research is to study the motion of blood flow and its dynamic relation to the movement of the heart valves in the left ventricle. One way to study the mechanics in the heart is by using a computational method known as the Arbitrary Lagrangian-Eulerian (ALE). The ALE is a common application in engineering used to solve problems pertaining to structural and fluid mechanic analyses and in this work, the approach is adopted to solve two problems; the fluid problem (i.e. the motion of the blood) and the structure problem (i.e. the movement of the valves). The method employs the use of reference frames to represent the classical Lagrangian and Eulerian systems. The Lagrangian reference frame is used to study the structure problem and the Eulerian reference is used to study the fluid problem.

The Lagrangian reference frame investigates structural deformation by fixing its frame on the structure of interest. As the structure deforms, the frame deforms with it. The deformation captured by the frame is the structural movement of the valves. The Eulerian reference frame studies the motion of fluid by setting its frame on the fluid material and allows the fluid to cross through the frame to study the flow. Fluid has velocity and so, as the fluid flows through the frame, the Eulerian calculation measures the differing velocity in and out of each frame section. This measurement captures velocity information of the blood and it can be used to study the flow motion. In view of the fact that the mechanics in the heart requires an interaction between the valves movement and the blood flow, solution to the interaction is derived by setting the Lagrangian and Eulerian reference frames on a single computational grid. Coupling of both reference frames produces solution to the fluid-structure problem and a graphical simulation can be derived to display this dynamic interaction in the heart.

1.4 Research Background

In modern studies of the fluid-structure interactions of the heart, several researchers around the world have been identified to incorporate the ALE approach in their work. A group of researchers from the Eindhoven University of Technology has developed tissue engineered heart valves by analyzing how the geometry and material properties influence the movement of artery and heart valves and the flow vicinity in the heart (de Hart et al. 2000). Simulations of valve dynamics in a simplified left ventricle flow model using the ALE method can be seen in (de Hart 2002). The ALE approach has also been used to study the fluid-structure analysis of the structural and the fluid dynamic behavior for cardiopulmonary bypass (Guadagni et al. 2001). Another work incorporating the Lagrangian-Eulerian formulation to study the incompressible viscous flow on a finite element platform can be seen in (Hughes et al. 1981). Fluid-solid interaction of the valves leaflets motions have been investigated by means of the ALE couplings to derive two-dimensional model of the bi-leaflets valve (Cheng et al. 2003) and three-dimensional model of the bi-leaflets model (Cheng et al. 2004). Numerical analysis of fluid-solid interactions for blood flow on arterial structures is given careful attention in some works (Hose et al. 1998, Rutten 1998). From these experimental works, additional information pertaining to the heart's boundary positions and velocity information can be observed. It is reported that it has been over four decades, attempts have been made to obtain a constitutive relation for blood and in recent studies continuum models addressing the shear-thinning behavior and viscoelasticity of blood through complex mathematical derivations has been analyzed (Kyeleswarapu 1996).

Modeling of mechanical heart valves began 30 years ago with the two-dimensional (2D) immersed-boundary method of Peskin (Peskin 1972) and has continued to this day as methods have improved and computational power has increased. Huang et al. (1994) performed 2D, time-accurate simulations of a tilting-disk heart valve using a grid resolution of over 90,000 nodes with steady inflow conditions. Three-dimensional analysis of a tilting disk valve under steady flow conditions has been performed (Shim and Chang 1997). Steady, 2D, finite-element and laminar simulations of a bileaflet valve has been created (King et al. 1994). In their 2D geometry, they assumed that the flow was symmetric between the two leaflets. (King et al. 1996, and King et al. 1997) later extended this work to 3D and performed laminar simulations using one-quarter of the valve geometry (i.e., assuming that the flow is symmetric with respect to both symmetry planes of the valve).

Aluri and Chandran (2001) performed 2D and 3D simulations to investigate cavitations potential during the closure of a mechanical mitral valve using grids with 2048 nodes in 2D and 56,200 nodes in 3D. Lai et al. (2002) used a grid of 9830 nodes in 2D coupled with an arbitrary Lagrange-Euler solver to investigate the effect of leaflet-tip geometry on the pressure in the vicinity of the valve during closure. Rosenfeld et al. (2002) found that even in 2D, resolving the fine details of the flow near the leaflet required 80,000 nodes for grid-independent solutions. de Hart (2002) simulated the fluid-structure interaction in the human aortic valve through both opening and closing phases using a Lagrange-multiplier-based fictitious-domain method coupled with a finite-element method for the fluid. In his simulation, only one-sixth of the valve cross-section was modeled using 20,000 degrees of freedom for the fluid and 6,500 degrees of freedom for the valve structure.

1.5 Research Overview

The aim of this research is to simulate a simplified two-dimensional model of blood flow in the left ventricle of the heart by means of the Arbitrary Lagrangian-Eulerian (ALE) approach. Acquiring morphological information of the heart including its general and ultra structure of the anatomy is essential in understanding the geometric configurations of the organ being simulated. This is done through utilization of the reverse engineering method by scanning real porcine heart and reconstructs the scanned data into surface model. The most important feature of an ALE model is the insertion of partial differential equations (PDE) on the model boundaries. In order to achieve this target, creation of domains, subdomains and boundaries (with extensive definition of their points and edges in 2D solid modeling) is an important consideration.

In modeling the coupling for the fluid-structure interaction, a mesh movement technique is introduced. In this technique, the fluid domain is identified to be conveniently described with respect to an Eulerian reference frame while a Lagrangian formulation is considered a more appropriate approach for the structure domain. The moving mesh for the Eulerian reference frame handles the fluid velocity and is usually known as the mesh velocity. The moving mesh for the Lagrangian reference frame handles the structure displacement and is called the mesh displacement. It has been identified that the general PDE for the mesh movement is based on the equation of motion used in continuum mechanics and for the most part they are taken from respective domains such as the solid and fluid mechanics. Implementation of field variables identified from these domains is utilized in commercially available software, FEMLAB, with the intention to handle the mesh displacement and mesh velocity described in the model. Time dependent solver is considered most appropriate in

deriving the solution to non-linear PDE problems where two-dimensional post processing and visualization is provided for the display of the simulation results on a computer screen.

1.6 Research Scope

In this research project, a simplified model of the left ventricle geometry will be created. The modeling geometry generated must be able to incorporate constraints from governing constitutive equations and solve for the time dependent problem. It would have been impossible to view the two-dimensional object without a graphical simulation. So a visualization program displaying the blood flow will be supplied for the system. In addition, the motion animation of the valves in the left part of the heart should be seen upon completion of system development. In summary, the scope of this research project is laid out as follows:

- To review existing works on heart modeling with particular emphasis to the techniques and computational technologies used.
- To implement the ALE method on a finite element platform and test for model convergence and accuracy of the system.
- To review and study techniques involved in numerical and computational calculation of the fluid dynamics using the Navier-Stokes equations and its application in modeling the dynamic properties to the blood flow.
- To grasp the basis of fundamental laws of physics (conservation of momentum, conservation of mass, balance equation, etc.) and the constitutive equations of the materials in order to derive the governing differential or integral equations.

- To understand the environment in which the heart works in order to obtain meaningful boundary conditions.
- To solve the boundary-valued problems (differential equations with appropriate boundary conditions) analytically or numerically.
- To analyze data from existing physiological experiments and search for solution values to test the boundary-valued problems named.
- To reformulate and resolve (when necessary) the mathematical problem so that the theory and simulated experiments corresponds to each other, that is they are testing the same hypotheses.
- To compare the experimental results with corresponding theoretical ones. By means of this comparison, hypotheses made in the theory are to be justified, and, if they are, find numerical values of the undetermined coefficients in the constitutive equations.
- To survey practical applications of the theory and experiments and search for possible method of enhancement to extend the simulated model in future works.

1.7 Thesis Organization

The thesis is organized into six separate chapters. Chapter 1 forwards a prologue to this thesis. Chapter 2 provides a critical look at the existing research that is significant to the work being carried out. The goal of this chapter is to compile the studies which are relevant to the research. This chapter has focused on the techniques of the Arbitrary Lagrangian-Eulerian (ALE) approach and its mesh movement mechanism as these are the main methods featured in the theses. An overview of the heart anatomy has been thoroughly discussed with the inclusion of the cardiac mechanics particularly on the left part of the

heart. The methods analyzing the flow properties of the heart or the hemodynamics have been briefly revised.

Chapter 3 is at the heart of this thesis. Careful details on the construction pertaining to the two-dimensional ALE modeling are presented. The methods involved in the study of the fluid-structure interaction in the left ventricle have been extensively discussed. Tools involved in the development processes are revised and with this, algorithm that is the backbone of the modeling is also weighted with interest.

Chapter 4 delivers results from preliminary experimental work and the actual simulation work done. The numerical results have been illustrated with snapshots from the two-dimensional graphical simulation. Analysis of each model experiment pertaining to certain goal is described. Verification of the simulated results is done through comparison with cited previous works.

Chapter 5 provides the discussion on results stemming from implementations carried out in the analysis chapter. Theories used in the development are thoroughly investigated and discussion on several related issues highlighting the research contributions. Suggestion for future work is also presented at the end of the chapter. Chapter 6 ends the dissertation with a brief assessment of the whole research.

1.8 Summary

This chapter forwards a preface to the dissertation by introducing the research objective and motivation. The research background is given special attention with inclusion of previous work done in similar areas of the research. The overview and scope provide an insight to the framework of the research. The chapter ends with a brief summary on the contents of each chapter of the thesis.

Chapter 2

Literature Review

**What we call the beginning is often the end
And to make an end is to make a beginning.
The end is where we start from...**

T. S. ELIOT, "Four Quartets"

2.1 Overview

The literature review is a critical look at the existing research that is significant to the work being carried out. The goal of this chapter is to compile the studies which are relevant to the research.

2.2 The Heart Anatomy

The human heart is positioned in the thoracic cavity between the lungs. The usual weight of the human heart is normally about 0.5 % of the specimen. For an instance, the weight of the heart for a man of 70 kg is 350 g. The heart is enclosed within the pericardium, which is composed of two layers; the visceral and the parietal pericardium. The two pericardial layers are separated by a thin lubricating fluid film. The heart functions as a pump whose sole function is to perfuse the whole body with circulating blood. The mechanical pumping motion of the heart produces friction and the thin lubricating fluid film is reported to reduce this friction. The heart wall itself is composed of three layers: the outer layer or epicardium, the middle, muscular layer or myocardium, and the inner endothelial layer or endocardium.

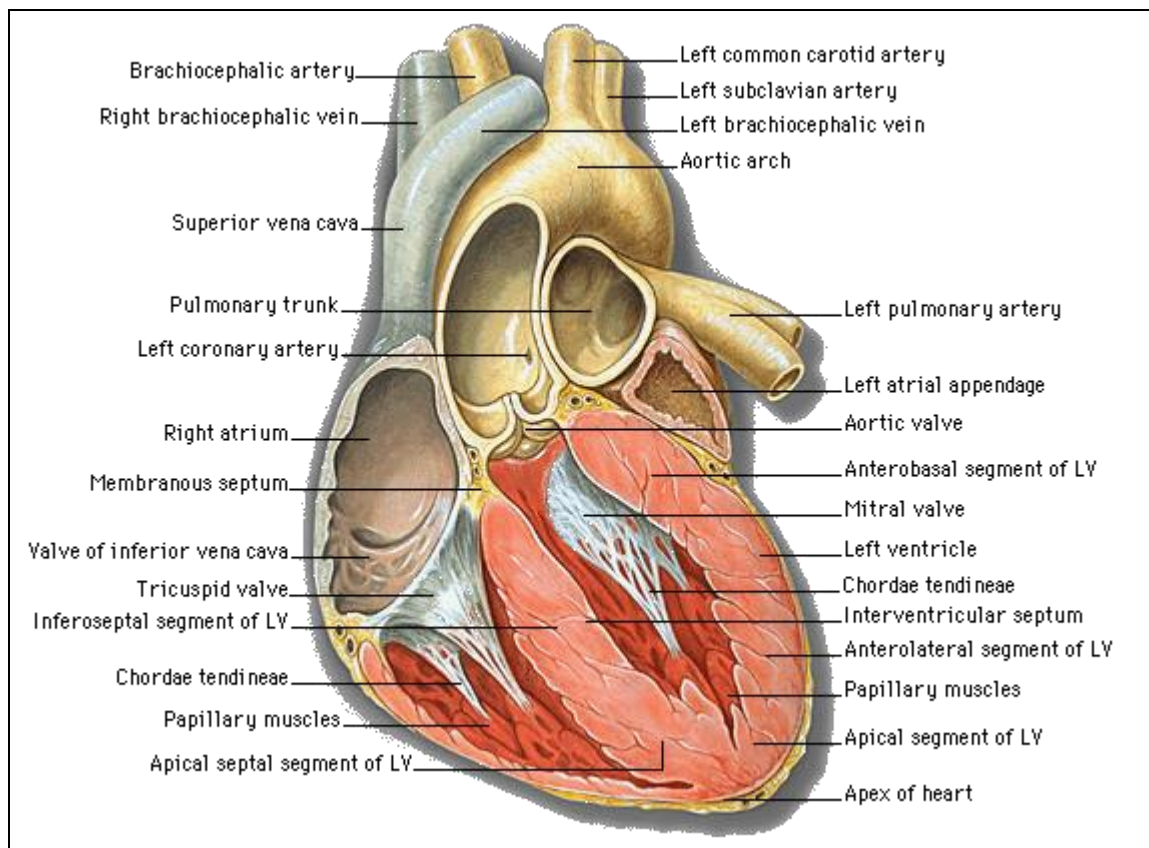


Figure 2.1: Gross Anatomy of the Heart (Atlas of Echocardiography 1999)

The human heart is divided into four chambers. The “upper” chambers of the heart, the atria, are anatomically separated from the “lower” chambers or ventricles by a fibrous ring. The four cardiac valves are situated within this ring. Based on the functional point of view, the heart is divided into right- and left-sided pumps, with the sole purpose is to propel oxygen deficient blood into the pulmonary circulation and oxygenated blood into the systemic circulation, in that order.

The direction of blood flow in the circulation is according to the illustration depicted in Figure 2.2; starting from the venae cavae, to the right atrium (RA), right ventricle (RV), pulmonary artery, lungs, pulmonary veins, left atrium (LA), left ventricle (LV), aorta, arteries, arterioles, capillaries, venules, veins, and back to the venae cavae.

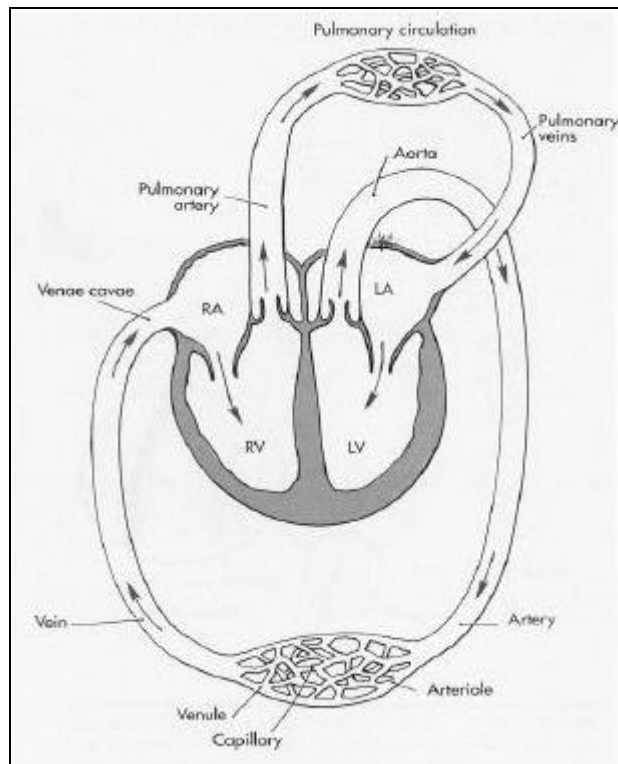


Figure 2.2: The sequence of blood flow in the circulation (Price and Wilson 1992)

2.2.1 The Left Heart

The left and right sides of the heart are separated by the septum (Figure 2.3). The left heart is composed of the left atrium (LA) and the left ventricle (LV). The LA receives oxygenated blood from the lungs via the pulmonary veins and there are no valves that separate the pulmonary veins from the LA. Because of this reasoning, alterations in the LA pressure are reproduced into the pulmonary domain, and acute elevations in the LA pressure have been depicted as the cause to pulmonary clogging. The LA is a thin-walled, low-pressure

chamber. Blood flows from the LA into the LV through the mitral valve. The mitral valve is a bicuspid valve with two valve cusps or leaflets. The leaflets are delicate, yet durable. The cusps of the valve are attached to thin strands of fibrous tissue called chordae tendinae. The chordae tendinae tissue extends to the papillary muscles, which are the muscular projections arising from the ventricular wall. The mitral valve assures one-directional blood flow from LA to LV, i.e. the mitral valve prevents backflow from the LV into the LA during LV contraction and ejection. The thick musculature of the LV ensures the ability to develop high pressure during ventricular contraction. The LV and the aorta are separated by the aortic valve, consisting of three cuplike cusps, secured to a fibrous ring. The valve prevents backflow from the aorta into the ventricle during LV relaxation and filling.

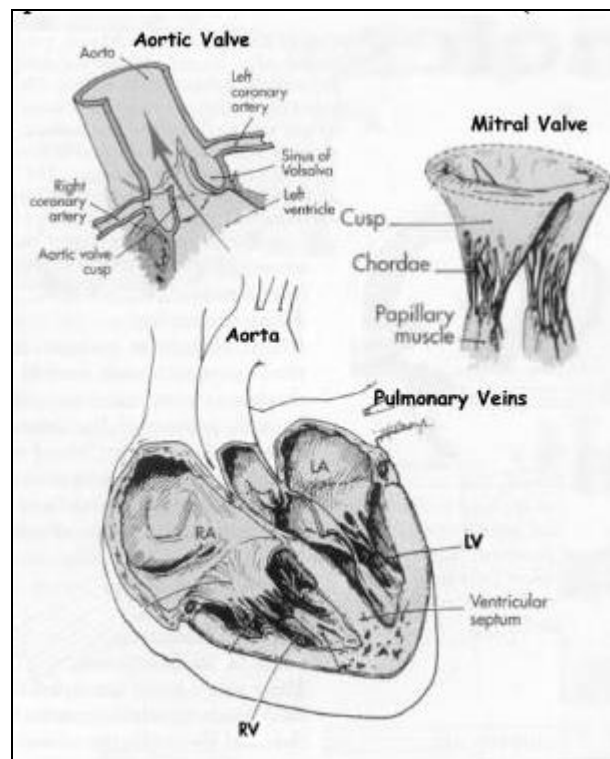


Figure 2.3: Anatomy of the human heart, aortic valve and mitral valve (Price and Wilson 1992)

2.2.2 The Cardiac Mechanics

Figure 2.4 represents the pressure and the flow events during the cardiac cycle (Yellin 1995). The cardiac cycle is the cycle of events that occurs as the heart contracts. The timing of the events can be situated within the cardiac cycle using the ECG diagram on top of the figure. The cardiac mechanics is divided into two major ventricular events; the systole and diastole. In the diastole phase, the heart ventricles are relaxed and the heart fills with blood. In the systole phase, the ventricles contract and pump blood into the arteries.

2.2.2.1 Systole

During ventricular systole, LV pressure is reported to rise from 0 to 120 mmHg. The moment it rises above the aortic pressure, the aortic valve is forced to open and blood is ejected from the LV into the arterial system. The volume ejected by each ventricle per minute is said to be the cardiac output (CO). Average cardiac output in humans during these resting conditions is 5-6 l/min (Chandran 1992). However, cardiac output is not the same to everyone; it varies to meet the demands of the peripheral tissues for oxygen and nutrients and may be as high as 30 l/min during peak exercise in trained athletes. The volume of blood ejected by each ventricle per beat is said to be the stroke volume (SV). During systole, there is approximately two thirds of the volume of blood in the ventricle is ejected at the end of each diastole (end-diastolic volume, EDV). This portion of ejected blood is known as the ejection fraction (EF; $EF = SV/EDV$). The residual ventricular volume, the one third left at the end of systole is referred to as the end-systolic volume (ESV).

2.2.2.2 Diastole

The diastolic portion of the heart cycle can be subdivided into four phases; the isovolumic relaxation, rapid or early filling (E-wave), diastasis (L-wave) and atrial contraction (A-wave). In the first phase, between the time of aortic valve closure and mitral valve opening, LV pressure drops exponentially from the aortic pressure level to the pressure level existing in the LA. In the next phase, the early filling (E-wave) begins when pressure in the LV falls lower of that in the LA, forcing the mitral valve to open and the LV to begin filling. The early filling phase corresponds with and is reported to be dependent on continued LV relaxation. This phase ends the moment the pressure in the two chambers is equalized. Although this rapid filling comprises only about 30% of diastole, it accounts for up to 80% of LV filling volume. The third phase is the diastasis. Small amount of filling, if any, comes from pulmonary vein flow (L-wave). With increased heart rate this phase shortens more than the other three. The fourth phase, atrial contraction (A-wave), contributes for 15% to 25% of LV filling volume under normal conditions but can contribute as much as 40% if LV relaxation is impaired.

Basically because relaxation is an energy consuming and therefore is considered an “active” process which commences during the second half of the ejection phase, sometimes the isovolumic relaxation phase and early filling phase are considered to be the end of systole (Brutsaert et al. 1993, Brutsaert and Sys 1989, Gillebert and Sys 1994). By this definition diastole only comprises diastasis and atrial filling. Consequently, in this definition diastole accounts for about 50% of the cardiac cycle at normal heart rates, contributing for only 15% to 25% of the LV volume. Although this approach offers some advantages in understanding cellular and mechanical events, it introduces a difficult

terminology for the clinician who, based on phenomenological evidence, is convinced that ejection ends with, and diastole commences after aortic valve closure.

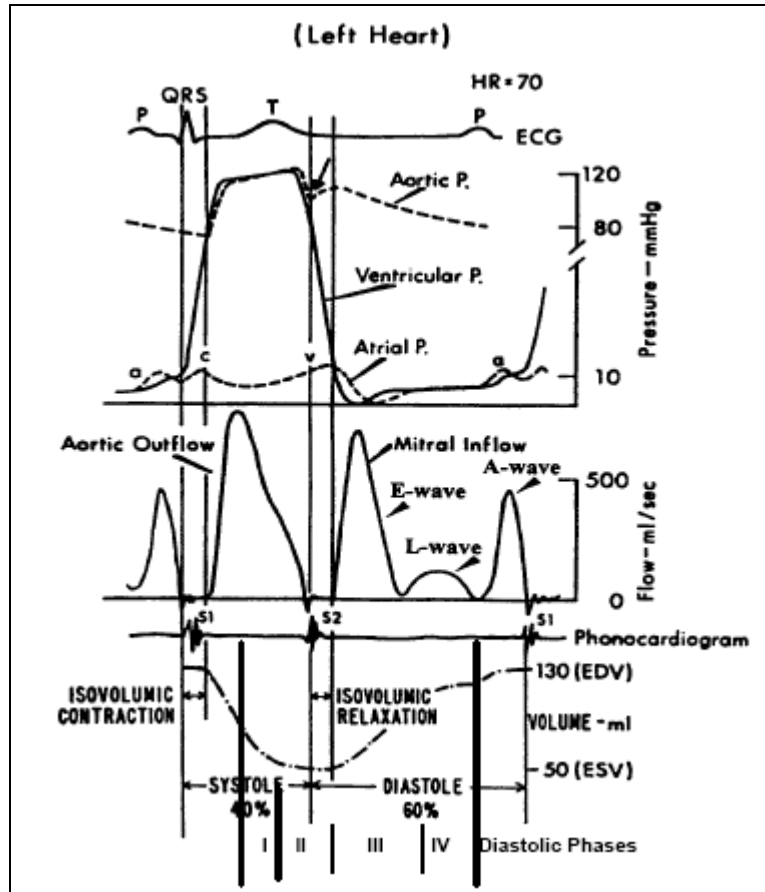


Figure 2.4: Pressure, flow and volume events during the cardiac cycle (Yellin 1995)

2.2.3 The Windkessel Theory

The simplest theory of the cardiovascular system is the Windkessel theory proposed by Otto Frank in 1899. The idea has been stated earlier by Hales (1733) and Weber (1850) in Fung (1981) and in the modern research the theory is re-introduced in Jacobsen (1999) and evaluated in both Jacobsen (1999) and, Adeler and Jacobsen (2001). The goal behind this theory is to model the after-load of the heart introduced to improve the outflow conditions at the aortic sink.

In this theory the aorta is represented by an elastic chamber, and the peripheral blood vessels are replaced by a rigid tube of constant resistance. Inflow to the aortic sink is supplied by the ventricle chamber during contraction where part of this inflow is sent to the peripheral vessels and part of it is used to distend the elastic chamber. The Windkessel model was introduced to improve the outflow conditions at the aortic sink. Originally, the outflow was determined by a linear resistance model (similar to the one for the atrial source), but this gave an unrealistic pressure.

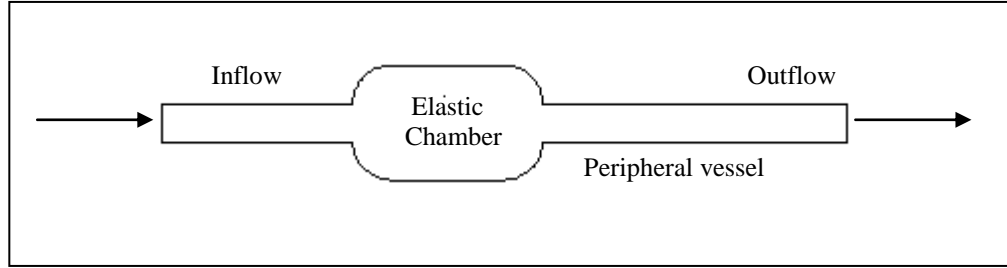


Figure 2.5: Simple representation of the aorta in the Windkessel Theory

Q is the inflow (cm^3/sec) into this system from the heart. Part of this inflow is sent to the peripheral vessel and part of it is used to distend the elastic chamber. If P is the blood pressure (pressure from the aorta or the elastic chamber), the flow in the peripheral vessel is equal to p/R , where R is the peripheral resistance. For the elastic chamber, its change of volume is assumed to be proportional to the pressure. The rate of change of the volume of the elastic chamber with respect to time t is therefore proportional to dp/dt . Let the constant of proportionality be written as K and so on equating the inflow to the sum of the rate of change of volume of the elastic chamber and the outflow p/R , the differential equation governing to the pressure p is

$$Q = K \frac{dp}{dt} + \frac{p}{R} \quad (2.1)$$

A primary effect of the use of the Windkessel model is that to obtain a simulated aortic outflow profile which reproduces a characteristic feature of the measured one, namely that the upstroke has a duration of about one half of that of the downstroke. The normal pumping history of the heart; the periodicity and the steady state response of the aorta to a periodically beating heart are shown in Figure 2.6. The equation given is in good correlation to the experimental data on the total blood flow, Q with blood pressure p , particularly during the diastole. Hence, in spite of the simplicity of the underlying assumptions, the model is quite useful to study the ventricular activities on the heart.

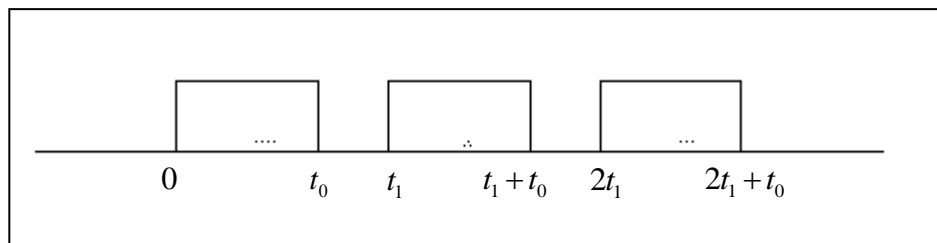


Figure 2.6: Some Pulse Waves in the Beating Heart

2.3 Dynamics of the Blood Flow (Hemodynamics)

The term hemodynamics refers to the principles that govern blood flow in the cardiovascular system. These basic principles of physics are the same as those applied to the movement of fluids in general. The concepts of flow, pressure and resistance are applied to blood flow to and from the heart and within the blood vessels.

2.3.1 Velocity of Blood Flow

The velocity of blood flow is the rate of the displacement of blood per unit time. The blood vessels of the cardiovascular system vary in terms of diameter and cross-sectional area. These differences in diameter and area, in turn, have profound effects on velocity of flow.

The relationship between velocity, flow, and cross-sectional area which depends on vessel radius or diameter is as follows:

$$v = Q/A \quad (2.2)$$

Where

v = velocity of blood flow (cm/sec)

Q = flow (ml/sec)

A = cross-sectional area (cm²)

Velocity of blood (v) is linear velocity and refers to the rate of displacement of blood per unit time. Thus, velocity is expressed in units of distance per unit time, which is cm/sec. Flow (Q) is the cross-sectional area of a blood vessel (e.g. aorta) or a group of blood vessels (e.g. all of the capillaries). Area is calculated as $A = \pi r^2$, where r is the radius of a single blood vessel (e.g. aorta) or the total radius of group of blood vessels (e.g. all of the capillaries).

2.3.2 Relationships between Blood Flow, Pressure, and Resistance

Blood flow through a blood vessel or a series of blood vessels is determined by two factors: the pressure difference between the two ends of the vessel and the resistance of the vessel to blood flow. The pressure difference is the driving force for the blood flow, and the resistance is an impediment to flow. Blood flow (Q) is directly proportional to the size of the pressure difference Δp or pressure gradient. The direction of blood flow is determined

by the direction of the pressure gradient and always is from high to low pressure. An example, during ventricular ejection, blood flows from the left ventricle in to the aorta (not in the other direction) because pressure in the ventricle is higher than pressure in the aorta. Furthermore, blood flow is inversely proportional to resistance (R) deriving the equation next;

$$Q = \Delta p/R \quad (2.3)$$

Increasing resistance such as by vasoconstriction would decrease flow, and decreasing of resistance such as vasodilation increases flow. The major mechanism for changing blood flow in the cardiac mechanics is by changing the resistance of blood vessels. The flow, pressure and resistance relationship can be used to measure the resistance of the entire systemic vasculature, that is the total peripheral resistance, or it can be used in measurements of resistance in a single organ or single blood vessel.

2.3.3 Resistance to Blood Flow

The blood vessel and the blood itself constitute resistance to blood flow. The relationship between resistance, blood vessel diameter or radius and blood viscosity are described by the Poiseuille equation

$$R = \frac{8\eta l}{\pi r^4} \quad (2.4)$$

where

R = resistance

η = viscosity of blood

l = length of blood vessel

r = radius of blood vessel

The most important concepts expressed in the Poiseuille equations are as follows. First, resistance to flow is directly proportional to viscosity of the blood; as an example, as viscosity increases the resistance to flow also increases. Second, resistance to flow is inversely proportional to the fourth power of the radius of the blood vessel.

2.3.4 Laminar Flow and the Reynold's Number

Ideally, blood flow in the cardiovascular and in the heart is laminar, or streamlined. In laminar flow, there is a parabolic profile of velocity within the blood vessel, with the velocity of blood flow highest in the center of the vessel and lowest toward the vessel walls. The parabolic profile develops because the layer of blood next to the vessel wall adheres to the wall, and, essentially, does not move. The next layer of blood (toward the center) slips past the motionless layer and moves a bit faster. Each successive layer of blood toward the center moves faster yet, with fewer adherences to adjacent layers. Thus the velocity of the flow at the vessel wall is zero, and the velocity at the center of the stream is maximal. Laminar blood flow conforms to this orderly parabolic profile.

2.3.5 Turbulent Flow

When an irregularity occurs in a blood vessel (e.g. at the valves or at the site of a blood clot), the laminar stream is interrupted, and blood flow may become turbulent. In turbulent flow, the fluid streams do not remain in the parabolic profile but, instead, the streams mix radially and axially. More energy (pressure) is required to drive turbulent flow than to drive a laminar blood flow. Energy is wasted in propelling the blood radially and axially. Turbulent flow is often accompanied by audible vibrations called murmurs.

The Reynold's number is a dimensionless number that is used to predict whether blood flow will be laminar or turbulent. It considers a number of factors, including diameter of the blood vessel, mean velocity of flow, and viscosity of the blood. Thus

$$N_R = \frac{\rho d v}{\eta} \quad (2.5)$$

where

N_R = Reynold's number

ρ = density of blood

d = diameter of blood vessel

v = velocity of blood flow

η = viscosity of blood

If Reynold's number is less than 2000, blood flow will be laminar. If Reynold's number is greater than 2000, there is an increasing likelihood that blood flow will be turbulent. Values greater than 3000 always predict turbulent flow. The major influence on Reynold's number in the cardiovascular system is changes in blood viscosity and changes in the velocity of blood flow. Inspection of the equation shows that decrease in viscosity cause an increase in the Reynold's number. Likewise, narrowing of a blood vessel, which produces an increase in velocity of blood flow, cause an increase in the Reynold's number.

2.3.6 Newtonian Property

Is blood a Newtonian fluid? A Newtonian fluid is one which exhibits the following property. The shear stress, or resisting force τ , and velocity gradient, or rate of deformation du/dy are linearly related by

$$\tau = \mu \frac{du}{dy} \quad 2.6)$$

where μ is the coefficient of viscosity. The question of whether blood is a Newtonian fluid is still standing. The composition of blood would seem to indicate that it is indeed not a Newtonian fluid. In fact, studies seem to indicate that plasma by itself is a non-Newtonian fluid. However, under certain restrictions, such as those imposed on this problem, it is sufficient to assume blood acts like a Newtonian fluid. Indeed, all modeling of pulsatile blood flow accepts this assumption. It is only when the scale of the problem is so reduced, as in capillary modeling, that the Newtonian fluid model breaks down.

2.4 Computational Fluid Dynamics (CFD) and the Navier-Stokes Equations

2.4.1 CFD approach in Hemodynamics

Blood in physiological conditions may be considered as incompressible. In the arteries, the flow can be considered a continuum. That is, the elements of blood seem to be continuous with each other, with no empty spaces in between. In fact, even though blood is composed of many different elements, the continuum hypothesis implies that every point in the fluid represents a fluid element, and that the properties at that point, represent the properties of that fluid element.

Studying blood flow in arteries belongs to the multidisciplinary field of bioengineering (Bellhouse 1972). It combines the knowledge base of engineering and medicine. Blood flow in arteries is covered under hemodynamics (Fung 1997, Fung 1993). Beside theoretical work, experimental studies and clinical measurements advanced our understanding in the past two centuries.

The equations are a set of coupled differential equations and could, in theory, be solved for a given flow problem by using methods from calculus (Batchelor 1967). But, in practice, these equations are too difficult to solve analytically. In the past, engineers made further approximations and simplifications to the equation set until they had a group of equations that they could solve. Recently, high speed computers have been used to solve approximations to the equations using a variety of techniques like finite difference, finite volume, finite element, and spectral methods hence bring forth this area of study called Computational Fluid Dynamics or CFD. With the development of modern computers, CFD was added, as an independent field, to theoretical and experimental studies of fluid motion,

also used potentially in numerical modeling of physical phenomena in the arterial flows as well.

2.4.2 The Navier-Stokes equation

The Navier-Stokes equation is a standard equation that describes the flow of continuum matter in fluid form - which can be a liquid like water, or a gas like the air. The equation describes the change with time of the density and velocity of the fluid. Most traditional CFD algorithms require the solution of the Navier-Stokes (N-S) equations to handle to these continuum requirements. The details of the solution process depend upon the details of the flow to be solved. The solution process for an incompressible flow can be very different than that for a compressible flow.

2.4.2.1 The Navier-Stokes Equation and the Incompressible flow

In situations in which the density is approximately constant, the flow may be termed as incompressible. The Navier Stokes equation for fluid flow:

$$\rho \frac{\delta u}{\delta t} - \eta \nabla^2 u + \rho(u \cdot \nabla) + \nabla p = F \quad (2.7)$$

where

$$\nabla \cdot u = 0$$

are deduced for incompressible Newtonian flow. However, a generalized version of the Navier–Stokes equation which allow for variable viscosity in non-Newtonian fluids can be derived as follow:

$$\rho \frac{\delta u}{\delta t} - \nabla \cdot [\eta(\nabla u + (\nabla u)^T)] + \rho(u \cdot \nabla)u + \nabla p = F \quad (2.8)$$

where

$$\nabla \cdot u = 0$$

The following variables and parameters appear in the equations:

η is the dynamic viscosity

ρ is the density

u is the velocity field

p is the pressure

F is a volume force field such as gravity

These applications are general enough to account for all types of incompressible flow such as the blood. These equations describe how the velocity, pressure, and density of a moving fluid are related. The equations were derived independently by G.G. Stokes, in England, and M. Navier, in France, in the early 1800's. The equations are extensions of the Euler Equations and include the effects of viscosity on the flow. The equation is actually a vector equation obtained by applying Newton's Law of Motion to a fluid element and is also called the momentum equation (further discussion in Section 2.7.6). It can be enhanced using the energy equation and the mass conservation equation (refer Section 2.7.5), which are also called the continuity equations. However the term Navier-Stokes equations are usually used to refer to all of these equations.

2.4.2.2 The Navier-Stokes Equation and Time Dependency

The Navier-Stokes equation consists of a time-dependent continuity equation for conservation of mass, conservation of momentum and for the conservation of energy. There are several independent variables in the problem, the x and y spatial coordinates for the two-dimensional domain, or x , y , and z for a three-dimensional domain, and the time t . These components of the velocity vectors plus three other dependent variables; the pressure p , density ρ , and viscosity plays major factor in defining the equation. The u component is the velocity vector in the x direction, the v component is the velocity vector in the y direction, and the w component is the velocity vector in the z direction. All of the dependent variables are functions of all four independent variables. The differential equations are therefore partial differential equations (PDEs) and not the ordinary differential equations (ODEs).

Notice that all of the dependent variables appear in each equation stated in the previous section. In order to solve a flow problem, there are at least five equations to be solved simultaneously; which are why it is called a coupled system of equations. There are actually some other equations that are required to solve this system.

2.5 The Arbitrary Lagrangian Eulerian (ALE) Modeling

ALE stands for Arbitrary Lagrangian Eulerian. It is an extensive numerical approach used to solve domains in engineering which require combination of both the classical Lagrangian and Eulerian reference frames and widely exercised on problems that analyze fluid structure interactions systems. It has been recognized that ALE has the capability to analyze fluid and structural motions when the material strain is large and where severe

deformation of flexible structures take place. Both reference frames, the Lagrangian and the Eulerian, on their own, have also been recognized to solve most problems.

2.5.1 The Lagrange Reference Frame

The Lagrange reference frame is commonly used in solid mechanics. It sets up a reference frame by fixing a grid to the material of interest then as the material deforms the grid deforms with it. For an example, a solid structure with little material flexibility, that is, a structure which has a slight amount of deformation would typically uses the Lagrangian approach because as the grid deforms under a certain applied load or pressure, the pattern of deflection is synchronously mapped out by the Lagrangian grid according to the deformation. The grid would also define the exact displacement of each particle, which could be manipulated to beneficially track the order of motion or mechanics of the solid properties. Having to track the displacement of all particles allow each individual sections of the grid to always contain the same amount of mass, and thus the method has been recognized to automatically satisfy the conservation of mass.

For more flexible structure with higher sense of elasticity, high pressure and load supply would result in a much larger deformation and could also reach the point of excessive distortion. Excessive distortion would chart the grid with critical deformation, where division of the grid plays a major role to determine the accuracy of the bending. Larger deformation has been identified to require smaller grid sections, as tracking severe bending would entail a finite measurement of the grid to accommodate the change. It is hence easier to track the regions predicted to have critical distortion with smaller grid sections. The definition of the size of the grid sections directly governs the design of the time steps as

they are based on the size of the smallest section of the grid. The particles of a structure or a solid model are usually in place and in a mode of unified attachment towards each other, giving opportunity for the Lagrangian grid to map the deformation.

In the domain of fluid mechanics, it has been recognized that fluid particles do not stay as tight as the solid particles and that fluids are not cohesive. So if a grid is mapped out onto a fluid, finite size of grid sections would not be sufficient to track the motion of the fluid as the fluid particles will travel independent of each other and diverge in space. The movement would result in mapping of excessive distortion with the possibility of the individual grid sections that try to follow certain particle to overlap each other, providing an unreasonable prediction of the fluid motion. In short, the Lagrangian method is considered as not the easiest solution for a fluid mechanics problem.

2.5.2 The Eulerian Reference Frame

The Eulerian reference frame, which is fixed in space, is the typical framework used in the analysis of fluid mechanics problem. It allows for material with specified load or pressure to flow through the grid as it is with the Lagrangian frame, but this time without tracking the path to of any of the individual particle. In order to predict the flow of the fluid across the grid, the Eulerian approach solves the problem by measuring the net flow through a certain area. In the case of the Lagrangian, conservation of mass is directly preserved as all the grid sections has been initialized with equal amount of mass, for the Eulerian, conservation of mass is taken into account openly by measuring the flux in and out of each grid section. This feature guarantees a thorough tracking of the fluid in motion only that it

is not an elegant approach to adequately track the path of any element, particularly the fluid free surfaces.

2.5.3 Coupling of the Lagrangian-Eulerian Reference System

The arbitrary Lagrangian Eulerian (ALE) method combines the two classical approaches. Both reference frames are used to allow special design of two grids; one that is flexible and another that permits for material to flow through it. In reference to the word arbitrary, ALE in essence takes the best part of both frames and merges them into one. This is helpful in problems with large deformations as ALE is applicable to allow tracking of the particle material to some extent but when the grid deforms excessively and distorts the aspect ratio of the grid beyond an acceptable point, it switches the grid and measures the flux of the material during the adjustment. The significant difficulty of the ALE approach is deciding how much to allow a grid to deform and how much flux to allow. This is usually done by setting a limit on the distortion of a segment of a grid and once it deforms past the limit, then the part of the grid is remeshed.

2.5.4 Controlling Equations in ALE

The ALE requires the input of several variables in order to allow for numerical calculations of the model so that it closely resembles the real world situations. These numerical entities are the fundamental elements that control and make the governing equations to work. Size, boundary conditions, free surfaces and starting velocities, and several of the intrinsic characteristics of the material; the density, viscosity, strength, Young's modulus, shear modulus, and bulk modulus are of important considerations. All these variables are to be put in a specific order to assure the accuracy of the controlling equations. The controlling

equations have been identified as the properties that depict the movements of the computer model, hence become the main element that ensures the succinct of the ALE simulation. Several controlling equations have been considered in the fluid - structure modeling.

2.5.5 Function of the Navier-Stokes Equation in the ALE

The Navier Stokes equations have been used to track the conservation of momentum needed to monitor the fluid motion in the simulation (Baaijens 2001). The partial differential equations (PDEs) especially the Weak Form equations, is used to observe the conservation of mass which is crucial when there is large deformation and remeshing of the grid occurs. When there is no deformation and the mesh stays constant as can be seen in the Eulerian approach, there is no need for the conservation of mass since there is no mass flux and the mesh remain constant by default. There is also the boundary conditions that requires particular attention, as boundaries to the model accepts the initial condition values, allow for directions to the fluid flow and structural motions and they graphically outlines all two dimensional motion that took place in the simulation.

2.5.6 Computational Grid Mapping

The grid requires a standardize mapping with each of the individual elements to be homogenous and of the same material. In application to a finite element environment, this is important because the computer treats each individual element in the mesh as equal material all through out (refer to Section 2.8). The boundaries dividing the domains and subdomains of interest are also better seen with this approach as it is often difficult to determine where the boundary lies between the individual materials. Using partial differential equations, the controlling equations are then applied to both grids individually,

creating matrix equations that allows for insertion of material properties and initial boundary conditions. The mesh generated by the procedure may have hundreds of individual grid squares resulting in simultaneous solving of large matrices for a problem. This can lead to multiple days of computing time and is the reason to consider setting of small time steps to the finite element solver.

2.6 The Balance Laws Formulation

In the previous subsections, literature survey on the ALE modeling has been made comprehensive to ensure a general understanding of the approach taken in this project. The goal of this section is to apply and use the conceptual knowledge and represent a numerical overview on the ALE using the Balance Laws formulation which governs its mechanical behavior. Throughout the following explanation, formulation extracted from Knobbe (2004) is used to accentuate the mathematical principle of the method.

2.6.1 Fundamentals Theory of the Balance Laws

Basically, the ALE approach in a finite element environment is used for its numerical approximation to master balance laws for an arbitrary set of quantities (ϕ). Balance equations are equations that represent the fundamental physical laws. In the mechanical world, these include laws expressing conservation of mass, momentum, energy and some form of the second law of thermodynamics. Such balance equations hold for all materials, e.g., solids, fluids, viscoelastic material and rigid bodies. In a global balance law, the material time rate of change of the total amount of the property over a given body of material, is considered as balanced by the sum of the fluxes ($j\phi$), which cross the surface plus the sum of the body forces ($\sigma\phi$). In other words, it can be said that the time rate of

change of a quantity is equivalent to the actions of the surroundings on the surface of the volume (V) and the actions of the surroundings on the volume itself.

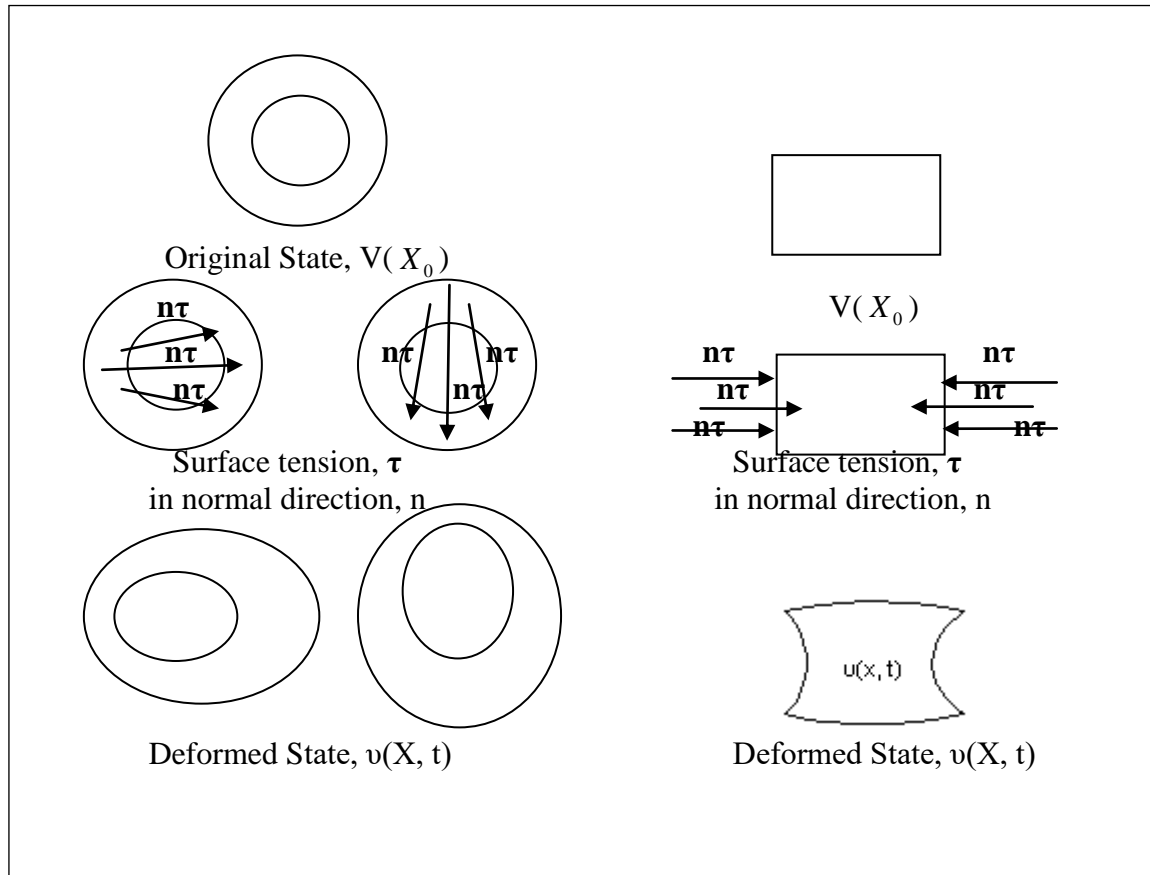


Figure 2.7: Sample Body of Material Undergoing Deformation

In Figure 2.7, $V(X)$ is considered to be a volume of material at reference time $t = 0$. This may be an entire body of material, or a part of a larger body in its original state. At a later time step, the material body goes through a deformation and at this point the volume that this body takes at the time is $v(x, t)$. Following the global balance law, it has been stated that the only way the total amount of property ϕ can change is through an amount crossing its boundary (flux) or by a body force acting throughout the material. These quantities are taken as the input sources to the fluid – structure problem and they are entitled to changes

due to any combination based on the surface sources, i.e. the flux, and the volumetric sources, i.e. the body forces.

2.6.2 Quantities representing the Balance Laws

For each balance law they are different quantities representing $\{\phi, j_\phi, \sigma_\phi\}$. For the conservation of mass, the quantity being conserved is mass; the flux is zero (the definition of the body includes all the material), and the body force also zero. For the conservation of momentum, the quantity being conserved is linear momentum, the flux is force, and the body force is gravity.

$$\frac{d}{dt} \int_{\chi|_t(\Omega_z)} \Phi dV|_z = - \int_{\chi|_t(\Omega_z)} n \cdot j_\phi dS + \int_{\chi|_t(\Omega_z)} \sigma_\phi dV \quad (2.9)$$

where $\chi(\Omega Z, t)$ is the spatial location of the body at time (t), dS is the surface of the body, and n is the elemental area that denotes the outward pointing normal direction to the surface (recall that n is a unit vector). The integration has been defined using the Eulerian framework over the body, because the quantities ϕ and σ_ϕ are defined per unit of special volume and $n \cdot j_\phi$ is defined per unit spatial area, but the time derivative is material (keeping χ fixed). Integrands in above equation depend on moving spatial coordinate y and time t . Since the body or material configuration (ΩZ) may move, the spatial volume occupied by the material $\chi(\Omega Z, t)$ may change in time.

The material over which the global balance law is defined may consist of the entire body or certain parts of the body. The boundary however must enclose the same material throughout the deformation. It has been noted that the first term of the right hand side of the equation, which represents the flux of a quantity across the boundary, the symbol n is defined to be the unit vector out, a positive surface integral means that there is a net flux out, resulting in the decrease of the total amount of ϕ . The integration limits are determined by a moving material configuration Ω_Z , where the corresponding spatial coordinates are specified by physical motion

$$y = \chi(z, t) = \chi|_t(z) \quad (2.10)$$

2.6.3 Localizing the Balance Law

The difficulty of using directly equation (2.9) is that it is an integral equation. Fortunately, for many materials, the balance law can be localized. The ALE formulation (Hughes et al 1981) is used to attain an equivalent localized system of PDE equations for calculating domains with arbitrary moving boundaries. The system of PDEs is spatially discretized by a finite element method (i.e. the Galerkins method, Hughes 2000). These equations are integrated numerically with respect to time. In subsection 3.5.2, the governing concept of the ALE formulation has been explained. With the derivations of spatial motion ξ as additional degree of freedom and the physical motion χ , a physical velocity v is introduced as material derivative which is the time derivative at constant material coordinate z of the physical motion.

$$\frac{d}{dt} \chi(z,t) \Big|_z = \nu(\chi(z,t), t) = \nu(y,t) \quad (2.11)$$

Consequently, a spatial velocity ν is also defined as time derivative at constant material coordinate x resulting in:

$$\frac{d}{dt} \xi(x,t) \Big|_x = \nu(\xi(x,t), t) = \nu(y,t) \quad (2.12)$$

A generalized form of Reynolds Transport Theorem for an arbitrary region $\Omega(t)$ can be derived for the ALE formulation:

$$\frac{d}{dt} \int_{\Omega(t)} \Phi dV = \int_{\Omega(t)} \frac{d\Phi}{dt} + \Phi(\nabla \cdot \nu) + \nabla \cdot [(\nu - v) \otimes \Phi] dV \quad (2.13)$$

It is noted that the single term of the left hand side in equation (2.9) is broken into three terms. Material derivative of quantity ϕ is converted in a combination of local time derivative, volume dilatation (shown by divergence of spatial velocity) and convective flow. The equation changes the sequence of time differentiation and volume integration and since the integration is over an arbitrary volume, the integrand has to be equal to zero. This generates another set of PDEs of equation, i.e.:

$$\frac{d\Phi}{dt} + \Phi(\nabla \cdot \nu) + \nabla \cdot [(\nu - v) \otimes \Phi] = -\nabla \cdot j_\Phi + \sigma_\Phi \quad (2.14)$$

In this equation, the term denoting volume dilatation is considered to be a source term, as a changing geometry results in a changing density Φ . The term $(\nu - \nu)$ denotes deviation of the physical velocity instead of the spatial velocity which depicts deformation of material configuration on the reference grid but not the spatial configuration.

2.6.4 Balance Laws Assumptions

Several assumptions are necessary to localize the balance laws: it is presumed that equation (2.14) holds for all possible volumes $V(X)$, i.e. not just the entire body but also all parts of the body; domains and subdomains included. Another necessary assumption is to assume that the integrand is smooth or continuous. These hypotheses hold for many materials but not all – for example, if the material contains a discontinuity, such as a crack, then the integrand is not smooth and localization of the balance law will not be successful. Thus it is plausible for the project to use a solid model of the left ventricle albeit in two dimensional and with much simplification as the order of the PDE equations entail for perfect and continuous geometrical structure. The necessity to create a flawless solid model for the analysis made consideration for a three dimensional model of the left ventricle a complication since there would be a lot more simplification and modification to the structure which is expected to consume unnecessary time expenditure. If these assumptions are followed in the text, then equation (2.14) has justified a local balance law which is in the form of the equation below:

$$\frac{d\Phi}{dt} + \nabla \cdot (\Phi \nu) + \nabla \cdot j_{\Phi} - \sigma_{\Phi} = 0 \quad (2.15)$$

2.6.5 Conservation of Mass

For the conservation of mass the quantity being conserved is mass (whereby ϕ is density). In the localization process, it has been assumed that mass is conserved everywhere locally – therefore supposedly mass cannot disappear in one place and re-appear someplace else. Because of this the equation of mass is often called the continuity equation. Substituting $\phi = \rho$ (density) and $j\phi = 0$ (because the boundary is a material boundary no mass can cross the boundary), and $\sigma\phi = 0$ (because it is assumed no mass is generated inside) into equation (2.15) generates the following continuity equation:

$$\frac{d\rho}{dt} + \nabla \cdot (\rho v) = 0 \quad (2.16)$$

$$\frac{D\rho}{Dt} + \rho \nabla \cdot v = 0 \quad (2.17)$$

Equation (2.16) is the Eulerian form of the continuity equation and equation (2.17) is the same equation written in terms of the material time derivative. The continuity of the Eulerian form shows that there is a continuous change in the density of the flux, which indicates this approach to be compatible to represent the continuous flow of the blood in the left ventricle.

Using the balance law, another continuity equation is derived:

$$\frac{D}{Dt} \int_{V(X)} \rho j dV = 0 \quad (2.18)$$

In equation (2.18) it is shown that the total amount of mass is fixed in time, and this amount is equal to the amount at some reference time:

$$\int_{V(X)} \rho j dV = \int_{V(X)} \rho_0 j_0 dV \quad (2.19)$$

Assuming that the total amount of mass is constant over any sub-volume, as with the arguments discussed for equation (2.9), a continuity equation for the Lagrangian framework is obtained as follows:

$$\rho_0(X) = \rho(X,t) j(X,t) \quad (2.20)$$

The continuity in the formulation denotes a continuous deformation of the material configuration which indicates the approach is suitable to track the movement of the deforming valve leaflets due to input pressure from the blood flow.

2.6.6 Conservation of momentum

The Newton's Second Law of motion has been implemented to conserve the momentum in the ALE model. Momentum can be defined as "mass in motion." A moving object such as the motion of the valve leaflets is considered to have momentum – it has its mass in motion (Cebeci and Bradshaw 1977). The amount of momentum which an object has is dependent upon two variables: how much mass is moving and how fast the mass is moving and these two are represented in the Newton's Second Law as mass and velocity. The relationship

between an object's mass m , its velocity v , and the applied force F is $F = mv$. Velocity and force are vectors and in this law the direction of the force vector is the same as the direction of the velocity vector. The force part of the Newton's law has two components; body forces and surface forces both denoted using the symbols g and τ . The term g is usually the gravity vector, and τ represents the contact forces which is a function of the unit normal to the surface.

2.6.7 Surface Traction and the Stress Tensor (Cauchy's stress tensor)

τ has units of force per unit area and it is a function of position, X . It is also a function of boundary dv . In Figure 2.7, there is a depiction of a traction vector, τ acting at a material point X_0 . It has been considered X_0 to be on the boundary of the body and the force the body experiences at the surface due to the pull on X_0 is called the traction vector. The governing theorem for the traction vector is as follows:

$$\tau = n \cdot t \tag{2.21}$$

Here, n indicates the normal direction in which the traction vector points. n in general also functions as the effect the external material has to orientate the surface since traction is a linear transformation of the unit surface normal.

2.7 Understanding the Finite Element Method

This section describes the Finite Element Method (FEM), and its approximations to handle a PDE problem which has a finite number of unknown parameters. In order to solve the problem for each geometry object, the FEM allows for discretization of the elements that makes up the object geometry into finite size partitions. The FEM incorporates the shape function to derive possible forms of the approximate solution.

2.7.1 The Mesh

The starting point for the finite element method is a mesh, a partition of the geometry into small units of a simple shape. In 1D the method partitions the subdomains into smaller mesh intervals. The endpoints of the mesh intervals are called mesh vertices. In 2D, the method partitions the subdomains into triangles, and these triangles are usually known as the mesh elements. Two-dimensional objects can have curved boundaries and so the triangular mesh elements are considered as an approximation in FEM. The sides of the triangles are called mesh edges, and their corners are called mesh vertices. A mesh edge must not contain mesh vertices in its interior. Similarly, the boundaries defined in the geometry are partitioned (approximately) into mesh edges (boundary elements) that must conform with the triangles if there is an adjacent subdomain. There might also be isolated points in the geometry and these are usually considered as the mesh vertices.

Similarly, in 3D, the method partitions subdomains into tetrahedrons (mesh elements), whose faces, edges and corners are called mesh faces, mesh edges, and mesh vertices, respectively. It partitions boundaries in the geometry into triangular boundary elements (mesh faces) and it partitions geometry edges into mesh edges. The isolated geometry

vertices in the object are partitioned and considered as mesh vertices, which is sometimes known as the node-points. The mesh vertices are usually only a subset of the node points. The term mesh element is usually used to describe any of the mesh elements; mesh faces, mesh edges, or mesh vertices. When considering a particular d-dimensional domain in the geometry (that is, a subdomain, boundary, edge, or vertex), then its mesh elements is the d-dimensional mesh elements contained in the domain.

2.7.2 The Finite Elements

After obtaining a mesh, approximations to the dependent variables is introduced. For the case of a single variable, u , the idea is to approximate u with a function that can be described with a finite number of parameters called degrees of freedom (DOF). Inserting this approximation into the weak form of the equation generates a system of equations for the degrees of freedom.

2.7.2.1 A simple example: linear elements in 1D

Assuming that a mesh consists of just two mesh intervals: $0 < x < 1$ and $1 < x < 2$, the linear elements means that on each mesh interval the continuous function u is linear. Thus, the only thing needed to know in order to characterize u uniquely is its values at the node points $x_1 = 0$, $x_2 = 1$, and $x_3 = 2$. Denoting these as $U_1 = u(0)$, $U_2 = u(1)$, $U_3 = u(2)$, the degrees of freedom can be written as follows:

$$u(x) = U_{1\varphi_1}(x) + U_{2\varphi_2}(x) + U_{3\varphi_3}(x) \quad (2.22)$$

where $\varphi_i(x)$ are in the form of piecewise linear functions. Namely, $\varphi_i(x)$ is the function that is linear on each mesh interval, which is equal to 1 at the i^{th} node point, and equal to 0 at the other node points. For example,

$$\varphi_1(x) = \begin{cases} 1-x \\ 0 \end{cases}$$

where

$$0 \leq x \leq 1 \text{ and } 1 \leq x \leq 2$$

The $\varphi_i(x)$ are called the basis functions. The set of functions $u(x)$ is a linear function space called the finite element space. For better accuracy, another finite element space corresponding to quadratic elements can be considered. Functions u in this space are second-order polynomials on each mesh interval. To characterize such a function, new node points are introduced at the midpoint of each mesh interval: $x_4 = 0.5$ and $x_5 = 1.5$. The corresponding degrees of freedom $U_i = u(x_i)$ is also introduced. Then, on each mesh interval, the second-degree polynomial $u(x)$ is determined by the degrees of freedom at the endpoints and the midpoint. This in return derives:

$$u(x) = U_{1\varphi_1}(x) + U_{2\varphi_2}(x) + U_{3\varphi_3}(x) + U_{4\varphi_4}(x) + U_{5\varphi_5}(x) \quad (2.23)$$

where the basis functions now have a different meaning. Consequently, the function that is quadratic on each mesh interval is equal to 1 at the i^{th} node point, and equal to 0 at the other node points as seen in the next example.

$$\varphi_1(x) = \begin{cases} (1-x)(1-2x) \\ 0 \end{cases}$$

where

$$0 \leq x \leq 1 \text{ and } 1 \leq x \leq 2$$

In general, specification of a finite element space in the FEM is set by applying a set of basis functions. In order to simplify the description of these basis functions, the introduction of local coordinates (or element coordinates) is useful. A mesh element of dimension d in an n -dimensional geometry (whose space coordinates are denoted as x_1, \dots, x_n) can be considered.

2.7.3 The Lagrange Element

The preceding examples are special cases of the Lagrange element. The Lagrange element is usually considered with an *order*, a positive integer usually depicted using the symbol k . The function u in the finite element space are normally the piecewise polynomials of degree k . This indicates that, on each mesh element, u is a polynomial of degree k . In order to describe such function it is suffice to give its values in the Lagrange points of order k . These are the points whose local (element) coordinates are integer multiples of $1/k$. For example, for a triangular mesh in 2D with $k = 2$, this means that there are node points at the corners and side midpoints of all mesh triangles. For each of these node points p_i , there exists a degree of freedom $U_i = u(p_i)$ and a basis function φ_i . The restriction of the basis function φ_i to a mesh element is a polynomial of degree (at most) k in the local coordinates such that $\varphi_i = 1$ at node i , and $\varphi_i = 0$ at all other nodes. Thus the basis functions are continuous and the following constraint is derived:

$$u = \sum_i U_i \varphi_i \quad (2.24)$$

The Lagrange element of order 1 is often called the linear element. The Lagrange element of order 2 is known as the quadratic element and all Lagrange elements are available with all types of mesh elements.

2.7.4 Curved Mesh Element

Using higher-order elements (that is, elements of an order > 1), is a good option since the solution has smaller error. However, the error also depends on how well the mesh approximates to the true boundary. In order to keep errors in the finite element approximation and the boundary approximation at the same level, it is wise to use curved mesh elements. Curve mesh elements are distorted simplexes that can be used to approximate a boundary better than ordinary straight mesh elements (if the problem's boundary is curved). Mesh element is usually considered as the image of a standard simplex. For mesh elements that do not touch the boundary, they are straight and so there is no reason to make them curved. It is often better to use the same order k here as for the order of the (Lagrange) element. This is referred to as using isoparametric elements. The use of isoparametric elements means that u is not a polynomial in the global coordinates (if $k > 1$), but they exist only in the local coordinates.

2.7.5 Weak Constraints

The boundary conditions in any fluid simulation are expressed either in terms of the fluid velocity at the boundary or the velocity gradient at the boundary. These are called Dirichlet and Neumann boundary conditions. A method for imposing a Dirichlet boundary condition for a fixed boundary in the FEM is by using the weak constraints. Weak constraints are representation of an alternative way to discretize *Dirichlet* conditions as opposed to the pointwise constraints described earlier. The idea is to regard the Lagrange multipliers $\mu(d)$ as field variables and thus approximate them with finite elements. This concept also introduces corresponding test functions $v(d)$. Multiplying the Dirichlet conditions with these tests functions and integrating them together can be useful to solve the case of a stationary problem in 2D:

$$\begin{aligned}
 0 &= \int_{\Omega} W^{(2)} dA + \int_B W^{(1)} ds + \sum_P W^{(0)} \\
 &- \int_{\Omega} v \cdot h^{(2)T} \mu^{(2)} dA - \int_B v \cdot h^{(1)T} \mu^{(1)} ds - \sum_P v \cdot h^{(0)T} \mu^{(0)} \\
 0 &= \int_{\Omega} v^{(2)} \cdot R^{(2)} dA \\
 0 &= \int_B v^{(1)} \cdot R^{(1)} ds \\
 0 &= \sum_P v^{(0)} \cdot R^{(0)}
 \end{aligned} \tag{2.25}$$

Sometimes the constraints can be modified to involve derivatives from dependent variables and with this, the Lagrange multiplier term can be improved with terms accounting for the dependence. These weak equations can be added to form a single equation. This treatment of the Lagrange multipliers as ordinary variables has thus produced a weak equation

without constraints. This can be useful if the Lagrange multipliers are of interest in their own right. It also makes it possible to modify the coupling term involving the Lagrange multiplier. The formulas just presented implement ideal constraints. In some situations, non-ideal constraints are useful, in particular, when the constraint involves non-tangential derivatives on the boundary. On the boundary, replaced the above Lagrange multiplier term by

$$-\int_B v \cdot \mu^{(1)} ds$$

Using non-tangential derivatives in the constraint yields a better discretization because the Lagrange multiplier term (the constraint force) applies only on the actual boundary and not on the elements adjacent to the boundary. Both the non-ideal constraint and the ideal constraint variant of weak constraints are available when weak constraints are applied. Combining pointwise and weak constraints is beneficial if there are both types of constraints for some variable but if the constraints are in adjacent domains, the resulting discretization does not work. The pointwise constraints can be obtained from the (ideal) weak constraints formulation by using the basis functions:

$$\delta(x - x_{mj}^{(d)})$$

for the Lagrange multipliers and their test functions, that is, let

$$\mu^{(d)} = \sum_{m,j} \Lambda_{mj}^{(d)} \delta(x - x_{mj}^{(d)}) \tag{2.26}$$

where δ is Dirac's delta function.

2.8 The Software FEMLAB

FEMLAB is the engineering tool, first released in 1999, that performs equation-based multiphysics modeling in an interactive environment based on partial differential equations (PDEs).

2.8.1 Advantages of the Software Package

Solving PDEs is a challenge which requires time in order to set up the underlying equations, material properties, and boundary conditions for a given problem. The FEMLAB package provides a number of application modes that consist of predefined templates and user interfaces with equations and variables for specific areas of physics. Special properties allow the selection of, for instance, analysis type and model formulations. The application mode interfaces consist of customized dialog boxes for the physics in subdomains and on boundaries, edges, and points along with predefined PDEs. A set of application-dependent variables makes it easy to visualize and postprocess the important physical quantities using conventional terminology and notation.

2.8.2 Predefined Boundary Conditions in FEMLAB

FEMLAB offers predefined boundary conditions in the modeling. There are used regularly in the fluid dynamics problem and has been noted with high interest in the research being carried out. In the project direct use of these boundary conditions for two-dimensional problem have been applied in modeling the boundary of the ventricle wall, the valve leaflets, and also the inflow and outflow of the blood through the system.

2.8.2.1 Inflow / Outflow Velocity

At an inflow or outflow boundary the fluid's velocity field is specified as

$$\mathbf{u} = (u, v, w) = (u_0, v_0, w_0)$$

in 3D; in the 2D case, the last component is dropped.

2.8.2.2 Outflow or Pressure

Using the total stress tensor form, this boundary condition states that the total force on the boundary is a pressure force defined by p_0 :

$$\mathbf{T} = -p_0 \mathbf{n}$$

Using the viscous stress tensor form, the pressure is set to p_0 , and the viscous force is zero:

$$p_0 = 0$$

$$\mathbf{K} = \mathbf{0}$$

This means that the implementation of the outflow condition for the total stress tensor form uses a Neumann boundary condition, which provides a better-posed problem than the Dirichlet boundary condition in the viscous stress tensor form. The latter boundary condition can still be useful, for example, if coupling of pressure to pressure field defined by another application mode is in an adjacent subdomain. An alternative is to model the Dirichlet boundary condition for the pressure with direct implementation in the equation system by editing the boundary coefficients using the total stress tensor form.

2.8.2.3 Slip or Symmetry

A slip condition means that the normal component of the velocity is zero

$$\mathbf{n} \cdot \mathbf{u} = 0$$

and that the tangential component of the viscous force vanishes

$$\mathbf{t} \cdot \mathbf{K} = 0$$

in 2D, and

$$\mathbf{t}_1 \cdot \mathbf{K} = 0$$

$$\mathbf{t}_2 \cdot \mathbf{K} = 0$$

in 3D. This condition is equivalent to a symmetry boundary condition.

2.8.2.4 No Slip

A no-slip condition means that the fluid's velocity equals that of the boundary, usually zero. This condition is normally use for static walls.

$$\mathbf{u} = \mathbf{0}$$

2.8.2.5 Normal Flow or Pressure

At a straight-out outflow boundary using the total stress tensor form, the normal component of the total force on the boundary is a pressure force defined by p_0 . Also, the tangential components of the velocity are zero. In 2D, this becomes:

$$\begin{aligned} \mathbf{t} \cdot \mathbf{u} &= 0 \\ \mathbf{n} \cdot \mathbf{T} &= -p_0 \end{aligned}$$

In 3D, the boundary condition is:

$$\begin{aligned} \mathbf{t}_1 \cdot \mathbf{u} &= 0 \\ \mathbf{t}_2 \cdot \mathbf{u} &= 0 \\ \mathbf{n} \cdot \mathbf{T} &= -p_0 \end{aligned}$$

Using the viscous stress tensor form, the pressure is set to p_0 , and the tangential components of the velocity are zero. Also, the normal component of the viscous force is zero. In 2D this condition reads:

$$\begin{aligned} \mathbf{t} \cdot \mathbf{u} &= 0 \\ p &= 0 \\ \mathbf{n} \cdot \mathbf{K} &= 0 \end{aligned}$$

2.8.2.6 Neutral

FEMLAB treats a neutral boundary as if there were no boundary, which means that the total or viscous force vanishes. For the total stress formulation, this means that

$$\mathbf{T} = 0$$

For the viscous stress formulation,

$$\mathbf{K} = 0$$

2.9 Conclusion

The literature survey is an essential aid in understanding the many contributing areas for the research undertaken and knowledge from these domain expertises is included in the modeling and visualization in the project research. This chapter has focused on the techniques of the Arbitrary Lagrangian-Eulerian approach and its mesh movement mechanism as these are the main methods featured in the theses. An overview of the heart anatomy has been thoroughly discussed with the inclusion of the cardiac mechanics particularly on the left part of the heart. The methods analyzing the flow properties of the heart or the hemodynamics have been briefly revised. Although blood is extremely complex to be described in full detail, the basic principles presented are useful to capture the essential properties of blood flow.

Chapter 3

Methodology

**I hear and I forget.
I see and I remember.
I do and I understand.**

Confucius

3.1 Overview

The heart is considered as non-manufactured products or as an organic object. Recreation of the 3D shape of the heart is necessary to help with the understanding of its fundamental morphology, general and ultra structure of anatomy and to know its geometric configuration. A feasible approach to digitize the heart is by using the reverse engineering method. From raw heart data to digitized and reconstructed heart surface, the model is only then ready to be transferred to the finite element platform for the ALE analysis and modeling. The reconstructed heart provides the geometry that is the shape of the heart. In creating a model, the dynamic that is the physics have to be explored and incorporated virtually into the computer.

3.2 Geometrical Modeling

The main objective of this project is to simulate the blood flow pattern in the left ventricle of the heart, which requires extensive ALE modeling on the simplified 2D ventricle's boundary. The model is supposed to show the simplified inner structure of the left ventricle with the right geometrical allocation of its chamber's sub-domains and valves. In consideration of this, the data acquired should be able to give forth as much information of the organ aforementioned; with results that is applicable to use in later software environment for the ALE modeling. Regions of interest that is paid particular attention during the data acquisition are the chambers outer and inner structures and the valves.

3.3 Acquisition of the Heart Data

A simplified surface model of the heart is needed for the purpose of preparation and acceptance of analysis in a finite element environment. Using the reverse engineering approach, raw data that represents the heart and essentially the left ventricle (LV) has been captured and used to recreate a sensible geometrical model that allows for visual penetration of its complex structure. Among expectations of the outcome from this session are for the model to encompass parameters that contributes to proper measurements of the fundamental aspect of the left ventricle such as the general structure of its walls in axial direction, diameter and shape of the ventricle valves (the mitral and the aortic), and the radius angle of those working valves that positions them at such in the chamber. The generated model is to be tuned in a format that will be recognized in finite element setting for the 2D ALE modeling.

3.3.1 Reverse Engineering Processes

The process of duplicating an existing component, subassembly, or product, without the aid of drawings, documentation, or computer model is known as reverse engineering. Reverse engineering can be viewed as the process of analyzing a system to identify the system's components and their interrelationships, create representations of the system in another form or a higher level of abstraction and to create the physical representation of that system. Reverse engineering enables the duplication of an existing part by capturing the component's physical dimensions, features, and material properties. Reverse engineering of mechanical parts involves acquiring three-dimensional position data in the point cloud using laser scanners or computed tomography (CT). Representing geometry of the part in terms of surface points is the first step in creating parametric surface patches.

A good polymesh is created from the point cloud using reverse engineering software. The cleaned-up polymesh, NURBS (Non-uniform rational B-spline) curves, or NURBS surfaces are exported to CAD packages for further refinement, analysis, and generation of cutter tool paths for CAM. Finally, the CAM produces the physical part. It can be said that reverse engineering begins with the product and works through the design process in the opposite direction to arrive at a product definition statement (PDS). In doing so, it uncovers as much information as possible about the design ideas that were used to produce a particular product.

In this session, reconstruction of the inner left ventricle's surface data for the ALE modeling in finite element software is described in graphical detail. This process has been identified with several major steps. Beginning with generation of point cloud data using a laser scanner, the scanned data is optimized to ensure the quality of the collected points by sampling and gap filling and finally ending with the creation of a surface wrap of the model.

3.3.1.1 Generation of Points Cloud data

An external scanner, GOM ATOS II was utilized to allow for generation of point data by hand-scanning the physical heart. The white-light scanning device, sometimes called a 3D scanner, collected the "raw" (x,y,z) point data on the left ventricle and directly mapped the points into Software Version 5, a platform that employs point data manipulation. The points are then stored as ASCII text files in the order they were entered, relative to the local coordinate system. During the digitizing process, the white light signal transmitted keeps track of the distance between the coordinate points. The generated sequences of points were

organized in a fairly random form, called point clouds of data. The distance was initially set to 0.01 inches but it was later reset to 1.0mm, adjustment made so as to accommodate the varied attention on simpler to more complex structure of the left ventricle. Further discussion on the topic is prepared in Section 2.9.7 of the literature review. The single arrow markings in both Figure 3.1 and Figure 3.2 indicate the similar location of the mitral valve in both outer and inner left ventricle, where the inner structure is a sub domain of the outer.



Figure 3.1: Generations of points cloud data of the outer layer of the left

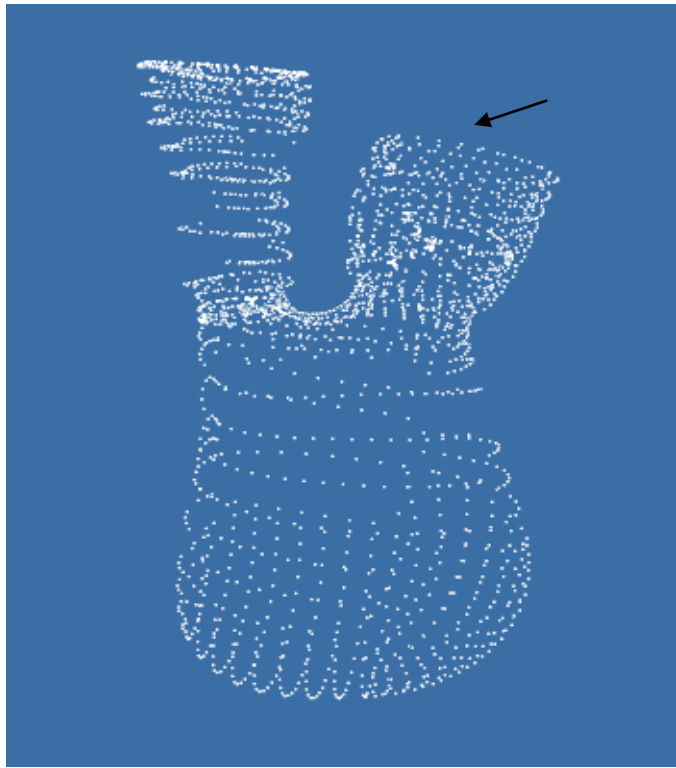


Figure 3.2: Generation of points cloud data of the inner layer of the left

To accurately scan all its sides, the organ is realigned each time it is moved. Three alignments points have been used as reference points so that the physical organ can be repositioned easily during the digitizing process. This is to be done when there are regions of the heart that could not be reached from the original position and when greater detail is needed in a particular region. The next figure presents more view of the outer side of the left ventricle that has been captured.

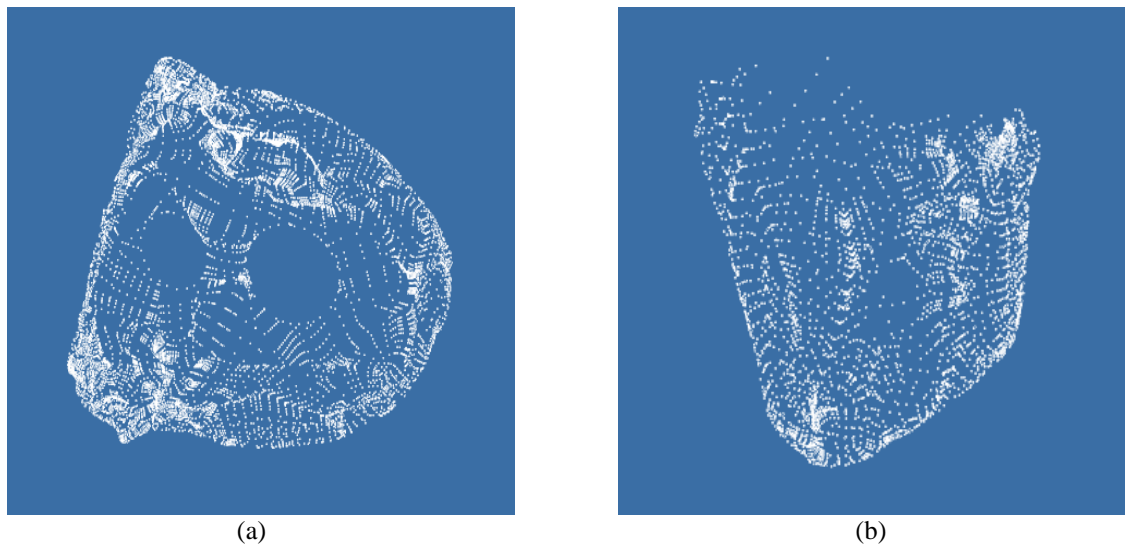


Figure 3.3: More views on the outer side of the left ventricle. (a) Top half of the outer left ventricle and (b) bottom half of the outer left ventricle

In Figure 3.3(a), the top half of the outer left ventricle is shown with two rings depicting the location of the aortic valve (left) and the mitral valve (right). Note that the aortic ring is much smaller than the mitral's, suggesting the valves to be of different diameter size and perhaps structure. In Figure 3.3(b), the bottom half of the outer left ventricle can be seen.

Among regions of the structure that are given considerable attention during this digitizing session are the valves themselves. The two working valves have been scanned separately from the ventricle's chamber body in order to gain better view of their geometrical structures. They are aligned and scanned thoroughly using the same method as scanning the left ventricle illustrating the points cloud obtained on the front view of the aortic cylinder, the front view of the mitral cylinder, the top view of the aortic semilunar and the top view of the mitral bicuspid. Results from the scan are shown next.

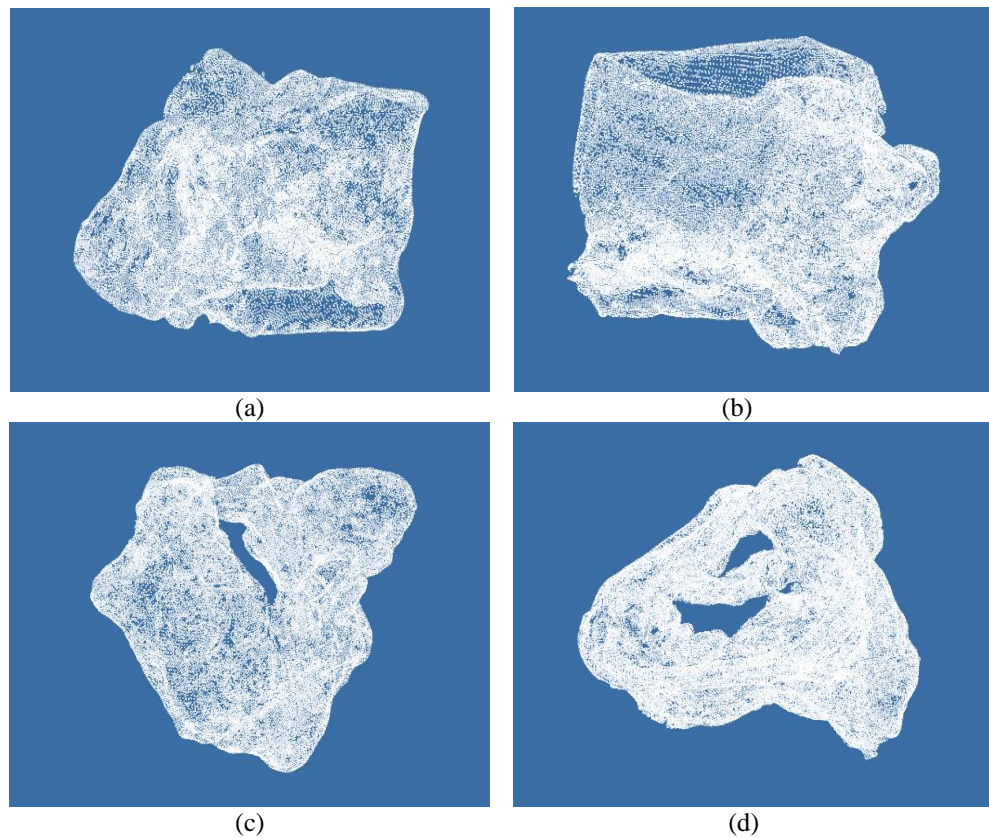


Figure 3.4: Generation of point clouds data on the left ventricle valves. (a) the aortic cylinder, (b) the mitral cylinder, (c) aortic semilunar valve and (d) mitral bicuspid valve.

Both valves, the aortic and the mitral, are noted to have been different in terms of structural representation, having the opening of the aortic valve to be semi lunar in shape, and the mitral valve consisting two segmented regions of unequal size. Again the difference here is considered to directly affect their functional aspect particularly to accommodate the blood inflow from the left auricle into the ventricle’s chamber and the blood outflow from the ventricle through the aortic valve. Since the recreation is targeted on just the basic shape of the inner left ventricle for use in a fast-moving, dynamic simulation, the accuracy of the scanning is not critical and the data size sampled was kept to be minimal. A summary of the number of points collected from the digitizing process are as depicted in Table 3.1 below.

Table 3-1: Number of points sampled for each structure scanned.

Geometrical Structure	Points Cloud Collected
Outer Left Ventricle (full)	260705
Top half of the Left Ventricle	12853
Bottom half of the Left Ventricle	4706
The Aortic Valve	87610
The Mitral Valve	59886
The Inner Left Ventricle	3375

3.3.1.2 Optimizing Scan Data

Optimization of the scanned data has been proposed to eliminate data that is not sufficiently captured. One of the problems encountered during the scanning process was to get the scanning beam to squarely face the heart at all times. The organic heart comprises of mostly rounded and free-form features so the resulting scans are at times prone to having overlapping data of scanned regions. Preservation of best data was adequately maintained by eliminating data parallel to the scan beam.

Scanning is also considered to be a ‘noisy’ operation and at times a certain amount of error is introduced to the scanned data. This is due to factors such as small vibrations in the scanning device, low accuracy of scanner calibration, or inadequate preparation of the physical object’s surface. The noise is identified by rough, uneven appearance on the surface model. Two errors have been mainly discovered to occur during the process: Gaussian noise and salt and pepper noise. The latter one occurs mostly at the valve edges, where the laser beam of the scanner hits two surfaces, resulting in a mean and erroneous data value. Noise reduction is carried out to reduce the noise with respect to the heart’s surface curvature. At a minimum reduction it is observed that noise in the curvature regions of the valve is higher as compared to reduction of noise at other smoothness, resulting in clearer depiction of the valve edges at medium and maximum reduction. It has also been

noted that high noise reduction has lead to large lost of data in the flatter regions suggesting that highest reduction is not necessarily convenient in order to maintain the quality of the data.

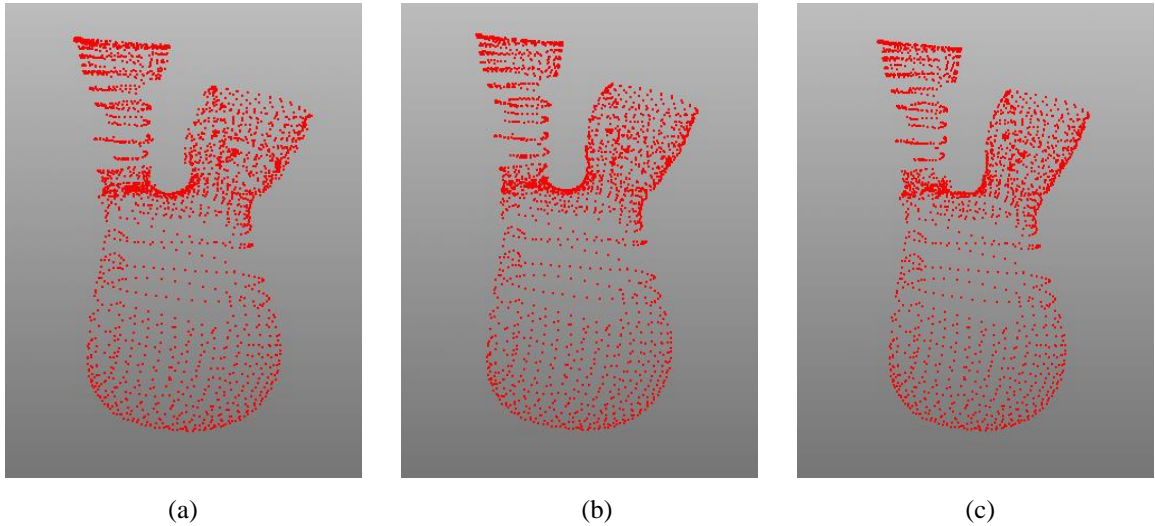


Figure 3.5: Results of noise reduction on the heart's surface curvature at (a) minimum noise reduction, (b) medium noise reduction and (c) maximum noise reduction

3.3.1.3 Sampling

A smaller set of points is often easier to work with. To sample points is to choose a smaller set of point representative of the original scan data. Two methods proposed for point sampling are the curvature and the uniform sampling. Uniform sampling, uniformly lessens the number of points in a point set. Subdivision of the model space into equally sized cubical cells deletes all but one from each cell. It is still however maintains the accurate representation of the point cloud model.

The model recreated is expected to have a clear delineation of its wall edges and sub domains for later boundary modeling. In consideration of this, sampling of the heart's curves is also considered a necessity. Curvature sampling samples points based on the

model surface curvature so as to produce an accurate wrap model with fewer points; points that lie in a high curvature region remain in order to maintain the accuracy of the surface curves, and points in flat regions requiring less detail have a large number of points that is deleted. Having points in a point set reduced, has practically lessened the storage space used, leading to an increase in the processing speed. Figure 3.6 portrays the curvature sampling at (a) 30, (b) 65 and (c) 100 sample percentage, showing that points on curved areas are more prominent after sampling is done.

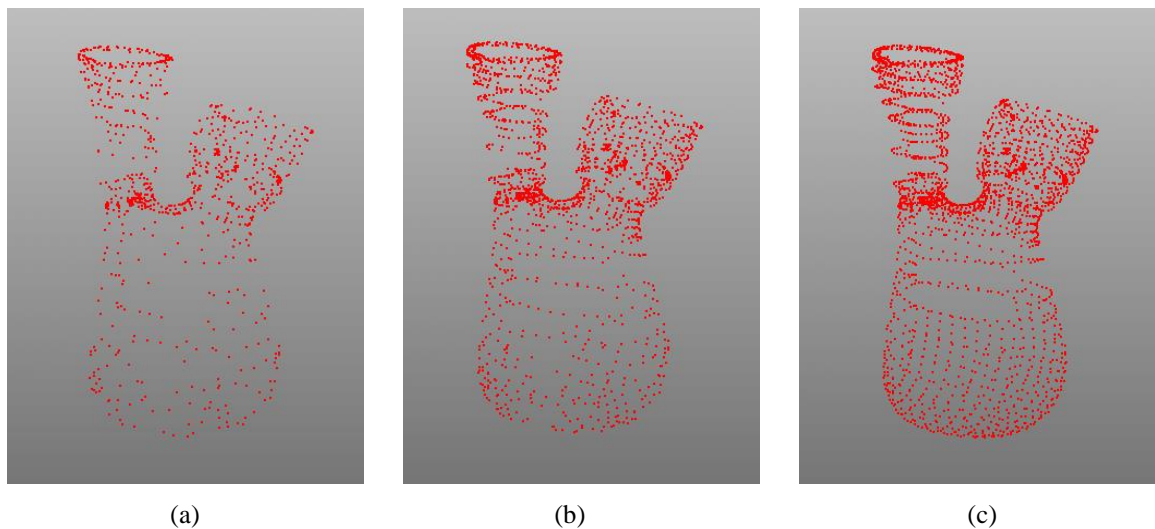


Figure 3.6: Results from curvature sampling on the surface model at (a) 30% curvature sample, (b) 65% curvature sample and (c) 100% curvature sample

3.3.1.4 Surface Wrapping

The wrap operation is done to construct a polygonal surface as seen in Figure 3.7. The process of surface wrapping takes the inner left ventricle model after curvature sampling, joins disconnected surfaces, and removes interior and overlapping surfaces. The main benefit of this process is that it drastically reduces time spent on surface preparation. The curvature samples obtained have been organized in accordance to three groups of points

distance measurements, 10mm, 5mm and 2mm. All samples were plot in xyz global coordinate.

At 10mm point distance, Figure 3.7(a), the model is seen with rough plotting that outlines the model's edges but lacking the data to wrap the surface. At 5mm point distance, Figure 3.7(b), the chamber's body has enough points data for generation of a surface wrap, but the valves is left with considerable holes after wrapping. At 2mm point distance, Figure 3.7(c), the points in the model are tightly connected to each other, with regions of the valves well covered and model has better chance to have a better quality surface wrap.

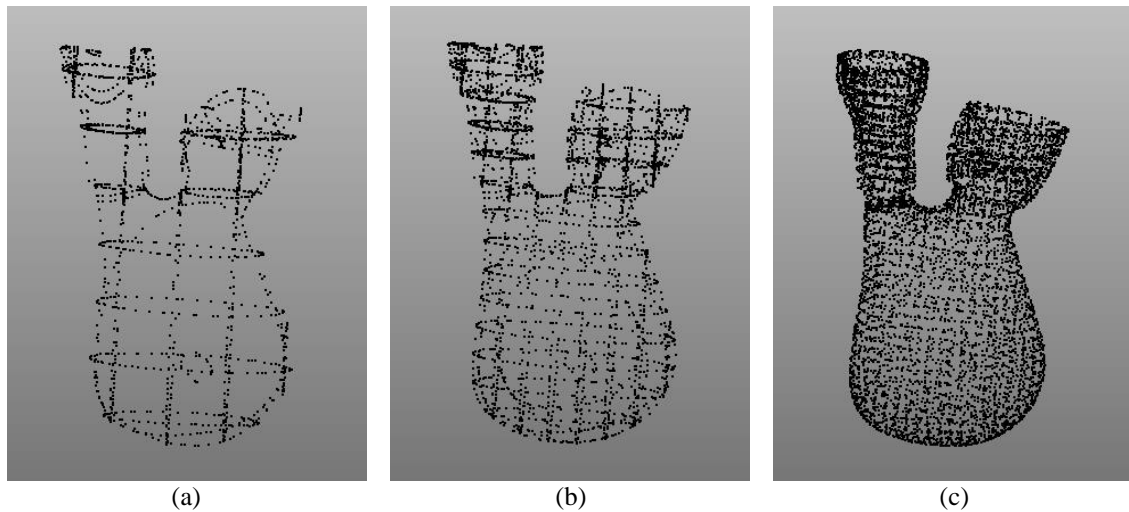


Figure 3.7: Results from polygonal surface reconstruction at (a) 10mm point distance, (b) 5mm point distance and (c) 2mm point distance

These point distance samples are then wrapped for surface creation. Figure 3.7(a) shows wrap surface at 10mm point distance resulting in poor surface wrapping of the model. Figure 3.7(b) shows wrapping at 5mm point distance, the chamber's body surface is seen in a better shape but the regions of the valves have a number of holes that needs a lot of patching and repair. Figure 3.7(c) shows wrapping at 2mm point distance, well determined

point sampling has lead to better preparation for a surface wrap of the inner left ventricle model.

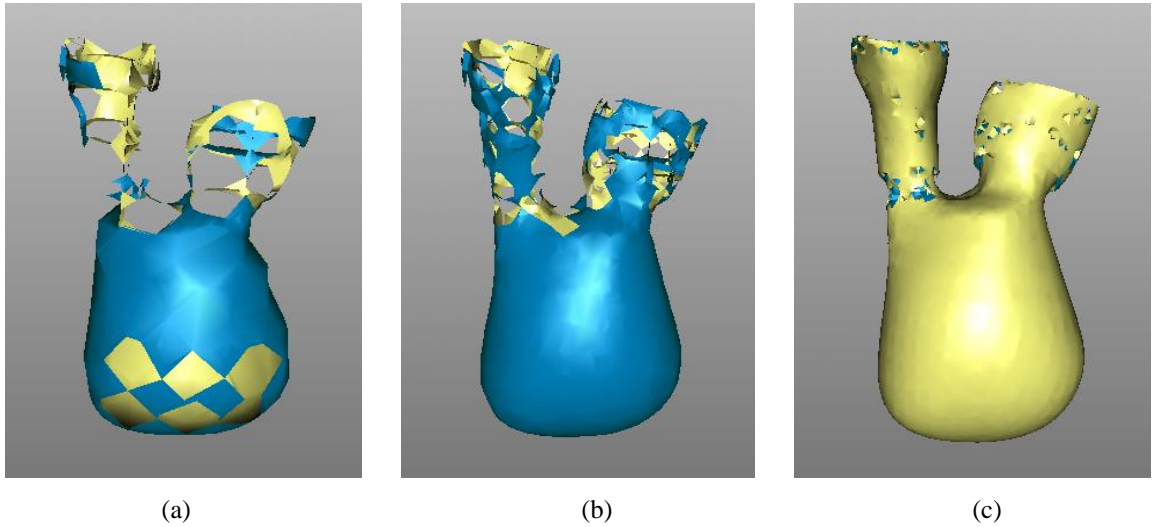


Figure 3.8: Results from surface wrapping on the left ventricle data. (a) Surface wrapping at 10mm point distance, (b) surface wrapping at 5mm point distance and (c) surface wrapping at 2mm point distance

3.3.1.5 Filling up the holes

Regions with missing data in the model are filled to close the gaps that may have been introduced during the scanning process. When the scan data is wrapped, these holes or gaps can appear in the surface of the model. The operation constructs a polygonal structure to fill the hole, and both the hole and the surrounding region are remeshed so the polygonal layout is organized and continuous. Some of the holes were filled up manually by marking the beginning and ending vertices of the hole. Some segments of the hole or boundary edge were filled partially, to clean up the boundary edge of an open surface, where there's no need for a complete closure of the particular surface. After holes are filled up, the number of points decreases whereas the number of triangles in the model has increased. A curvature based filling has been opted to ensure the polygonal structure used to fill holes in

high-curvature regions and is curved to match the surrounding area. For regions with flatter polygonal surface, flat filling is used which is more suitable for planar regions.

Figure 3.9(a) shows the left ventricle surface wrapped polygonal model. The valves are highlighted in yellow, and the ventricle's chamber in blue. The model's top view, Figure 3.9(b), provided an insight to the structure of the valves opening, located both at the cylindrical base. The semi lunar aortic and the bicuspid of the mitral's can clearly be seen in the wrapped surface model.

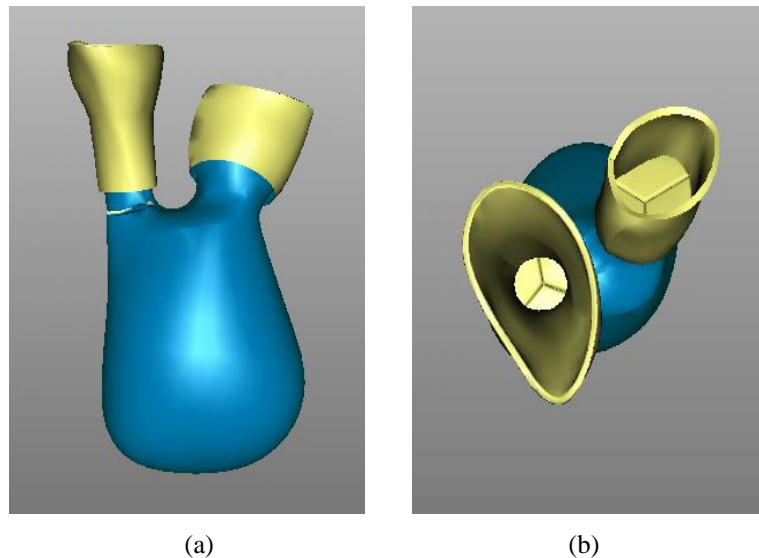


Figure 3.9: The left ventricle surface model. (a) model front view and (b) model top view

The resulting 3D surface model reconstructed from these tasks is used in the creation of a 2D solid model of the heart. It is a heavy requirement for the ALE modeling especially in a finite element environment. A simple 3D rendition of the model is available for display purposes (Refer to Appendix A).

3.3.2 Data Measurements

The surface model of the left ventricle has further been analyzed to get the measurements on some of the important boundaries. The ALE modeling requires an approximation of the diameters of certain section of the left ventricle. The aortic and mitral's are among those that were paid close inspection. Using these spatial information solid modeling for the ALE analysis can be carried out. The software measures regional shape of the left ventricle in terms of radial distance from a long axis (center axis) constructed from the centroid in between both the aortic and the mitral annulus to the most distant point on the left ventricle. Regional shape is analyzed as radial distance to the ventricular surface from the center axis. For orientation the centroid of the aorta at the level of the aortic valve is placed at 90 degrees. The left ventricle is then divided into several segments. Regional shape in each segment is calculated as the mean radial distance of the points lying within that segment to the center axis.

Figure 3.10(a) denotes the wrap surface of the inner left ventricle model with arrow markings indicating regions of interest that are to be considered for diameter and length measurements. Figure 3.10(b) shows the location for calculation of the crease angle between the aortic and the mitral valves. It has been discovered that the cylindrical part of the two valves are in a certain mode of angular attachment towards each other contributing to the manner in which the ejection fraction of the blood from the mitral's inflow and out to the aortic occurs. The crease angle computed shows a slanting of about 27.87 degree separation of the two working valves.

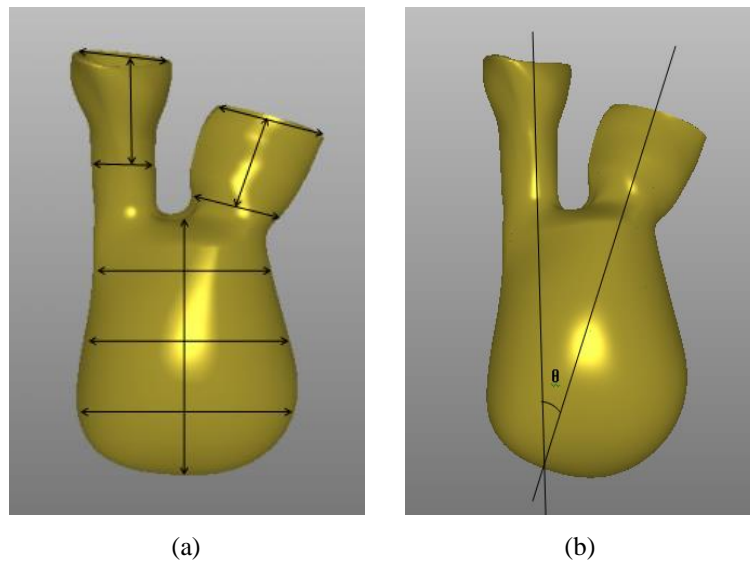


Figure 3.10: Regions of interest considered for the left ventricle measurements. (a) length and diameter measurements and (b) the crease angle calculation

Measurement is done using CAD software, which computes the distance between two manually defined points, singled out as labeling of [1] and [2] on the model. Color coded lines appear on the models with labels next to each line. The color corresponds to the axes in the model coordinates and provides an understanding of the distance on each of the axes. Highlighted in yellow is the distance with values of the axes calculated in millimeter. Note that the diameters obtained on the chamber's body are largest at the centre, with smaller width at the top and bottom of the body. It is a rather justified indication that a simplified version of the ventricle's body for the ALE solid boundary modeling should take the shape approximation of an oval. The detail measurements can be referred in Appendix B.

3.4 Solid Modeling

The preceding section discussed the reconstruction of the physical heart into a three dimensional surface model and during the process, important knowledge on the anatomy of interest has been gathered and thoroughly explained. The information then collected is now used for the creation of a two-dimensional (2D) solid geometrical model of the heart. This 2D solid geometry model has been identified as a strong requirement to cater to the many constraints a surface model has. A 3D surface model without doubt has enough attributes to give a good physical representation of the heart but it is not directly applicable to handle the complex mathematical and physical formulation of the ALE modeling especially in a finite element environment. The most important feature of an ALE model is the insertion of partial differential equations (PDE) on the model boundaries. In order to achieve this target, creation of domains, subdomains and boundaries; with extensive definition of their points and edges made 2D solid modeling of the geometrical heart an important consideration.

The 3D surface model would not be able to accommodate to these requirements and even if it could cater to the sort of meshing a finite element solver needs there is still a great need of a powerful computational supply to guarantee a complete calculation of the PDE equations in all three dimensions.

It has been a trade to simplify the properties of the solid geometry as complex geometrical representation would require a much harder effort to simulate since the main element to a simulation is the computation of the governing equations on the solid modeling. It would be wonderful to represent the left ventricle as a 3D model instead of 2D yet it is an unfortunate that the complex mathematical formulation needed in the calculation would delay the variables design resulting in a much longer computing hours and resources. The

coming subsections will first lay out the creation of the 2D solid modeling of the heart, and on with the ALE modeling, on the proposed finite element platform, FEMLAB.

3.4.1 2D Solid Modeling in FEMLAB

FEMLAB (Finite Element Method Laboratory) is a finite element platform which comprises tailored modeling solutions for several existing engineering domains; structural mechanics, chemical engineering and electromagnetics. The software facilitates modeling of all physical phenomena based on partial differential equations (PDEs), such as heat transfer, wave propagation and fluid flow. The model equations, or physics, are applicable in a ready-to-use form, or freely specified to suit any type of physical phenomenon such as linear, non-linear or time dependent analysis and simulations. Several problems can be combined and coupled in a single model, also called multiphysics, providing a very straightforward modeling process with a minimum of non-realistic assumptions.

3.4.2 Modeling of Curves and Solid Objects

The goal of this section is to describe the solid geometrical modeling in FEMLAB. The concepts of solid modeling and boundary modeling are to be explained. In FEMLAB two dimensional solid modeling and boundary modeling is the fundamental element for the creation of 2-D geometry objects. A hierarchical inheritance structure of the 2D geometry classes in FEMLAB is laid out as follows:

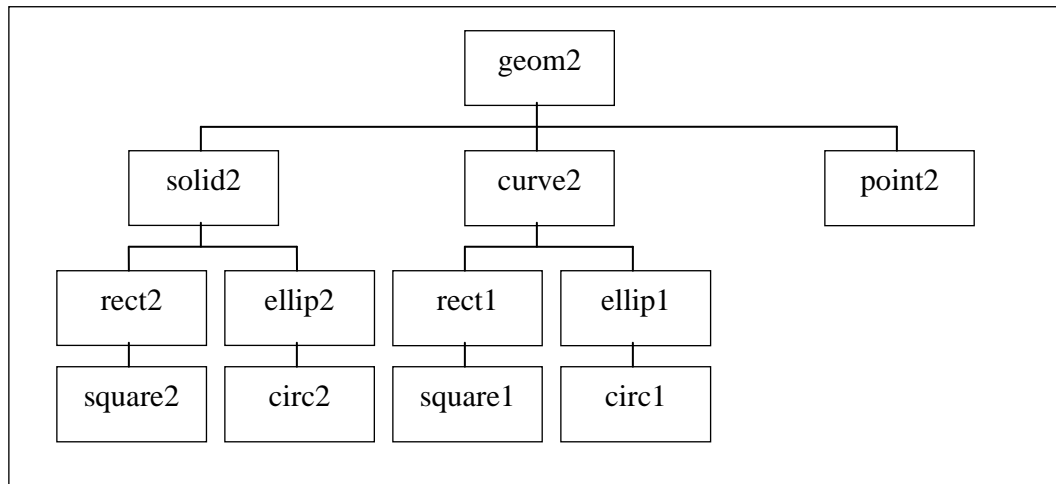


Figure 3.11: Hierarchical Inheritance Structure of the 2D Geometry Classes

In the hierarchical structure it can be seen that a 2D geometry object in FEMLAB contains object of the class geom2, solid2, curve2 or point2, all called as solid object, curve object, or point object respectively. Some of these objects on their own contain several other objects of a lower hierarchy; the solid has rect2, ellip2, square2 and circ2, and the curve object is represented by rect1, square1, ellip2 and circ1. The class geom2 is a super class of all 2D geometry classes. It is a hybrid object that combines the features of a solid object, curve object and point object. Recreation of the 2D left ventricle model in the project uses these features to handle both the boundary modeling and solid modeling required. Implementation of both modeling on the heart model is explained in the next subsections.

3.4.2.1 Curves / Boundary Modeling

Curves are considered as objects which represent the outline boundaries to solid objects. In the physical world the curves of an object are seen as lines with certain degree of proportionality; they could take the form of straight lines or arcs of circular or elliptical

attributes, and mathematically, they are read as production of a well constructed set of rational Bezier curves. A rational Bezier curve is a parameterized curve on the form

$$b(t) = \frac{\sum_{i=0}^P b_i W_i B_i^P(t)}{\sum_i W_i B_i^P(t)}, 0 \leq t \leq 1$$

where the functions

$$B_i^P(t) = \binom{P}{i} t^i (1-t)^{P-i}$$

are the Bernstein basis functions of degree n. $b_i = (x_i, y_i)$ are the controlling vertices, and w_i are the weights which should always be positive real numbers to get a properly defined rational Bezier curve. The maximum degree n of the curves is provided using a special function “fldegree”. A rational Bezier curve has a direction defined by increasing parameter t. This direction is used to uniquely determine subdomain number to the left and to the right of a curve.

The software package used to model the curves and solid objects utilizes a special draw mode that offers several ready-made functions of lines and arcs on a two dimensional grid axes as the platform. The spatial grid and axes has been used for the modeling with an equal x and y spacing, adjustment made to the settings so as to get the right view to model the geometry of interest. Using specified points as reference perimeter to denote the location of the start and end point of certain lines or arcs, lines are created using the line option and curves are modified using the 2nd and 3rd degree Bezier curves. The default names for the points are PT1, PT2, PT3, etc. and for the Bezier curves; B1, B2, B3, etc. and

these markings appeared on each of the created lines and arcs. Figure 3.12 shows some of the examples of the functions used in the early creation of the curves model. In Figure 3.12(a), B1 indicates a straight line in between two specified points, PT1 and PT2. In Figure 3.12(b), B2 is a boundary with a straight line from PT3 and PT5 and a 2nd degree Bezier arc pulled in the direction of another point, PT4. PT6, PT7, PT8 and PT9 in Figure 3.12(c) define the reference perimeters for the creation of the arcs and curves on B3. The aforementioned boundaries are highlighted in red for clarity.

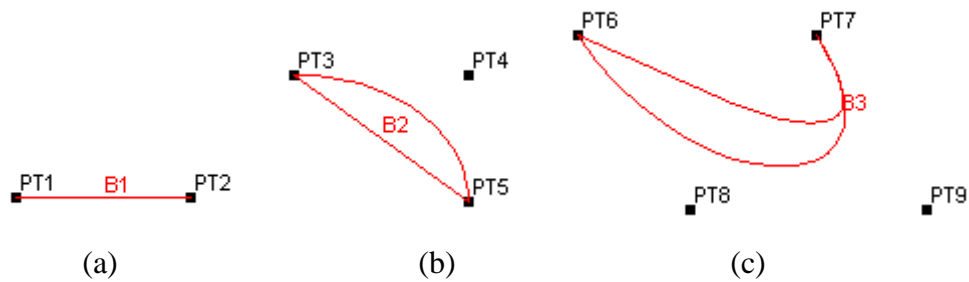


Figure 3.12: Example of functions used in the curves modeling.

These lines and arcs of curves went through further manipulation to get the right depiction for the geometrical representation of the left ventricle model. The surface model studied in the previous section has been compared to create a simplified version of the domain. Figure 3.13 shows the result of a comprehensive curve and boundary modeling of the two-dimensional replica of the left ventricle model. Stitching of the conjoining ends of the curves has been done to form several closed domains; B1 represents the boundary to the mitral cylinder, B2 is the boundary model to the ventricle's chamber body, and B3 represents the boundary to the aortic cylinder. In the figure, the two working valves of the left ventricle is described with boundary B4 and B5, both representing simplification modeling of the mitral and the aortic valves respectively. These isolated domains have been

constructed part by part using the information gathered on the geometry and careful comparison has been made with the corresponding domains identified in the surface model. The mitral valve on the right has been tilted according to the identified crease angle with the centroid of the aortic cylinder fixed at 90 degree for better orientation. These free boundaries have been assembled in such manner before they are coerced and laid on each other for the formation of solid objects. Explanation on the solid modeling of the left ventricle is carried out in Section 3.4.2.2.

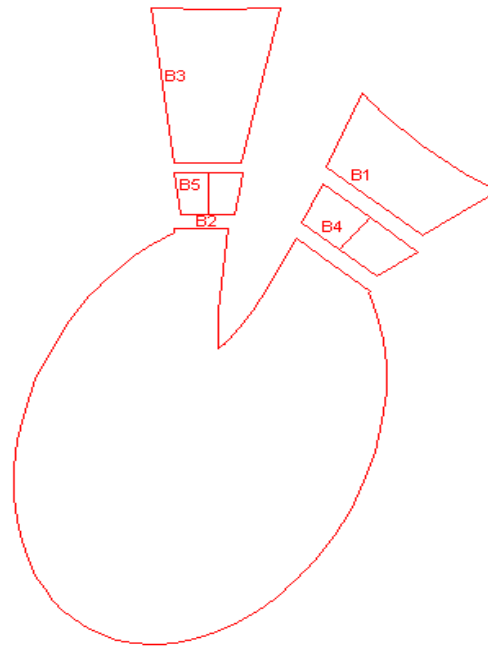


Figure 3.13: Boundary modeling of the left ventricle model with five different closed domains created separately.

Figure 3.14 provides an example of the modeling done to create the aortic cylindrical boundary, depicted as B3 in Figure 3.9. In Figure 3.14(a), a four-sided geometric shape (B1) created using the line functions and an elliptic curve (B2) has been used to roughly plot the boundary for the cylinder. The boundaries are split into several smaller regions; B3, B4, B5, B6, B7, B8, B9, B10 as seen in Figure 3.14(b). Three of the boundaries; B4,

B9, and B10 is deleted in Figure 3.14(c) resulting in the boundary model described in Figure 3.14(d). The geometry has been observed to have two curves; B7 and B8, protruding outside the cylinder body, which require further modifications to cut both boundaries into halves. In order to solve the problem, two additional lines have been added to part the excessive boundaries from the main region of the cylinder body as seen in Figure 3.14(e). Splitting of the elliptic curves and the new lines has introduced several new curves and lines sections; B5, B10, B11, B12, B13, B14, and B15, as seen in Figure 3.14(f). Leaving only the surrounding cylinder base that is described by B4, B8 and B9, and two of the elliptic curves; B13 and B14, all of the other unwanted boundaries have been deleted in Figure 3.14(g). The final product is depicted in Figure 3.14(h), a boundary model labeled as B3.

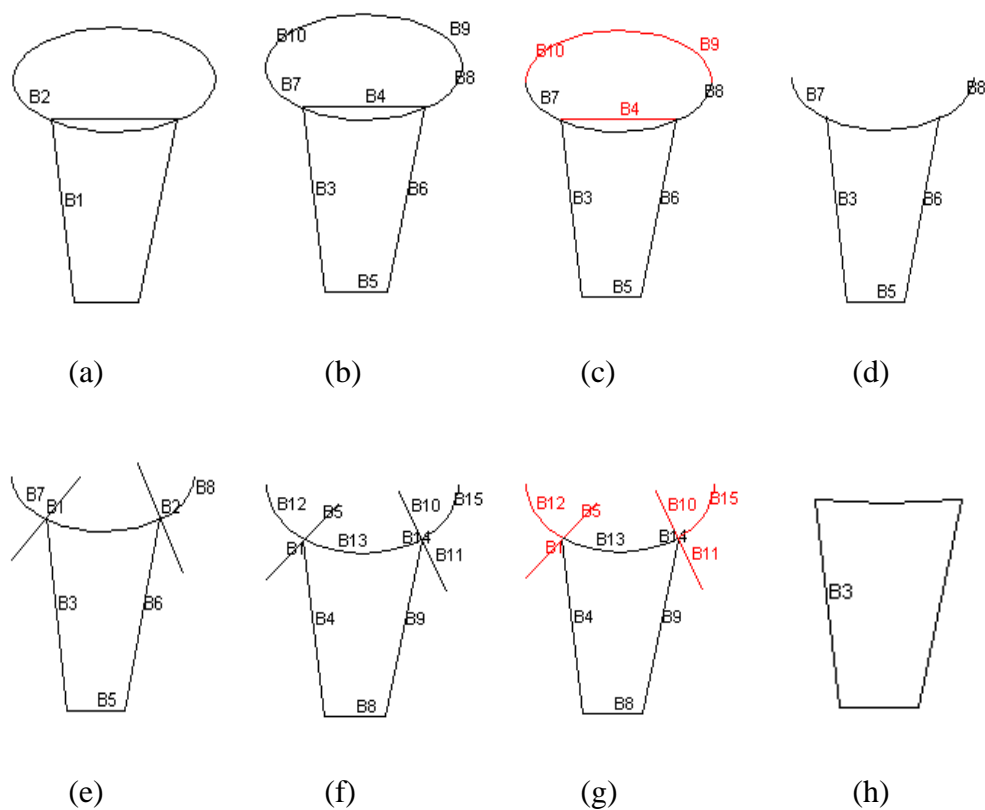


Figure 3.14: The curves modeling of the aortic cylinder

3.4.2.2 Solid Modeling

A solid object is allowed to have a boundary part and an interior part. It has been considered for the solid object created to consist of internal borders that separate internal subdomain as solid object always contain one or more subdomains. These subdomains are important to the ALE modeling as it is where specification of different material properties in different regions of a solid are made. Additional points and borders can be used to control the distribution of the mesh inside a solid object. This is useful for the post processing purposes. The boundary of a solid, including the borders, consist a number of edge segments. A solid is completely defined in terms of its boundary, and optimally its internal borders, and as such, it is said to have a boundary representation. For example, a primitive solid rectangle or a solid square has a boundary that consists of 4 line segments and one subdomain. A primitive solid circle or solid ellipse has a boundary that consists of 4 circular or elliptical arcs, and a single subdomain.

Formation of solid objects is done by using Boolean operations, a method that is considered suitable for rapid generation of complex geometries. Three major operations; union, intersection and difference are used on a set of primitive solid objects - square, rectangle, circle and ellipse. Objects that are formed as a combination of primitives are called composite solid objects. A composite object can have any number of boundary curves of different kind, e.g., lines or arcs. The actual number of boundary curves depends on how the composite solid was created. Composite solid objects have also been created using boundary modeling. The operators $+$, $*$, and $-$ are used to form the set of points for the resulting composite object. The operators; $+$, the set union operator, and $*$, the set intersection operator, have the same precedence. The operator $-$, the set difference operator,

has higher precedence. The precedence has been controlled by using parentheses. The resulting composite object is the set of points for which the set formula evaluates to true. By default, the set formula contains the union of all selected objects. Each geometry object is automatically given a unique name by the GUI. The default names of the circles are C1, C2, C3, etc; R1, R2, R3, etc., for rectangles; and E1, E2, E3, etc. for ellipses. Squares, although a square is just a special case of a rectangle, are named SQ1, SQ2, SQ3, etc. Composite objects are named CO1, CO2, CO3, etc. The name is displayed on the objects itself. Any names can be used as long as the object is not left blank. Alteration of the names and the geometrical properties of the objects can be done by editing them during the drawing.

In this section, formation of the solid modeling of the left ventricle from the boundary model is described. Coercing all curves object into solids has been done to each separated boundary B1, B2, B3, B4, and B5 individually. The function coerce to solid is a tool utilized to make sure the solid objects created are non-empty, since an object of the class curve consists only a boundary, which can either be open or closed. Figure 3.15(a) depicts the solid coercing done on the model's closed boundaries. All solid objects created are by default components of the class composite object, indication done using the symbol CO. In the figure, CO1 is the solid form of the boundary B1, CO2 represents the solid form of B2, CO3 the solid form of B3 and so forth. The solid models are then attached together using the union Boolean formulation resulting in the model described in Figure 3.15(b).

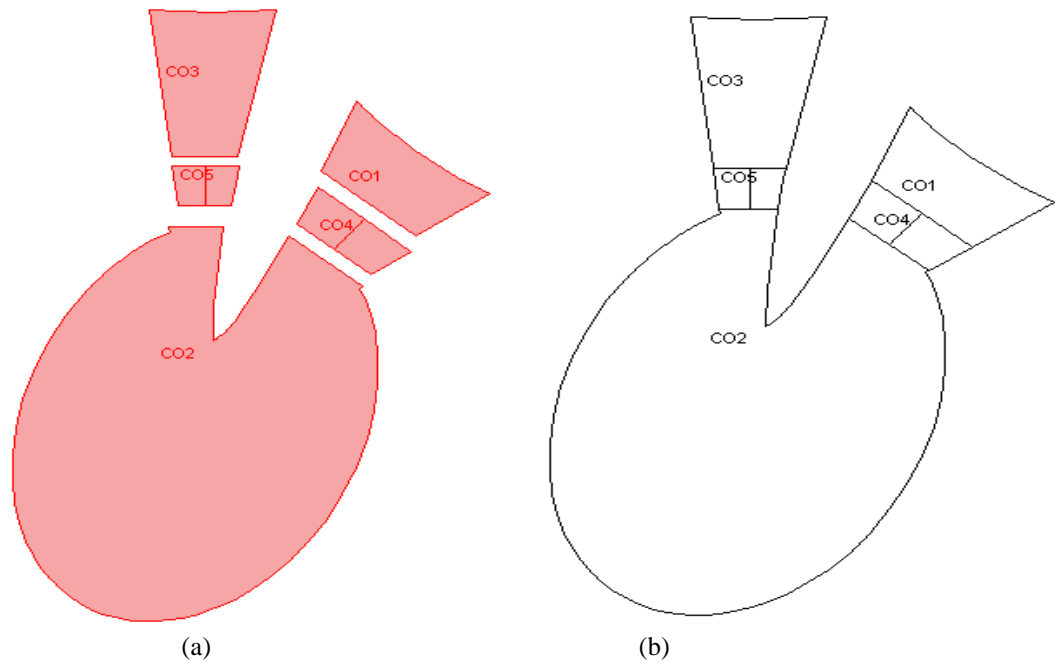


Figure 3.15: Solid Modeling of the Left Ventricle Model

Figure 3.16(a) shows the use of three rectangular objects; R1, R2, and R3 to create the model's prototype valves, with R2 and R3 tilted to several degrees according to the angle in which the sides of the valves stand. In Figure 3.16(b), the primitives have been patched and overlaid on top of each other using the function union to form a composite object, CO7 as seen in Figure 3.16(c). Splitting of the object using the function intersection and difference, as described in Figure 3.16(d) into singular divisions is important in order to distinguish the domains apart from each other for ease of manipulation. Unnecessary parts on the model are selected and are seen in red in Figure 3.16(e). These objects are dismissed by deleting them one by one resulting in the geometry in Figure 3.16(f). The lines inside the geometry are identified as interior boundaries and have been erased to form a simplified version of the left ventricle valves, represented as CO5 in the Figure 3.16(g).

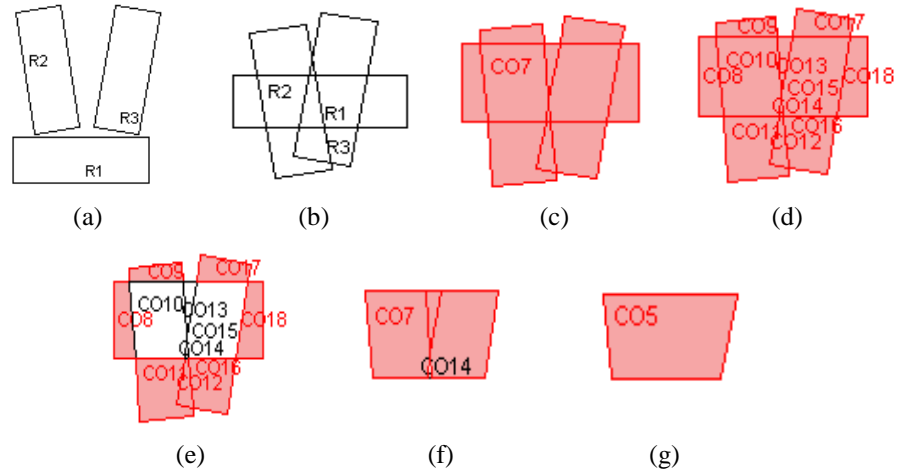


Figure 3.16: The solid modeling of the aortic valve

3.4.2.3 Subdomains and the Split Operation

When using the union operation, internal borders will partition the resulting solid into subdomains. These subdomains can be used to specify different material properties of the model. It is possible to split a solid with more than one subdomain into collection of minimal solids that consists of only one domain each. This operation has been used on the solid valve, seen to contain only singular domain in Figure 3.16(g), for the creation of the simplified valve leaflets. In a 2D representation of the left ventricle, it has been identified that the motion assumed to mimic the opening and closing of the valve's leaflets is a continuous linear horizontal movement of lefts and rights from the valve's boundary edges towards the centre of the valve's orifice and vice versa. In the design framework, the valve has been considered to have two subdomains, with each solid domain representing specific moving boundary conditions to cater to the periodic opening and closing of the leaflets. The illustration in Figure 3.17(a) indicates the conceptual design of the subdomains using boundary modeling. A vertical boundary line is used to split the valve into two subdomains,

with each subdomain defined by three boundary edges and the line splitting in the middle. B3, B4, B1 and B6 represent the first subdomain on the left and B3, B5, B2 and B7 represent the other on the right. Both boundary subdomains are coerced into solid models as seen in Figure 3.17(b). In the simulation, certain boundary calculation will force the specified material properties of the solid subdomains in a mode of horizontal movement; from boundary B1 right towards the center, B3, synchronously with the movement of boundary B2 to the left reaching the center B3, the motion indicating the closing of the valve. Periodically, another set of boundary calculation will reverse the movement of the solid properties from the centroid axis, B3, out to the right reaching the boundary B2, and to left towards the boundary B1, indicating the opening of the valve.

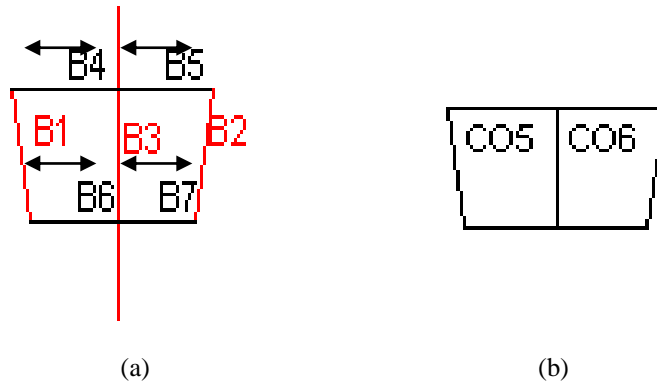


Figure 3.17: (a) Conceptual design of the subdomains using boundary modeling and (b) coercion of the boundary subdomains into solid

The simplification of the left ventricle using two – dimensional boundary and solid model created is considered ready for use as basic in the ALE modeling on FEMLAB. The approach in discussion is specifically and extensively laid out in the next section to model the blood flow and the movement of the mechanical valves leaflets. Starting with the conceptual settings of the Lagrange and Eulerian reference grids, the manipulation of the controlling equations on geometry curves and domain boundaries using partial differential

equations, the insertion of the field variables and PDE equations to represent mesh displacement and mesh velocity, the initialization of boundary conditions, the meshing of the solid domains and subdomains for integration of the time steps, and finally the explanation on the type of solver used on the two-dimensional problem.

3.5 Modeling ALE on the Left Ventricle

The opening and closing behavior of the valve is a delicate interaction not only between the blood flow and geometrical and stiffness properties of the heart valve leaflets, but also, the interaction must consider the influence of the aortic and mitral's roots and walls stiffness properties, which can change the characteristics of the inflow and the outflow of the blood in the ventricle chamber considerably. Numerical analysis of the opening and closing behavior is complicated by the two - dimensional finite motion of the very flexible leaflets in a compliant system of fluid and structure. In modeling the mesh movement in this fluid-structure interaction, the fluid domain is identified to be conveniently described with respect to an Eulerian reference frame while a Lagrangian formulation is considered a more appropriate approach for the structure domain.

However, these formulations are conceptually incompatible on a single domain; they are so differing individually as to be incapable of harmonious combination or coexistence together. The reason being is because of the characteristics in which both reference frames behaves; the Eulerian sets a fixed grid, non-movable, that only allows for flux to flow through it, prediction of the flow done by measuring the net flow across a certain region, while the Lagrangian sets a similar grid only this time the grid is fixed to another movable reference frame together with a material of interest and then as the material deforms the

grid deforms with it. Another character that is defining to the diversity of the two grids is the way they handle the controlling equations that govern the model. For example, in the case of the Lagrangian, conservation of mass is directly preserved as all the grid sections has been initialized with equal amount of mass, but for the Eulerian, conservation of mass is taken into account openly by measuring the flux in and out of each grid section (further discussion on the matter of mass conservation can be referred to in Section 2.7.5 of the literature review). And so, in order to solve this problem, the use of an Arbitrary Lagrange - Eulerian (ALE) formulation is introduced.

The word arbitrary in itself brings forth the meaning of a value or a quantity of function that is introduced into the solution of a problem. The arbitrary function alternately switches any value or form derived from a solution so that the solution may be made to meet special requirements according to the physics of a problem. One example of the physical problem analyzed in the project is the expansion of the aortic and mitral boundaries caused by internal fluid pressures. In the fluid domain, the internal fluid pressures are initialized and calculated on the fluid mesh using the net flow method and the result is shared with the structure domain to see its impact on the boundaries. The result from the impact is then used to update the internal fluid pressures and the process iterates until the system reach a state of convergence. This back and forth characteristic of the physical problem invokes a continuous adaptation of the fluid mesh and requires for a special method such as the arbitrary to monitor the changes in the domain without having to do modification to the topology geometry. However, with respect to the large leaflet motion immersed within the computational fluid domain it is generally difficult to adapt the fluid mesh in such a way that a proper mesh quality is maintained without changing the topology. In the matter of controlling the mesh quality, which is also a rather important physical issue, the arbitrary

behavior of the ALE is considered beneficial as it can direct the system to perform remeshing on a particular area with decreasing mesh quality.

In this project the software package FEMLAB is identified as a prime preference for the reason that it supply for both Lagrangian and Eulerian settings, carries the idea of association between moving meshes from both fluid and structure domains in the ALE modeling, provides facility to handle coupling between the reference systems, allows for separate and combined PDE calculations (when necessary) on the multiple boundaries and domains of the geometry, sets the mesh in a finite element environment, and utilizes a predefined time-dependent solver for the PDEs calculation which provide solution to the proposed physical problem. The finite element platform utilized by FEMLAB is also identified most appropriate as the base to model the mesh movement.

3.5.1 Modeling Mesh Movement for the ALE

The software package FEMLAB utilizes the finite element environment and the ALE to form the basis of the moving mesh method. Two methods; mesh displacement and mesh velocity, have been suggested for the determination of the mesh movement. It has been identified that the general PDE for the mesh movement is based on the equation of motion used in continuum mechanics and for the most part there are taken from respective domains such as the solid and fluid mechanics. Implementation of field variables identified from these domains is utilized in FEMLAB with the intention to handle the mesh displacement and mesh velocity in the model.

Mesh displacement is defined as function of the Cartesian spatial coordinate and time. An analogy used to describe mesh displacement is to assume the mesh to have isotropic and elastic-like behavior, which is similar to the refined theory of solid mechanics. In order to demonstrate the techniques used in the project, the valve structure has been programmed with density and a Neo–Hookean hyperelastic behavior summarized in Table 3.2 below.

Table 3-2: Field Variables Representing Properties of the mesh Displacement

Mesh Displacement Field Variables	Values
Density (ρ)	960Kg/m ³
Coefficient (u)	6204106 N/m ²
Bulk Modulus	20u
Poisson Ratio (ν)	0.45
Elastic Modulus	1.017N/m ²

By means of the generalized Hooke’s law, the stress-strain relationship in the linear elastic behavior is numerically computed using the (Cauchy) stress tensor. The value of the stress tensor which is gained from the properties of the valve structure (as depicted in the Table 3.2) is used as input for the PDE equation that governs the mesh displacement. Mesh displacement is the method used to control the plane strain of the reference grid, which basically tracks where the mesh moves and the method is done by specifying the displacements using the surface tractions. Surface tractions are the load properties that tracks the movement made by a body that moves on the ALE grid. The tractions are given by properties such as the Poisson’s ratio (ν), body force in x – direction (K_x), body force in y – direction (K_y), and density (ρ), all acting as loads that affect the constrained movement of the structure.

Mesh velocity on the other hand is fundamentally used to track how fast the mesh is moving, movement identified as fluid motion of the blood with the velocity of the mesh observed by computing the net flux of the blood across the grid on specific areas. The fluid in the model is a blood-like substance with a density and dynamic viscosity in similar comparison to the discussion in Section 2.3 of the literature review. In brief, the properties are shown in Table 3.3.

Table 3-3: Field Variable Representing the Mesh Velocity

Mesh Velocity Field Variables	Values
Density	1060Kg/m ³
Dynamic Viscosity	0.0054Pa-1s

These initial loads for the mesh velocity are taken in the FEMLAB computation to help solve the partial differential equations on the original mesh. The generated results are boundary conditions that are used to set new inputs which serve the goal of producing a new set of mesh coordinate. Based on physics programmed for the boundary conditions in the new mesh, FEMLAB again solves the PDE at a different time step with new sets of displacement loads and velocity net flux. At each time step, adjustment to the mesh is done and along the process, creation of new mesh coordinates is completed which would record new movements to the mesh.

The process is iterated until it satisfies every time step specified. Consequently this would result in a constant mapping of change of the domain boundaries which depicts the deformation or distortion of the problem geometry. It can also be said here that the interaction between fluid and structure of the model comes from the coupling of the mesh

velocity and mesh displacement which are computed from the physics of the boundary conditions that governs the mesh movement problem. In the next subsection, determination of the left ventricle boundary conditions used to solve the PDE for the mesh movement is discussed.

3.5.2 Coupling of Reference System for the Mesh Movements

The basis of an arbitrary Lagrangian – Eulerian (ALE) formulation is the use of three separate coordinate systems:

- (i) The Eulerian reference system which is fixed in space for the mesh velocity (Ω_f).
- (ii) The Lagrangian reference system which moves with the material for the mesh displacement (Ω_s).
- (iii) The computational reference system (Ω_g) which can move arbitrarily in space.

Using solid modeling previously explained in section 3.4, the two - dimensional ventricle model is spatially discretized into triangular mesh containing information on the points, curves and edges. These points are considered an essential requirement to track the material in the Lagrangian system by using its point coordinates as reference on the movable grid. These material points are identified on the other two grids using their position vectors in both the Eulerian grid and the arbitrary reference grid. The governing concept of the ALE formulation is to let both Eulerian configuration and Lagrangian configuration moves and deforms independently over a fixed referential configuration.

This introduces the spatial motion ξ as the resulting degree of freedom generated by the Eulerian system. Consequently, it also introduces physical motion χ of the deforming solid material by the Lagrangian system. These two properties are created at any occurrence of movement or deformation on the two working grids but they are independent of each other, as it is emphasized that both spatial and physical motions have different spatial coordinates albeit being mapped onto the same arbitrary configurations. Figure 3.18 denotes the relation between various configurations and motions.

In order to track the physical movement of the material, physical quantities in the fluid–structure problem are defined with respect to the connection between the Eulerian and the Lagrangian systems, but this only cater to solving the physics of the problem. Simulation of a computational solution to the fluid–structure problem can only be made available by manipulation of a computational grid, and so in the case of this project the arbitrary grid has been identified to provide the base for this simulation. Linking the Eulerian system to the arbitrary grid and map the end result of the fluid – structure problem as a finite element formulation of the interaction can only be obtained if the Eulerian reference system is in direct relation to a computational reference system.

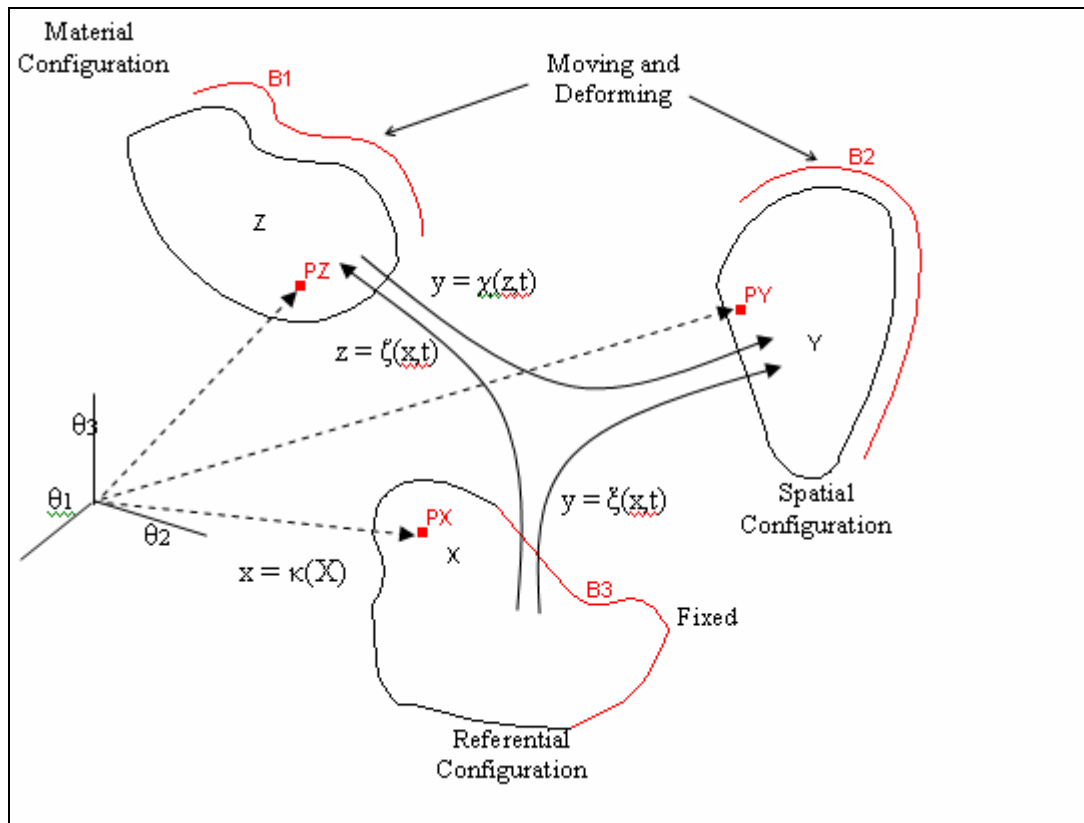


Figure 3.18: Relation between moving configurations and motions

In Figure 3.18, three grid configurations are shown; at the top left is the material configuration (PZ) which denotes the Lagrangian reference system, spatial configuration (PY) on the right hand side of the figure signifies the Eulerian reference system, and at the bottom, referential configuration (PX) is the arbitrary grid where all movement and deformation from both Lagrange and Eulerian systems are referred and mapped onto.

Several sample points, P_s , P_f and P_g has been used to illustrate the spatial relationship shared by the points. The three points are actually similar in the sense that they represent identical spatial configuration in the problem only that having been referred in three different systems does not allow them to have the same spatial coordinates. In other words,

a material point in the Lagrangian system is identified with its position vector P_f in the Eulerian system and P_g in the computational reference system (the computational grid).

B1, B2 and B3 are examples of changes that occurred in the systems. B2 demonstrate a change or deformation in the spatial configuration of fluid properties tracked by the Eulerian system, resulting in generation of spatial motion ξ . The information gathered from the spatial motion is sent to the awaiting Lagrangian system, and at the same time step it is also sent to the fixed computational grid for reference mapping. The Lagrangian system accepts the spatial motion information and uses it to calculate and observe the impact made by the fluid on the structure of the deforming solid material geometry. Subsequently this introduces physical motion χ with information on the deformation shown in the figure as B1 and this information is also mapped on the fixed computational grid for reference mapping. On the fixed grid, both B1 and B2 are mapped in accordance to their vector positioning and seen as B3 on the topology of the arbitrary grid. Three simple equations explain the coupling between the systems, which shows the representations of the domain derivatives in relation to each other.

These relations portrayed in the modeling are all based on the laws of continuum mechanics, such governing laws used are the balance laws which becomes the principle in deriving the PDEs for Eulerian and Lagrangian continuity equations in the conservation of mass, and Newton's second law that explains the conservation of momentum in the model. A more elaborate and comprehensive numerical explanation is laid out in Section 2.4.2.1 in the literature review.

3.5.3 PDE for the Mesh Movement

The aim of this section is to introduce several PDEs used in the ALE formulation to handle moving boundaries in a fluid – structure problem. In the preceding section, it has been explained that coupling of the reference systems for the mesh movement requires for the systems to be related to each other. The connection between the reference systems has been identified to follow the laws of continuum mechanics in order to derive the PDEs for both the Eulerian and Lagrangian equations. In accordance to the modeling for the left ventricle model, three PDEs; the Navier Stokes equations, Balance equations, and Weak form equations have been identified as most suitable for the task. The numerical account of the Navier Stokes and the Weak are laid out next, with description of the balance equation extensively covered in Section 2.7 of the literature review.

In FEMLAB, the formation of the ALE model is carried out by representing field variables as the mesh displacement and mesh velocity. A mapping from an original domain Ω to the deformed domain $\bar{\Omega}$ is considered and defined by

$$x(X,Y,t), y(X,Y,t), X,Y \in \Omega, x,y \in \bar{\Omega}, t \in \mathbb{R}^+ \quad (3.1)$$

with Jacobian inverse

$$\begin{bmatrix} I_{Xx} & I_{Xy} \\ I_{Yx} & I_{Yy} \end{bmatrix} = \frac{1}{D} \begin{bmatrix} y_Y & -x_Y \\ -y_X & x_X \end{bmatrix}, \text{ where } D = x_X y_Y - x_Y y_X. \quad (3.2)$$

Using the PDEs, FEMLAB solves the equations on the original mesh (of the original domain) but adjusts the equations to account for the mesh movements. The method covers situations in which the topology of the geometry does not change during the simulation and a suitable PDE for the mesh velocity exists, hence deriving the Navier Stokes equations in written form as

$$\begin{aligned}
& \int_{\Omega} (\tilde{u}_x(2\eta u_x - p) + \tilde{v}_y(2\eta v_y - p) + (\hat{v}_x + \hat{u}_y)\eta(u_y + v_x) + \\
& \hat{u}((u - \Psi_x)u_x + (v - \Psi_y)v_y) + \hat{v}((u - \Psi_x)v_x + (v - \Psi_y)v_y) + \\
& - \hat{p}(u_x + v_y) + \rho \hat{u} \frac{du}{dt} + \rho \hat{v} \frac{dv}{dt} - \hat{u}f_x - \hat{v}f_y) d\Omega = 0
\end{aligned} \tag{3.3}$$

in the moving coordinate system, where $\Psi = (\Psi_x, \Psi_y)$ is the mesh velocity and $\hat{\cdot}$ denotes a test function. The deformed velocity derivatives can be expressed using the original velocity derivatives

$$\begin{bmatrix} u_x & u_y \\ v_x & v_y \end{bmatrix} = \begin{bmatrix} u_x I_{Xx} + u_y I_{Yx} & u_x I_{Xy} + u_y I_{Yy} \\ v_x I_{Xx} + v_y I_{Yx} & v_x I_{Xy} + v_y I_{Yy} \end{bmatrix} \tag{3.4}$$

The integration of the Weak equations on the original domain derives a set of equations that can be solved on the fixed mesh.

$$\begin{aligned}
& \int_{\Omega} D((\hat{u}_x I_{xx} + \hat{u}_y I_{yx})(2\eta u_x - p) + (\hat{v}_x I_{xy} + \hat{v}_y I_{yy})(2\eta v_y - p) + \\
& (\hat{u}_x I_{xy} + \hat{u}_y I_{yy} + \hat{v}_x I_{xx} + \hat{v}_y I_{yx})\eta(u_y + v_x) + \\
& \hat{u}((u - \Psi_x)u_x + (v - \Psi_y)v_x) + \hat{v}((u - \Psi_x)v_x + (v - \Psi_y)v_y) + \\
& - \hat{p}(u_x + v_y) + \rho \hat{u} \frac{du}{dt} + \rho \hat{v} \frac{dv}{dt} - \hat{u} f_x - \hat{v} f_y) d\Omega = 0 \tag{3.5}
\end{aligned}$$

For the moving boundaries of the valve leaflets, a prescribed moving boundaries formulation has been used to solve for the mesh velocity using the Poisson's equation in the moving coordinate system. The following equation is used:

$$\int_{\Omega} D((\hat{\Psi}_{xx} I_{xx} + \hat{\Psi}_{xy} I_{yx})\Psi_{xx} + (\hat{\Psi}_{xy} I_{xy} + \hat{\Psi}_{yy} I_{yy})\Psi_{xy}) d\Omega = 0 \tag{3.6}$$

$$\int_{\Omega} D((\hat{\Psi}_{yx} I_{xx} + \hat{\Psi}_{yY} I_{Yx})\Psi_{yx} + (\hat{\Psi}_{yX} I_{Xy} + \hat{\Psi}_{yY} I_{Yy})\Psi_{yy}) d\Omega = 0 \tag{3.7}$$

$$\text{where, } \frac{dx}{dt} = \Psi_x$$

$$\text{and, } \frac{dy}{dt} = \Psi_y \text{ on } \Omega$$

with initial condition $x = X, y = Y$. Solving movement in the moving coordinate systems makes the problem nonlinear with higher degree of freedom but often allows for larger mesh movements. This consequently provides a velocity field for the boundary.

$$\Psi_x = U(t)$$

$$\Psi_y = V(t)$$

$$u = \Psi_x$$

$$v = \Psi_y \quad \text{on} \quad d\bar{\Omega}$$

3.5.4 Schematic Representation of the Mesh Movement Method

In this section, a schematic representation of the ALE method is offered. The idea is to scheme out the solution procedure between the passing interface of the fluid, structure and the arbitrary (computational) domain. Several constants have been identified as key elements to the model; surface traction, initial loads in the form of velocity, viscosity, and pressure data, all which are considered as boundary conditions to the three grid domains discussed in previous subsections.

In a physical problem where the goal is to monitor physical deformation made by fluid on a solid structure, the fluid domain is given the initial push. At the initial time step, the velocity field in the fluid domain Ω_f is computed using inflow velocity which generates information on the pressure p_f that is expected to press on the solid boundary. The interface software passes the pressure data as boundary conditions into the solid domain Ω_s .

In the structure problem, the deformation of the solid domain Ω_s is computed by calculating the traction vector using the pressure data obtained. This in return generates new boundary conditions for the structure in the form of boundary position (displacement) u_s and velocity information v_s . This information has been considered in the Balance and Weak Form calculation to update the movement of the material in the solid domain. Both u_s and v_s are then sent to the grid deformation problem and the fluid problem respectively. The grid accepts u_s from the solid domain and uses it as reference to map the deformation for the simulation.

During the deformation mapping, the weak form calculation derives the grid's velocity v_g and at the same time the computational grid is updated with new boundary positions. Derivation of v_g from the computational grid and v_s from the solid calculation are considered necessary in the ALE modeling as velocity information is essential to update the Navier Stokes equations for the fluid problem. This process iterates until it has satisfied all time step specification.

Additionally, to ensure full convergence, there is a facility in FEMLAB to assist for relaxation of pressure, displacement or both. There is also automatic remeshing of the fluid domain when the distorting mesh is too large and violates the quality constraints set for the model. This feature is necessary for systems such as the heart valves that feature severe topological distortion of the leaflets boundaries.

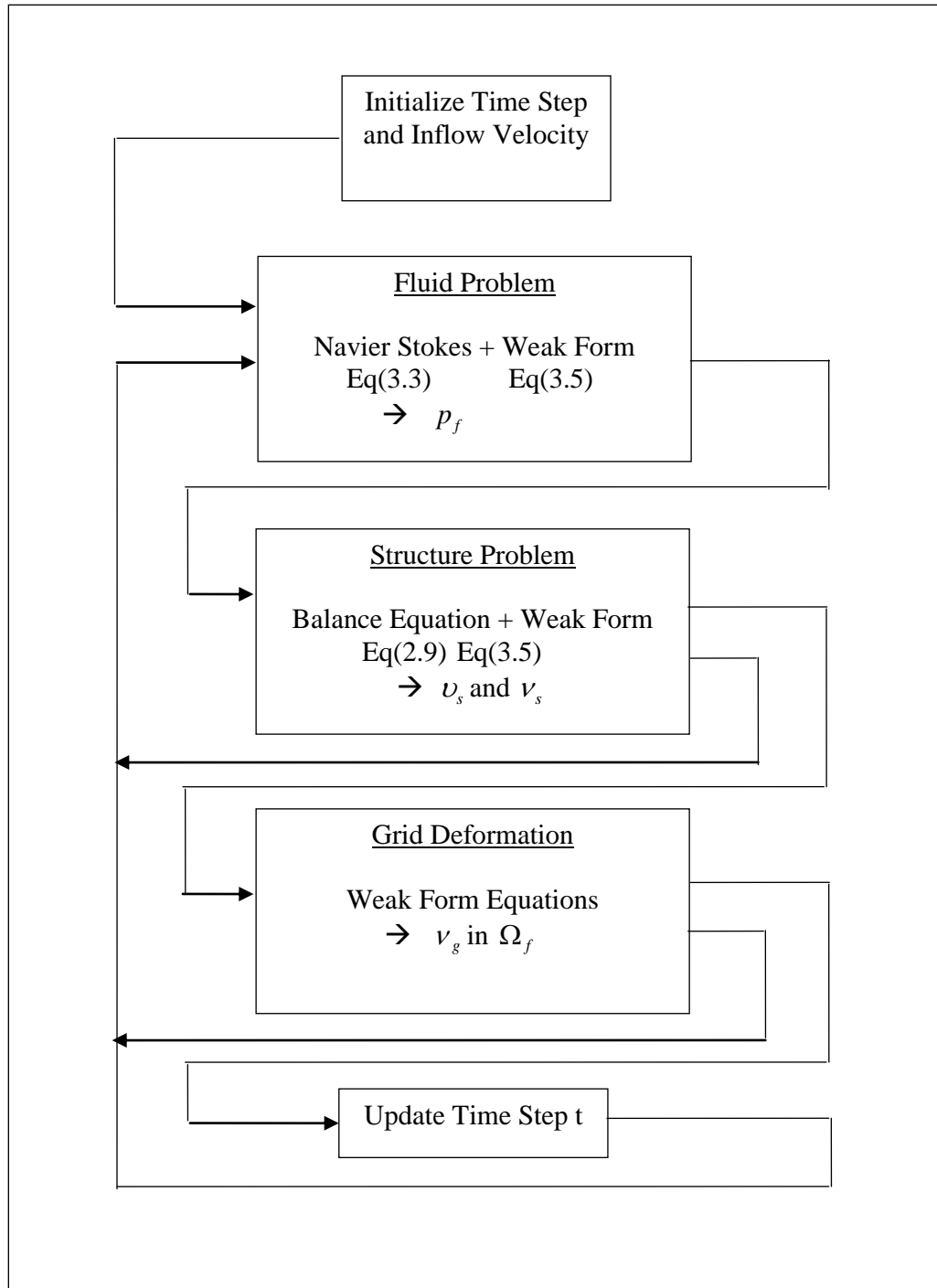


Figure 3.19: Schematic Presentation of the ALE Method

3.5.5 Assumptions for the Mesh Movement Method

Several important assumptions have been identified to model the suggested mesh motion in accordance to the laws of physics. Mesh motion is a degree of freedom generated when the ALE approach is used. It is expected that the degree of freedom is proportional to the capacity of movement of the mesh. Higher degree of freedom indicates a bigger capacity for the mesh to deform which allows for the ALE formulation to handle more delicate movement problem.

- (i) The first assumption is to ensure that the mesh motion is governed by a law of dynamics, which should be close in similarity to continuum mechanics (i.e. balance law, Eulerian and Lagrangian continuity equations, Newton's second law, Cauchy's tensor law).
- (ii) The second assumption is to identify that linear momentum of mesh elements is defined as parallel to linear momentum of a material volume.
- (iii) The third is to control the variables that act as the body force to the model. The underlying idea is that a region with larger variables production should have a refined mesh, while a region with less variables production could do with coarser mesh.
- (iv) The fourth assumption is to assume that traction can be used to act as the resisting force to the motion or deformation of the mesh elements. In this case, the traction is allowed to have values from the material or solid reference system or it can be changed to have values from the fluid reference system depending on the mode of resistance similar to either mechanical domain.

The fourth assumption deals with the issue of selecting the form for surface traction. It can be summarized that the two mesh approaches, selects the surface traction according to the physics of the problem. This resulted in the different forms of PDE settings on the geometry's boundaries for the mesh movement. The mesh displacement method utilizes the weak form formulation to handle the stress-strain relationship parallel to elastic materials in solid mechanics and the mesh velocity method exercises the Navier Stokes equation to derive surface traction based on an analogy to fluid mechanics.

3.5.6 Setting the Boundaries Physics for the Mesh Movement

In the preceding subsection, it has been identified that boundary conditions plays an important role in ensuring the convergence of the PDE calculations. Boundary conditions define the interface between the model geometry and its surroundings. When specifying boundary and interface conditions, the software differentiates between exterior and interior boundaries. An exterior boundary is an outer boundary of the modeling domain, while an interior boundary represents the dividing interface between two subdomains in the modeling domain. If an equation is deactivated in one domain, the interior boundary between the active and inactive domain becomes an exterior boundary for its variable for the reason that the interior boundary is then on the outside of the modeling domain for those fields. This in return voids the boundaries of the inactive domains. Figure 3.19 illustrates these boundaries.

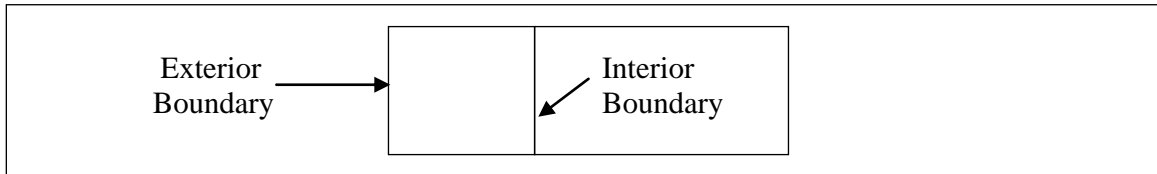


Figure 3.20: Interior and Exterior Boundary of a Domain

In accordance to the physics that defines the ALE modeling with its mesh movement problem, FEMLAB allows for settings of the model boundaries by specifying each line of the boundary in the model geometry with a suitable physical condition. In this setting, the boundaries are arbitrarily numbered analogous to the illustration depicted in Figure 3.21. Boundaries denoting the simplified aortic and mitral valves are highlighted in Figure 3.22 for better observation.

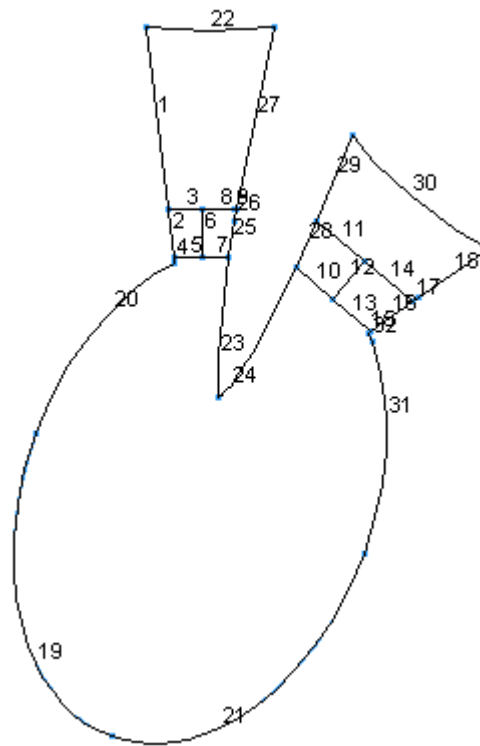


Figure 3.21: Boundaries Marked with Number

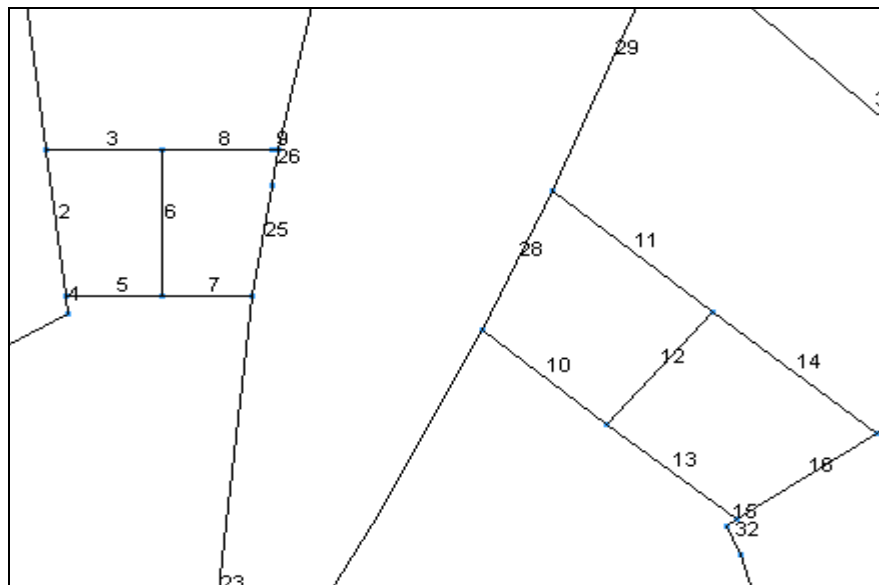


Figure 3.22: Closer Examination of the Valve Boundaries

Adjustments to each corresponding boundary lines begin with entering the appropriate conditions as shown in Table 3.4. The reasoning behind every condition set upon each numerically marked boundary for the mesh movement is specific to the physiological attributes identified. Refer to Section 2.8.2 for further explanation.

Table 3-4: Boundary Settings for the Mesh Movement

Boundary	1,15,17-21, 23-24,27, 29, 31-32	22	30	2,4,25-26	16,28
Type	No Slip	Inflow / Outflow Velocity	Outflow / Pressure	Inflow / Outflow Velocity	Inflow / Outflow Velocity
x-velocity (u_0)	0	0	0	pin_vel	pin_vel2
y-velocity (v_0)	0	$32*s*(1-s)$	$32*s*(1-s)$	0	0
Pressure (p_0)	0	1.0	1.0	0	0

3.5.7 Setting the Mesh on the Left Ventricle Model

The starting point for the finite element method is a mesh which is considered as a partition of the geometric model into small units of simple shape. The software FEMLAB facilitates a method called the Delaunay algorithm to generate 2D mesh on a solid model. For a 2D geometry such as the left ventricle model, the software utilizes partitioning of the subdomains into mesh elements which are in the form of infinitesimal triangular-shape units. These elements are considered as approximation for the reason that each boundary created can be curved in shape. The sides of the triangles are called mesh edges, and their corners are mesh vertices. A mesh edge must not contain mesh vertices in its interior similar to the boundaries which are defined in the geometry into partitions of mesh edges. These boundary elements must be conformed to all the existing triangles for every adjacent subdomain. Any isolated points in the domain geometry are also considered as mesh vertices.

The shape of the geometry and various mesh parameters determine the number of mesh elements. Using the mesh parameter features supplied by the software, specification of local mesh-element sizes is allowed to control the mesh distribution. All mesh parameters aim at prescribing the maximum allowed mesh element size, which indicates that the size of a mesh element must not be larger than the minimum prescribed local element size determined by all mesh parameters.

Table 3-5: Mesh Parameters Settings for the Geometry

Mesh Parameters	Example Values
Predefines Mesh Sizes	Normal
Maximum Element Size	1 (by Default)
Maximum Element Size Scaling Factor	0.3
Element Growth Rate	1.3
Mesh Curvature Factor	0.25
Mesh Curvature Cut Off	0.0003
Optimize Quality	On
Refinement Method	Regular

The maximum element size field dictates the maximum allowed element size which by default is 1/15th the size of the geometry. The maximum element size scaling factor comes into play when there is no maximum element size specified. Such as the case presented in Table 3.5, the software multiplies the maximum element size (which is 1 by default) by this scaling factor. The element growth rate determines the maximum rate at which the element size can grow from a region with small elements into a region with larger elements. The value must be greater or equal to one. The default value is 1.3, which means the element size can grow by a 30% approximation from one element to another.

The mesh curvature factor determines the size of boundary elements compared to the curvature of the geometric boundaries. The curvature radius multiplied by the curvature factor, which must be a positive scalar, gives the maximum allowed mesh size along the boundary. A lower value gives a finer mesh along curved boundaries. In the project this curvature factor is set as 0.25, lower than the software default value of 0.3 indicating finer mesh is used along the left ventricle curved boundaries. The parameter in the mesh curvature cut off prevents the generation of many elements around small curved parts of the geometry. This value, also a positive scalar, is set at 0.0003 by which a lot smaller than its

default value of 0.001. When the radius of curvature is smaller than the product of the mesh curvature cut off value times the maximum axis parallel distance in the geometry, the software considers the radius of curvature as being this product.

The optimize quality is set to function to control if FEMLAB carries out quality optimization during mesh initialization. It has been discovered that when trying to solve a problem that does not converged, or having solved a problem where the solution does not seem to properly resolved, there is often a need for resolving the problem using a finer mesh. In these situations it is sometimes easier to refine the existing mesh than to generate the mesh from scratch using finer mesh setting such as the mesh refinement method. The regular refinement method divides each element into four elements of the same shape in 2D. Figure 3.21 demonstrate the result of various mesh distribution considered in the project.

In order to initialize mesh for the left ventricle geometry, several mesh settings available in FEMLAB are studied. In Figure 3.23, several different type of mesh have been tested on the model. Each figure represents a specific allocation of mesh structure starting with the extremely coarse mesh depicted in Figure 3.23(a), up until the extremely fine mesh in Figure 3.23(h). In the early stages of the development, all eight settings have been implemented as a uniform distribution on the model on the Figure 3.24 summarized the elements generated for each mesh settings.

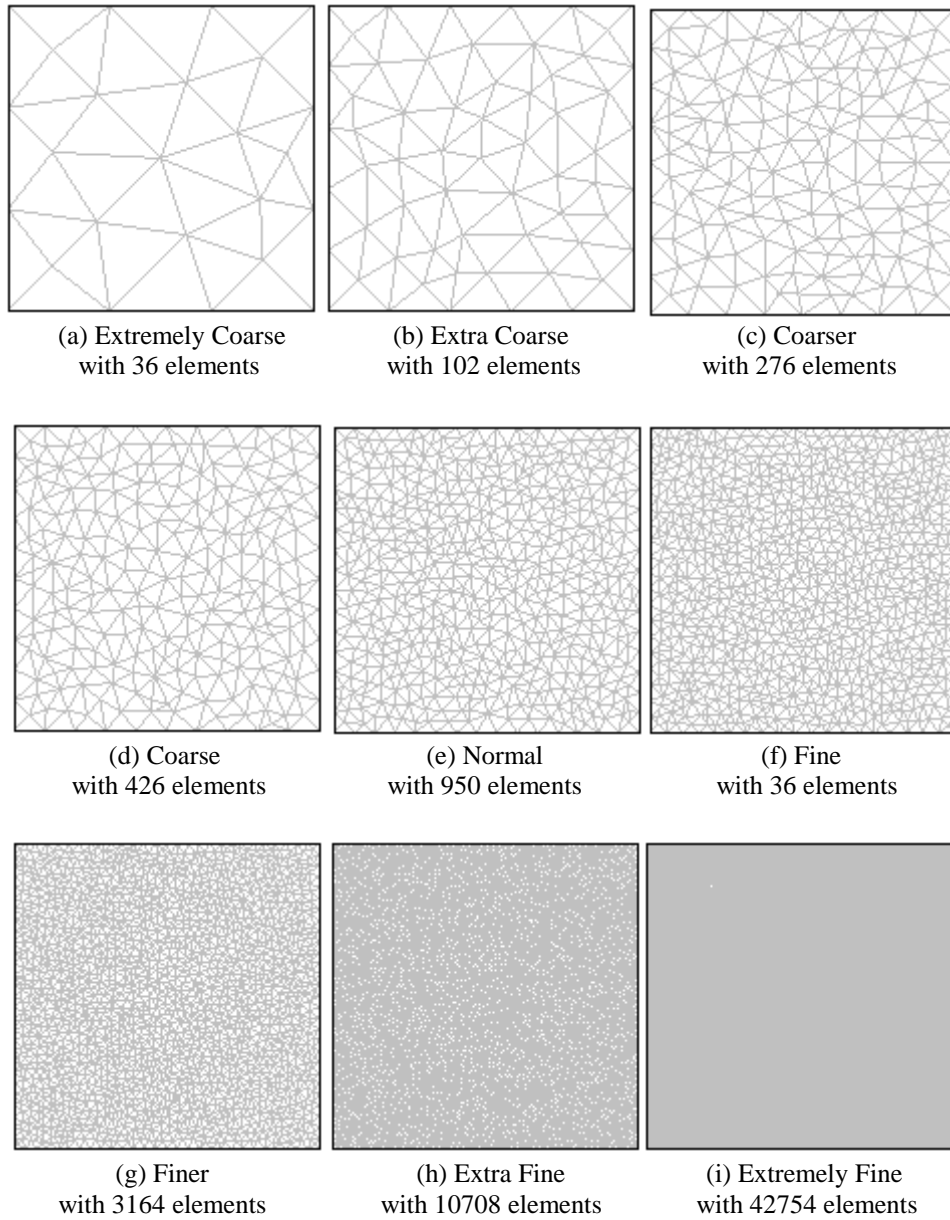


Figure 3.23: Varied Settings Available for the Mesh; Coarsest to Finest.

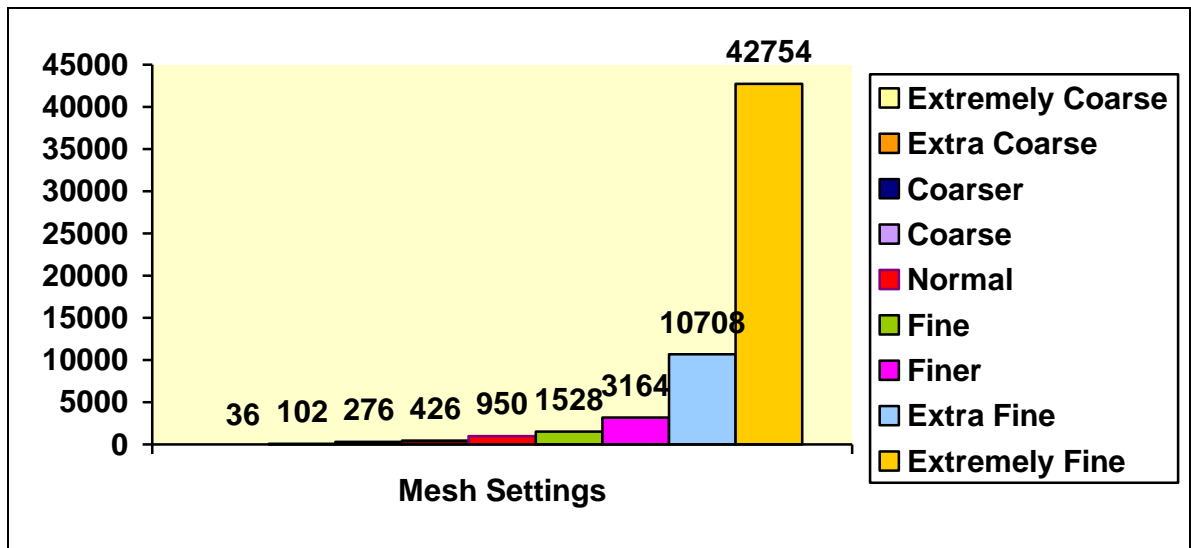


Figure 3.24: Several Different Mesh Settings for the Model

The Figure 3.25 next is used to show the mesh initialized on the left ventricle model. A coarser mesh has been used in most parts of the model; the domains of the aortic and mitral cylinders and the conical domain of the ventricle chamber. In order to maintain the mesh quality on areas expected to encompass a rather large deformation, estimation figured for the valve leaflet distortions, remeshing of the subdomains of the working valves has been employed with a more predefined mesh.

The base (coarser) mesh has been identified to comprise 222 boundary elements, 2247 number of elements and it is programmed with a minimum element quality of 0.4804. The predefined mesh, which can also be referred to as extended mesh, provides the left ventricle model with a total of 10482 numbers of degrees of freedom. This is an indication that areas in the model with finer mesh particularly the valve domains are considered to experience large toleration for deformation or distortion of its geometrical structures.

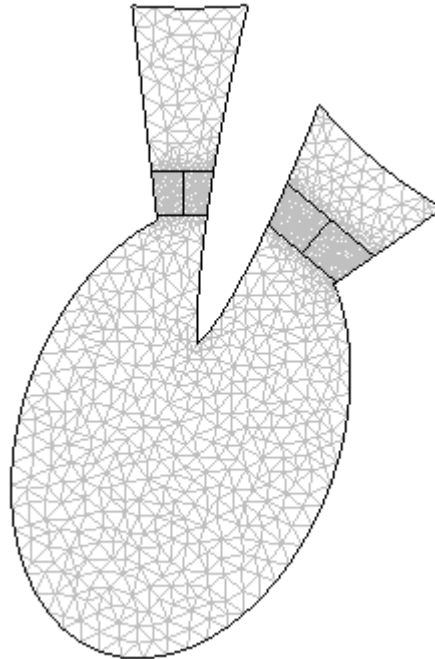


Figure 3.25: Meshing of the Left Ventricle Model

Remeshing of the valve domains, however, have been discovered to introduce artificial diffusivity, a finite element discretization difficulty mostly identified in hyperbolic problem such as the blood flow. It has been observed that detection of large diffusivity may prevent the solution from converging and with this reasoning a streamline diffusion technique has been used in the project to address the stabilization issue.

3.6 Solving the model

As noted, the underlying mathematical structure in FEMLAB is a system of PDEs and in solving the PDEs, FEMLAB utilizes the finite element method. In the project, simultaneous coupling of the three reference system described in Section 3.5.4 requires for the software to run the finite element analysis together with adaptive meshing and error control using a variety of numerical solvers. In order to reduce the complexity of the calculation the time

dependent solver in FEMLAB has been chosen for its unique feature and ability to mix domains of different space dimensions in the same problem, therefore simplifying the time dependency issue in the ALE model.

3.6.1 The time dependant solver

The goal of this section is to examine the time dependant solver, which is most appropriate in deriving the solution to non-linear PDE problems. The left ventricle model being simulated in the project is considered a non-linear problem basically for the two following reasoning; the first being the coefficients or material properties utilized in the model contains a dependable variable, i.e. the time (t), and secondly, having to exercise the Navier Stokes formulation among the underlying PDEs has always been considered as nonlinear unless the formulation takes in zero pressure (p=0) as input value, resulting in a special case of the linear Stokes formulation. .

In the time dependant solver, the output time is specified as vector using the syntax in the form of $t_0 : \Delta t : t_n$. The symbol t_0 is used to denote the initial time which is considered as 0 by default and t_n is the notation applied to show the last output time. Within this length the time step Δt can be designed and programmed in accordance to the dynamics of the model. The time stepping in the model is designed to follow this equation:

$$x(t) \rightarrow x(t + \Delta t) = x + dx \quad \text{for} \quad t \rightarrow t + \Delta t \quad (3.8)$$

It is sometimes essential for accuracy or performance to set the absolute and relative tolerance as they determine the limit for the error estimation in each integration step. It is also with benefits that the absolute tolerance is set to be smaller than the displacements for the reason that the displacements in most structural mechanics are considered small.

3.6.2 Settings for the time dependent solver

Several points discussed in Section 3.6.2 is summarized in the next table. Highlighted in the table are parameters used in setting the time dependent solver.

Table 3-6: Settings for the Time Dependand Solver

Parameter	Value
Times	0:0.02:1.5
Relative Tolerance	0.001
Absolute Tolerance	0.00010
Initial Time Step	0.0010
Maximum Time Step	1.0
Load Constraint	On
Constraint Constant	On
Mass Constant	On
Jacobian Constant	On
Constraint Jacobian Constant	On

The syntax 0:0.02:1.5 represents a vector of times starting at 0 with step 0.02 up to 1.5. The relative tolerance is set to be 0.001 with absolute tolerance defined at a very small scale of 0.00010. The absolute and relative tolerances determine the limit for the estimated error in each integration step. For accuracy of convergence, the initial time step of 0.0010 is set and with every 0.02 step, the solver calculates the PDEs and solves the equations for the Eulerian and Lagrangian domains. It has been identified that for coarser mesh, a bigger initial time may be used but it must be in accordance to the times settings of 0 to 1.5. Hence

determining the maximum time step as 1.0 and anything exceeding that limit would have been too big in ratio comparison to the decided times. In the setting, all constraints and constants is made available by setting them on.

3.7 Postprocessing and Visualization

For post processing, FEMLAB provides tools for plotting and postprocessing any model quantity or parameter to help analyze the results obtained from the time-dependent solver. Several tools for plotting have been utilized to study the parametric behavior in various experimental work (refer Section 4.2) and in the left ventricle simulations (refer Section 4.3).

In addition, animation has been utilized as it can be used to reveal the dynamics in a solution. Cross sectional of plots is considered important to the project as it can be used to interpolate within a domain for the reason to extract mesh-independent plots, and at the same time extend these plots in time or along parametric solutions. These domain plots supply for all the graphical figures shown in the Results and Analysis chapter and caters for the computation of numerical integrals of the model quantities.

3.7.1 2D Postprocessing and Visualization

In the project, standard plots in 2D have been identified to visualize the solution as part of the geometry. As explained in the previous section, the solution can appear as a combination of the various 2D plots – a surface, a contour, a deformed plot, a streamline plot, etc. These standard plots have been animated in time or along parametric solution and they are identified in this documentation as follows:

- Surface plots
- Contour plots
- Arrow plots
- Streamline plots
- Deformed shape plots
- Cross-section point plots

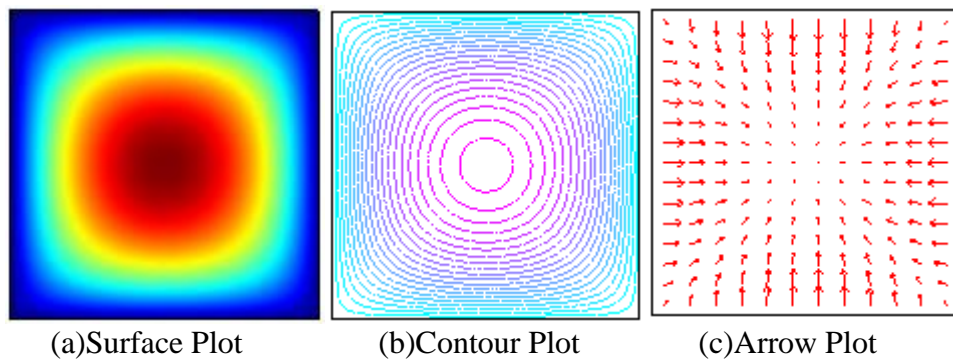


Figure 3.26: The Surface, Contour and Arrow Plot for the 2D Visualization and Postprocessing

Figure 3.26(a) shows the surface plot which is the default plot in the 2D visualization tool displaying quantity parameter as colored two-dimensional feature. In Figure 3.26(b), a contour plot is seen to describe a display of quantity parameter as a set of colored contour lines with constant values. In Figure 3.26(c), a 2D arrow plot visualizes a 2-component vector quantity on the domain. In this setting, the distribution of the arrows in position are done by explicitly locating the arrow coordinates using either a space-separated list of coordinate vector, for example `0:10:100` or `logspace(-1,1,30)`. The arrows can also be specified by independently positioning them as proportional or normalized in the x and y directions which help determine whether the plot gives arrows a length proportional to the magnitude of the vector field or a normalized length. Red is the default color for the arrow.

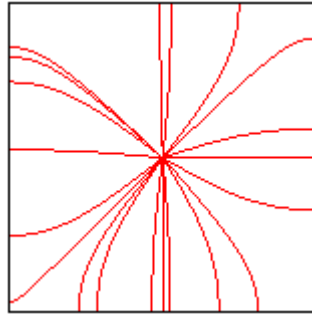


Figure 3.27: The Streamline Plot

As described in Figure 3.27, 2D streamlines visualize a vector quantity on subdomains of the model and it has been identified to be particularly important in visualizing blood flow in the project. The vector quantity visualized in the plot is defines the streamline appearances in similar order to the arrow plot specifications. Increasing the streamline starting points above its default value of 20 increases the total amount of the streamlines in a subdomain which is used in the blood flow modeling to highlight the difference in flow rate across a domain or subdomains in the left ventricle model. The following attributes highlights the streamline algorithm which further describes the function's effect.

- Calculation of streamlines is initialized by selecting a set of starting points which is controlled by the streamline start points and the number of start points.
- The algorithm then finds the vector of the given vector field at these points by interpolation which normalizes the vector field.
- The algorithm next integrates the points along the direction of the vector using the integration tolerance.
- At the new position, the algorithm finds vector values by interpolation and performs another integration.

This process stops if:

- It reaches a predetermined number of integration steps which is controlled by the maximum number of integration steps entry.
- The points end up outside the geometry.
- The points reach a “stationary point” where the vector field is zero. The stationary stop tolerance can be reset to control the empty vector field.
- The algorithm has used a predetermined amount of “time” for integrating. For this matter, the maximum integration time can be reset with another specification.

It is also possible to visualize a vector field by deforming the geometrical shape (refer to Figure 3.28). This plot type is considered primarily extended for visualizing the x and y displacements (noted using the symbol u and v) particularly for problem in structural mechanics. In the project this attribute is used to highlight the deformation defined by the Lagrange multiplier in the ALE simulation of the left ventricle model. Scaling of the deformation is set to 10% of the geometric domain.

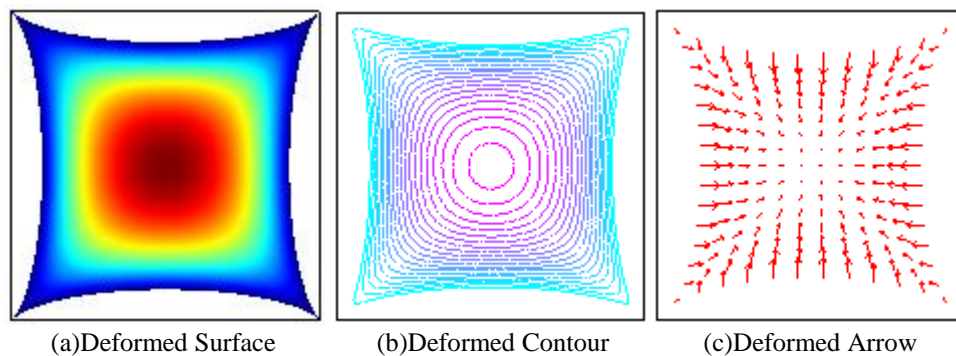


Figure 3.28: 10% Deformation of the Surface, Contour and Arrow Plot for the 2D Visualization and Postprocessing.

The 2D point cross-section plot is used to visualize a quantity in one or several point in time, along a parameter range, or for several eigenvalues. The plots are necessary to describe current plotted scalar or quantity based on the model's surface or contour data, resulting in presentation of the parameter in graphical order (refer to Section 4.3.2, Figure 4.14).

3.8 Conclusive Remarks

Careful details on the construction pertaining to the two-dimensional ALE modeling have been presented. The methods involved in the study of the fluid-structure interaction using mesh movement to depict the deforming leaflets under pressure from the blood flow in the left ventricle have been extensively discussed. Several important techniques deriving the tools involved in the development processes are revised and with this, algorithm that is the backbone of the modeling has been highlighted with interest.

Chapter 4

Results & Analysis

...For I Dreamt Last Night of Bloody Turbulence

William Shakespeare, "Troilus and Cressida"

4.1 Overview

In this chapter, comprehensive descriptions of the experimental results are first analyzed followed by a representation of the results obtained from the left ventricle simulation. Several important theories have been identified as important through the literature review, and these theories have been made practice in the methodology to generate several preliminary experimental works. Information gathered from each investigational model are extracted individually pertaining to several modeling scope discussed in the methodology several and the knowledge gained are merged together in the development process to help form a plausible simulation model of the heart's left ventricle.

4.2 Experimental Results

4.2.1 Incompressible Laminar Flow

Ideally, blood flow in the heart is laminar, or streamlined. In laminar flow, there is a parabolic profile of velocity within a blood vessel, and in the case of this project the blood vessels identified are the aortic and mitral cylinders. The velocity of the blood is depicted highest in the center of the vessel and lowest toward the vessel walls. A thorough discussion on the matter can be referred to in Section 2.3.4 of the literature review. In the earliest stage of the development, an experimental test has been carried out to simulate the incompressible and laminar attribute of the blood flow across a tube and a curved domain. Results of the tests are shown as follows:

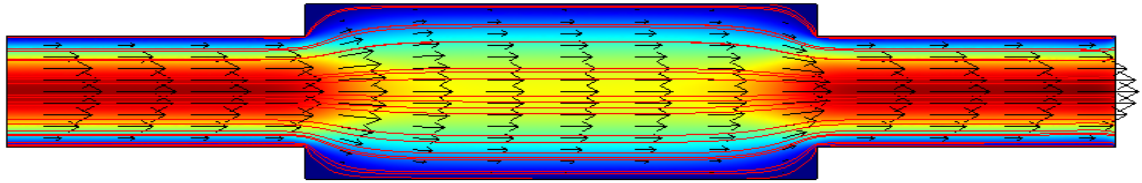


Figure 4.1: Laminar Flow in a Tube

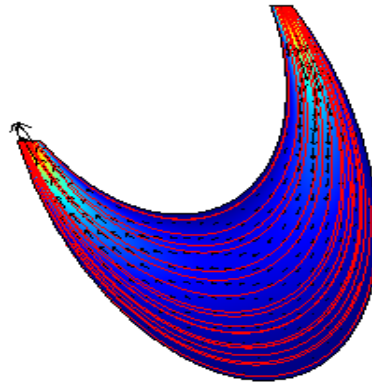


Figure 4.2: Laminar Flow Pass a Curved Domain

The two figures in representation described fluid as blood-like substance with a density of 1060Kg/cm^3 and dynamic viscosity of 0.005Nsec/m^2 . In Figure 4.1 the flow is designed to cross a tube-like channel and in Figure 4.2 the flow is seen to pass through a curved-like domain. The goal of these experiments is to examine the physics of the planes in relation to the passing incompressible yet a steady blood flow. Specifying an inflow of $s*(1-s)$ velocity, the blood is depicted to enter from the inlet boundary (indicated using arrow markers) with a parabolic velocity profile, passes through the two geometrical plane channels respectively and leaves through the outlet boundary in the absence of external forces.

The model computes the blood's velocity components $u = (u, v)$ in the x- and y-directions and its pressure p in the region defined by the geometry in the preceding figure. The PDE model for this application uses the stationary incompressible Navier-Stokes equations numerically tracked in Eulerian fashion based on the governing equation discussed in Section 2.5.2

$$\rho \frac{\delta u}{\delta t} - \eta \nabla^2 u + \rho(u \cdot \nabla)u + \nabla p = F$$

where

$$\nabla \cdot u = 0$$

This first equation represents the balance of momentum from Newton's second law (refer Section 2.7.6). The other relationship is the equation of continuity, where zero on the right-hand side states that the blood is incompressible. In this model, boundary conditions have been modified so that the average velocity at the inlet is of average 0.544 m/s. In order to obtain a corresponding parabolic velocity profile, the $(u, v) = (6V_{\text{means}}(1-s), 0)$ has been set where s is a boundary parameterization variable that runs from 0 to 1 along the boundary. The fluid nature of the blood is predicted to always stay stationary at the walls, so $(u, v) = (0, 0)$ is the appropriate boundary condition set along the boundary. At the exit boundary, it has been assumed that a constant static pressure, $p = 0$, is most suitable for the experiment. Despite the fact that it is a steady - state flow model, the experimental work has been identified to require initial conditions for the reason that the incompressible Navier-Stokes equations are nonlinear. In order to achieve a numerical solution, the nonlinear solver has been picked to solve the equations iteratively.

The result from this experiment shows the benefit use of the Navier Stokes equation as proposed in the methodology (refer to Section 3.53) to handle the incompressible and laminar aspect of the flow. Using a simple geometry to describe the steady state flow, information gained from this prototype is imported in later model as basics for the simulation of the blood flow particularly in the cylindrical domains of the mitral and aortic valves.

4.2.2 Incompressible Turbulent Flow

When an irregularity occurs in a blood vessel particularly at the valves or at the site of a blood clot, the laminar stream of the blood flow is disrupted and at this point the blood flow may become turbulent. In turbulent flow the fluid streams do not remain in the parabolic profile but instead the streams mix radially and axially. More energy is needed to drive turbulent flow than to drive laminar blood flow. Turbulent flow is normally estimated using the Reynolds number method, a dimensionless number used to predict the pattern of the blood flow; either it will be laminar or turbulent.

Using the same definition as the previous experimental work, another prototype is modeled with a slight change to the geometry configuration. Narrower inlet and outlet channels have been designed and this time a wider diameter channel is allocated in the middle as the connector in between. Taking into accounts the density and viscosity of the blood as defined in the previous section, the result is presented and analyzed in the next figures.

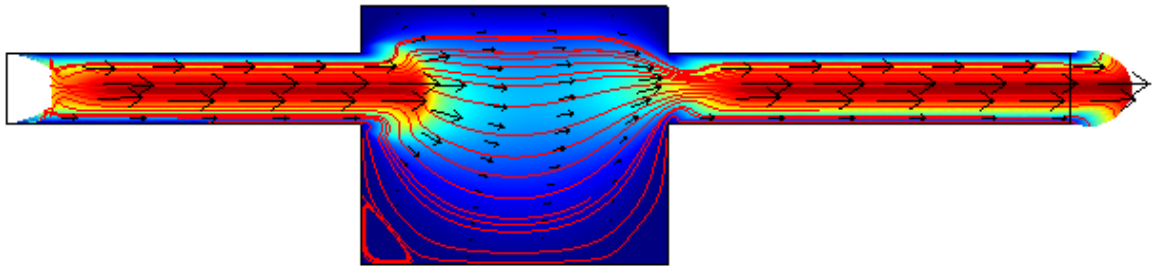


Figure 4.3: Incompressible Flow with Occurrence of Turbulent

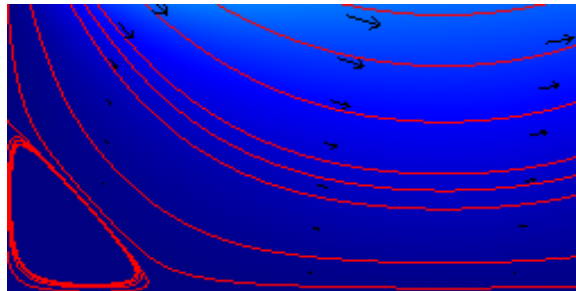


Figure 4.4: Occurrence of Turbulent in the Flow

In this flow prototype the blood is seen to enter as inlet from the left hand side and leave the geometry at the farthest right boundary. At the inlet, with the same specification of $s*(1-s)$ as velocity inflow, the blood current is seen to have the highest velocity along the center of the inlet boundary until it reaches the middle chamber, a bigger and much wider channel in diameter comparison. Here, part of the inflow is sent to the other peripheral channel on the right and part of it is used to inflate the middle chamber.

For such a fluid flow particularly the kind presented in the middle chamber of the experimental model, a velocity field with a boundary layer of thickness $\approx 1/\sqrt{Re}$ (i.e., Re being Reynolds number) can be expected at the walls. In order to resolve this steep solution gradient a few rows of elements is needed across the layer. It has been observed that for flow with bigger Reynolds number, the elements in the interior of the channel can be much

larger than those nearer to the walls. The model is then set up to solve the problem on a fixed isotropic mesh. The given input data is seen to correspond to a Reynolds number of

$$\text{Re} = \frac{0.544 \cdot 2 \cdot 0.0052 \cdot 1.23}{1.79 \cdot 10^{-5}} \approx 389$$

In order to show a clearer representation of the thickening boundary layer near the inner wall of the middle chamber, another mode of exemplary model normally known as the back step flow is used to elaborate the problem. The backward facing step is an interesting case for the studies of the performance and solution strategy of a turbulence model. In this experimental case, the flow is subjected to a sudden increase of cross-sectional area, resulting in a separation of flow starting at the point of expansion. Spatial variations in the velocity field cause production of turbulence outside the wall region and its interaction with the mean flow influences the size of the separation bubble. The size of the bubble, or the re-attachment length, is one of the quantities that must be predicted accurately by a turbulent model.

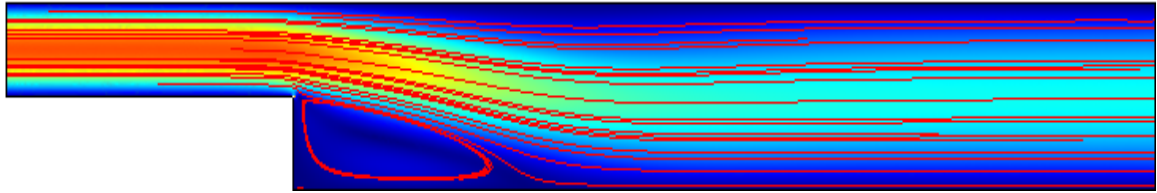


Figure 4.5: Backstep Flow with $V_{\text{mean}} = 0.1$

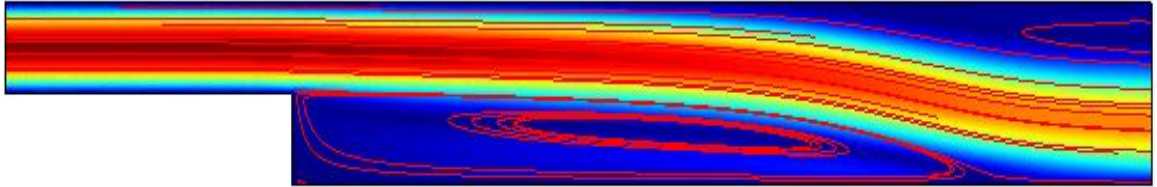


Figure 4.6: Backstep Flow with $V_{\text{mean}} = 1.0$

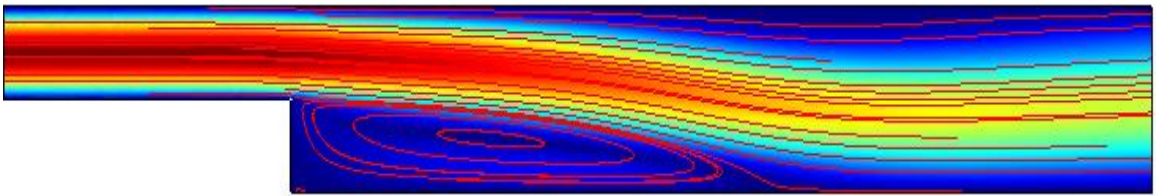


Figure 4.7: Backstep Flow with $V_{\text{mean}} = 0.5$

The preceding figures show the velocity fields in a streamline plot. A circular motion depicted behind each steps can be identified as recirculation regions which has the potential to expand with increasing Reynolds number. Three different experimental velocity values have been used to aid the experiment and the results have been recorded in the three figures presented. The distance from the step to the stagnation point where the flow reattaches to the lower wall is called the reattachment length. Using three different specifications of average velocity mean for all three experiments, the backstep flow in Figure 4.5 is seen with the shortest length of recirculation behind the step, accumulating to a low Reynolds value.

Increasing the velocity mean with a maximum value as seen in Figure 4.6 has created in generation of eddy or current flow which is observed to cross the outflow boundary, the ordeal indicating that there is an inflow through the assumed outflow boundary. This finding calls for the inclusion of more of the downstream region in the computational domain to get a reliable solution. For this matter the averaging velocity is rechecked and another mean value has been set to shorten the recirculation region, which in fact explains why the computational domain in the model presented in Figure 4.7 is slightly shorter than the one in Figure 4.6. A dimensionless number quantifying the recirculation region is the reattachment length divided by the step height. According to experimental data, this quotient is approximately 7.93 at a Reynolds number of 389.

4.2.3 Incompressible Flow with Pressure

The preliminary models tested in previous sections have idealized another experimental work to test for the incompressibility aspect of the flow in relation to the inclusion of the pressure factor. Including the pressure factor is necessary since there is a high relationship between blood flow, pressure and resistance (refer Section 2.3.2). As stated in the literature review, blood pressures are considered not equal throughout the cardiovascular system else the blood would not flow, since the flow requires a driving force (i.e., a pressure difference). The pressure difference has been identified as the driving force for blood flow, and the resistance is an impediment to flow.

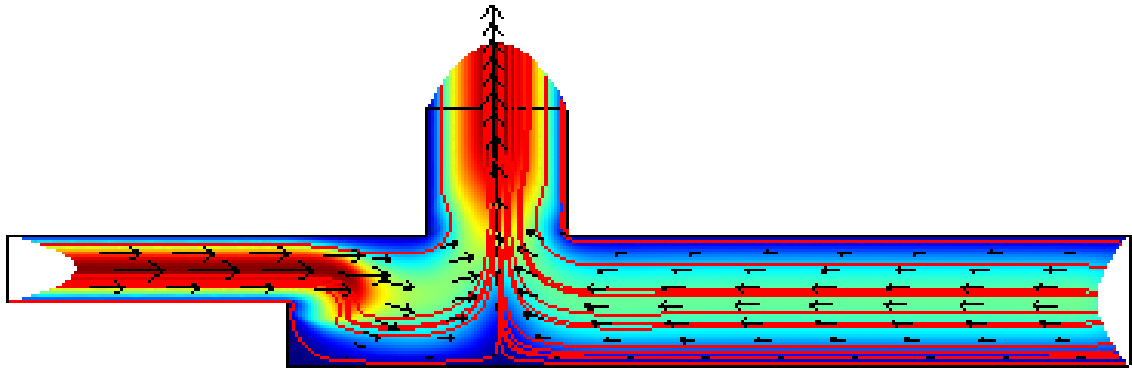


Figure 4.8: Flow with Pressure

In the experimental model depicted in Figure 4.8, the blood is seen to flow through a vessel like tube with two inlets and a channel outflow. A parabolic profile has been used to define the two end inlets but this time the incompressible profile is handled with the inclusion of the parameter pressure. The outflow channel in the middle has been defined without any pressure resulting in a difference of pressure distribution for the model. In this experimental simulation the blood is seen to travel in a steady state behavior along the vessel and out into the middle channel in a direct proportion to the size of the pressure difference or pressure gradient. This in return indicates that the direction of blood flow is governed by the direction of the pressure gradient which has always been defined as high to low. The result is comparable to the studies of the cardiovascular physiology; it has been observed that during ventricular ejection, blood flows from the left ventricle into the aorta (not in the other direction) because pressure in the ventricle is higher than the pressure in the aorta.

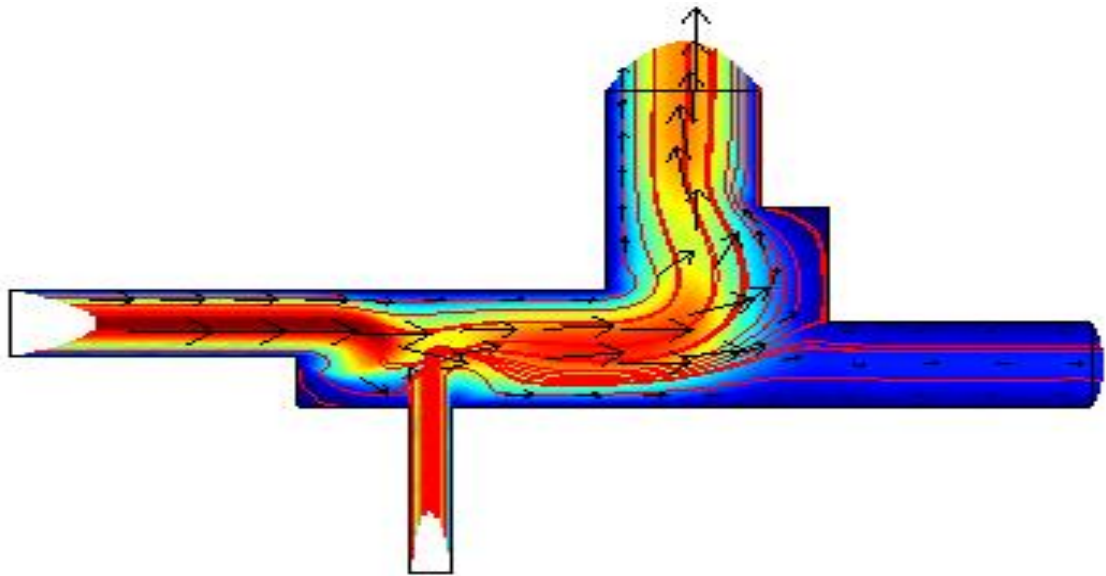


Figure 4.9: Pressure Flow with Resistance

Another preliminary work has been carried out to test the resistance theory. Defining the geometry as depicted in Figure 4.9, the geometry is modeled with two inlets of similar pressure. At the left hand side of the geometry, the blood is noticed to flow in a steady state from the inlet along the horizontal channel and is expected to leave through the outflow channel on the right. In order to test the resistance of the flowing velocity another inlet with the same pressure is created in between. Using a vertical tube half the size smaller, this second inlet carries a doubling pressure (due to the size) and gives forth a velocity flow in a normal direction towards the incoming flow from the left, resulting in a slight disruption of the parabolic profile of the flow. This small interference proves that blood flow is inversely proportional to resistance. It is clearly seen here in the experiment that increasing resistance would decrease flow and decreasing resistance would increase flow.

In order to handle the incompressibility factor for the model, the Navier-Stokes equation has been defined with Lagrange p2-p1 elements to stabilize the pressure. The 2nd-order Lagrange elements (p2) model the velocity components while linear elements (p1) model the pressure. These default element settings provide one order higher Lagrange elements for the velocity components than for the pressure. As this is a common benchmark problem in computational fluid dynamics, there has been no known exact solution, but experimental data is available (Gresho et al. 2000) making it possible to check the accuracy of the FEM solution.

4.2.4 The Stress Tensor Test

The stress tensor represents any force that the boundary exerts on the fluid. In a fluid flow example there can also be internal stresses due to the fluid pressure in addition to the stress resulting from viscous forces. The choice of stress tensor form directly affects the boundary conditions since boundary conditions depend on its pressure condition and different implementations provide different pressure settings. In order to simulate an application of stress tensor in an incompressible flow as proposed in the methodology (refer to Section 3.5.1), a neutral boundary condition can be used to set the viscous or full stress tensor for the flow. In this experimental Navier Stokes case, the pressure drop is modeled by setting the pressure at the outlet as equal to the pressure at the inlet minus a pressure drop. Using the momentum and continuity equations laid out in the literature review (refer Section 2.7.6), this formulation is derived for the model:

$$\rho \frac{\delta u}{\delta t} - \eta \nabla^2 u + \rho(u \cdot \nabla)u + \nabla p = F$$

where

$$\nabla \cdot u = 0$$

Here, ρ is the density, $u=(u,v)$ is the velocity field, p is the pressure, and η is the dynamic viscosity. A pressure drop from the left to the right boundary of the geometry drives the flow in the channel. At the walls, a no-slip boundary condition, $u=0$ has been set followed by the settings of three symmetric boundary conditions between the left and the right boundary of the geometry section. The velocities u,v are continuous and the pressure drops by a constant Δp from the left to the right boundary. The results show the expected flow behavior for the problem.

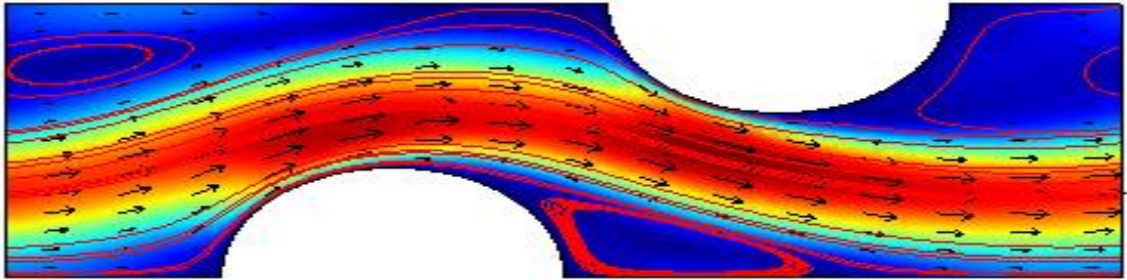


Figure 4.10: Incompressible Flow Pass Periodic Boundaries

In the geometry, an introduction of two periodic boundaries is necessary to better test the incompressible flow with a defining stress tensor condition. When using periodic boundaries, the boundary conditions need to fulfill the constraints imposed by the settings

for the periodicity. In this model the viscous stress tensor formulation is used resulting in definition of the neutral boundary condition as follows:

$$\rho \frac{\delta u}{\delta t} - \nabla \cdot [-pI + \eta(\nabla u + (\nabla u)^T)] + \rho(u \cdot \nabla)u = F$$

where

$$-\nabla \cdot u = 0$$

Extending the experiment further, it has been identified that there is a possibility to alter the fluid flow so that it uses the full stress tensor formulation. The reason is that with the full stress tensor formulation, the neutral boundary condition can be designed as

$$\rho \frac{\delta u}{\delta t} - \nabla \cdot [\eta(\nabla u + (\nabla u)^T)] + \rho(u \cdot \nabla)u + \nabla p = F$$

where

$$\nabla \cdot u = 0$$

In order to account for the full tensor stability, a new geometrical model has been designed with new boundary conditions and new periodic boundaries configurations. As seen in the following figure, the full stress tensor condition is seen to help stabilize the development of the velocity field and viscous layer as the fluid encounters two periodic walls. These boundaries have been designed at a very close proximity at the lateral boundaries forming a tight flow channel in the middle of the geometry.

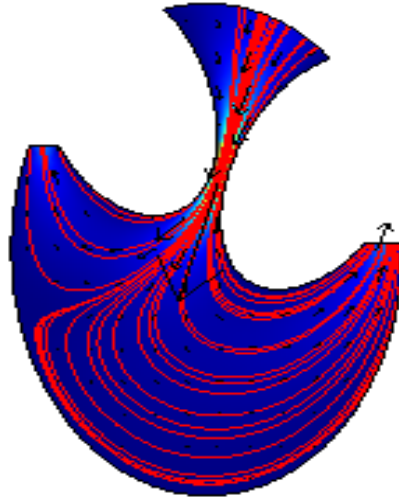


Figure 4.11: Flow Pass Tight Channel

Setting the average velocity of $14*s*(1-s)$ at the inlet, Figure 4.11 shows the fluid flow from the top boundary passed through the tight channel in the middle and into the hemispherical-shape chamber. A difference in the velocity profile in the model implies that the pressure profile is also periodic and having periodicity in the pressure indicates a pressure difference to the Navier Stokes model. This allows for the pressure properties to be discontinuous in the fluid flow.

4.2.5 The Poisson Test

The Poisson equation is identified as an important asset to solve for the mesh displacement in the moving coordinate system (refer to Section 3.51) of the ALE. Therefore general understanding of the Poisson properties is considered important in the experimental test being conducted. In this experimental model a Poisson equation has been programmed on a disc-like geometry to study the effect of pressure distribution on the mesh displacement of the model boundaries. Specifying a Neo-Hookean hyperelastic behavior as stated in Table

3.2 (refer to Section 3.5.3); the disc is given several different set of pressure constraints weighting at the center of the disc. Six different timestep plots are used to show the disc boundary movement in relation to the pressure gradient. Another circular boundary with a fixed mesh has been designed at the outer layer of the disc to show better depiction of the deformation. The results generated from the test are shown in the next figure.

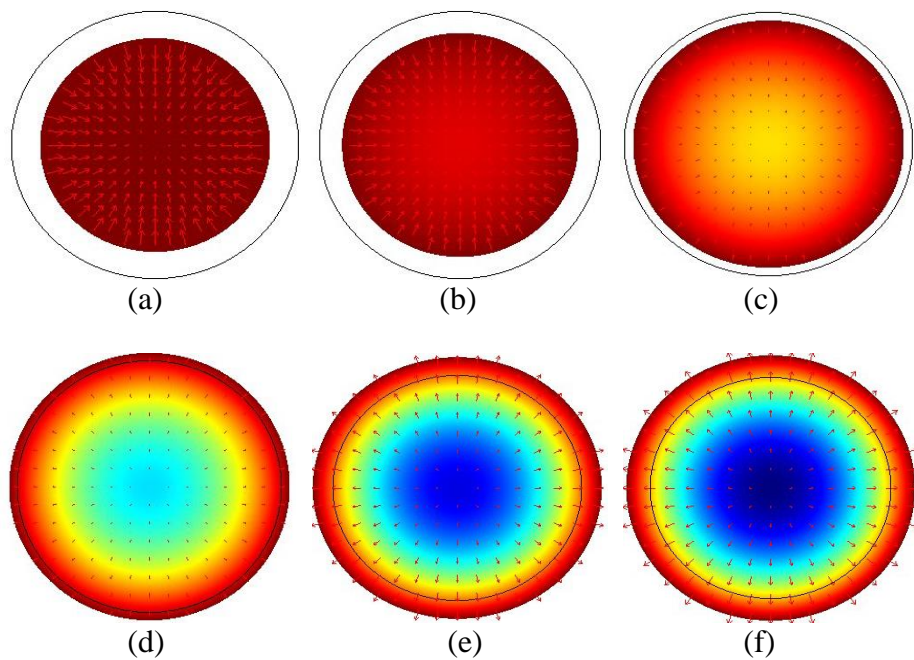


Figure 4.12: Results from the Poisson Test.

Figure 4.12 shows the disc at zero initialization of pressure. Note that the boundary of the disc stays static over time. Figure 4.12(a) is the result of the test at the first timestep. With a pressure different of 0.05, the moving boundary of the disc is seen to move discretely towards the outer layer in the second timestep. Positive development of the pressure shows further deformation of the boundary seen in Figure 4.12(c). Figure 4.12(d) is the deformation of the disc boundary leveling the fixed outer layer boundary. In Figure 4.12(e)

and Figure 4.12(f) higher pressure distribution has resulted in distortion of the moving boundary passed the fixed boundary.

4.2.6 The ALE Test

The results gained from Section 4.2.1, Section 4.2.2, Section 4.2.3 and Section 4.2.4 have been considered as valuable to the development of the left ventricle model as they supply sufficient knowledge on the major properties used in the ALE methodology; fluid flow tracked in Eulerian fashion and structural deformation depicted using the Lagrangian multipliers. In accordance to the extensive modeling presentation compiled in Section 3.5 of the methodology chapter, an experiment to simulate the ALE on a test model has been configured with the goal to study the mesh movement developed on the grid settings and to observe the domain deformation generated by the fluid-structure interaction.

Domain equations (Eq.3.1 to Eq.3.7) in Section 3.5 have been utilized to study the effects of mesh movement in a prescribed moving boundary. This experiment considers two cases. In the first case, the mesh velocity is prescribed and in the second case, the mesh velocity is left to vary freely. In this structural deformation, an incompressible inflow is seen to pass cross the disc-like geometry with a hole in the middle. The inflow and outflow of the fluid in the structure has been graphically expressed using the arrow and streamline markers, ensuing in experimental results as depicted in the following figures.

a) Results of the Mesh Movement in a Prescribed Moving Boundary

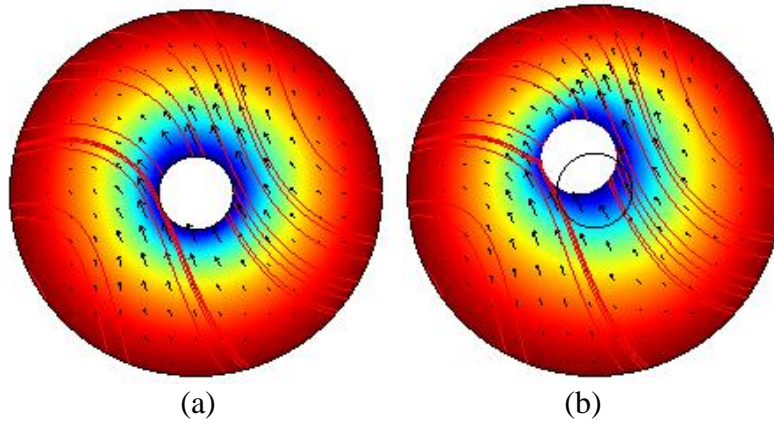


Figure 4.13: Mesh Movement in a Prescribed Moving Boundary

Figure 4.13(a) shows the mesh displacement and the mesh velocity at the initial stage of the simulation. A circular disc-like geometry with a moving smaller circular domain is designed to move according to the following pattern:

$$U = A \frac{2}{\pi} \left(-a \tan(t) \sin(t) + \frac{1}{1+t^2} \cos(t) \right)$$

$$V = A \frac{2}{\pi} \left(a \tan(t) \cos(t) + \frac{1}{1+t^2} \sin(t) \right)$$

Figure 4.13(b) represents the mesh movement on the prescribed moving boundary. In this case, the mesh displacement of the inner circular domain is recorded to move following the path of the stream flow. Comparing the velocity information from the two figures indicates that there is no major velocity change in the fluid domain; a suggestion that the mesh displacement has not affect the mesh velocity throughout the experiment.

b) Results of the Mesh Movement in a Free Moving Boundary

In the case of the free moving boundary, the mesh displacement is designed to be in a fixed coordinate system. The reason being is to simplify the equation for the mesh and to allow for smaller mesh movements. At the boundary, the wall has been implemented without any surface tension to minimize the constraints to the model under examination. These constraints have been implemented in a weak form by means of the Lagrange multipliers λ_x and λ_y . The corresponding weak terms $Y_x \lambda_x$ and $Y_y \lambda_y$ are added to the weak form of the PDE for the mesh movement.

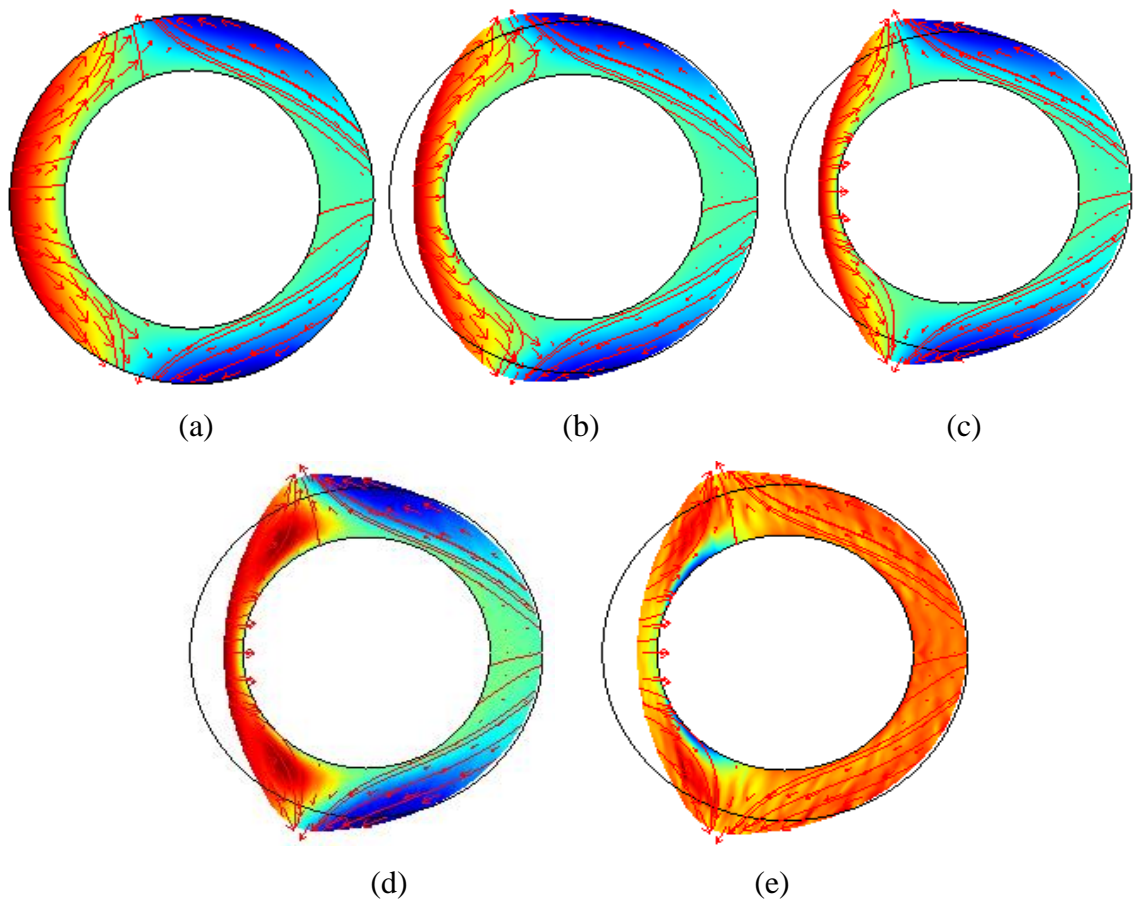


Figure 4.14: Mesh Movement in a Free Moving Boundary

The mesh displacement and mesh velocity at the initial phase can be seen in Figure 4.14(a). At the inlet on the left, the motion of the fluid is triggered by an initial velocity of a constant 1.0 and dynamic viscosity of 0.005Nsec/m². In Figure 4.14(b), Figure 4.14(c) and Figure 4.14(d) the flow is seen to move freely at the free boundary carrying the effect of the mesh velocity on the deforming boundary. Figure 4.14(e) shows a different domain plot to illustrate the pressure distribution on this simplified ALE model. In the plot, the pressure property is observed to depend mostly on the depth of the fluid.

4.3 Simulation Results

4.3.1 Incompressible Blood Flow through the Left Ventricle Model

The influence of the Neo-Hookean elasticity particularly of the walls or boundaries of the working valves has posed attention to the analyzed result relating to the calculation of the dimensionless parameter identified as an approximation of 500 Reynolds numbers, which corresponds to typical values in major arteries (Pedrizzetti et al., 1998). The flow dynamics analyzed in the rigid vessel of the ventricle chamber is seen to contribute to the instantaneous systolic and diastolic flow fields of the left ventricle model. The boundary layer of the mitral valve, developed during the acceleration, separates during systole and produces a small recirculating cell immediately at the downstream of the ventricle chamber. The separation phenomenon corresponds to the roll-up of the boundary layer and the formation of the vortex structure eventually traveling downstream (Pedrizzetti 1996).

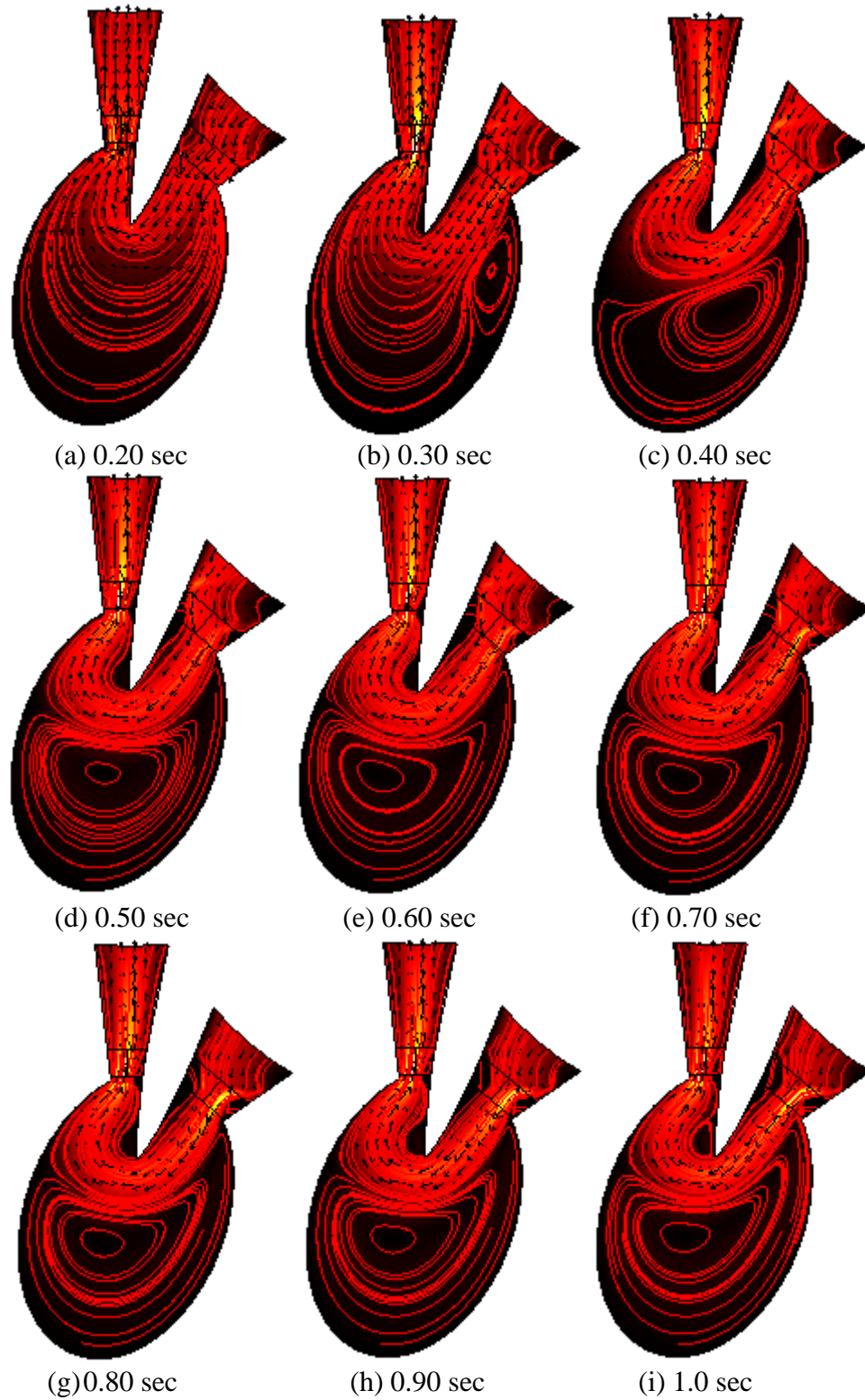


Figure 4.15: Velocity Profile in the Systolic and Diastolic Phase of the Left Ventricle Two Dimensional Simulation

Results of the two-dimensional left ventricle simulation are laid out in extensive graphical representation in Figure 4.15. Using nine different plots, the velocity profile in the systolic and diastolic phase in the one second simulation time is observed with the timestep separated at approximately 0.1sec per plot. Figure 4.15(a) and Figure 4.15(b) shows the left ventricle simulation before initialization and at the first point of initialization. At this beginning, a positive separation of vorticity indicates a persistent negative shear forces in the portion of wall downstream of the enlargement. The same flow fields are reported in Figure 4.15(c), Figure 4.15(d) and Figure 4.15(e). It can be observed that during systole the ventricle chamber is inflated with the incoming inflow from the mitral valve, pressuring the chamber to dilate and with that the flow is seen to accelerate at a maximum velocity profile throughout the chamber.

Figure 4.15(f), Figure 4.15(g), Figure 4.15(h) and Figure 4.15(i) shows the blood flow profile during diastole. At diastole the boundary layer is thicker because of deceleration and the streamlines show about a zero net flow. The deceleration decreases the flow rate indicating vessel shrinks, not seen in the simulation but is assumed to increase the actual discharge and bulk velocity from the ventricle chamber out into the aortic. During the acceleration, the synchronous deformation of the wall leads to a less extended separated region, while the contraction of the vessel during the deceleration phase of the imposed diastolic pulse tends to diminish the value of the negative tangential stress.

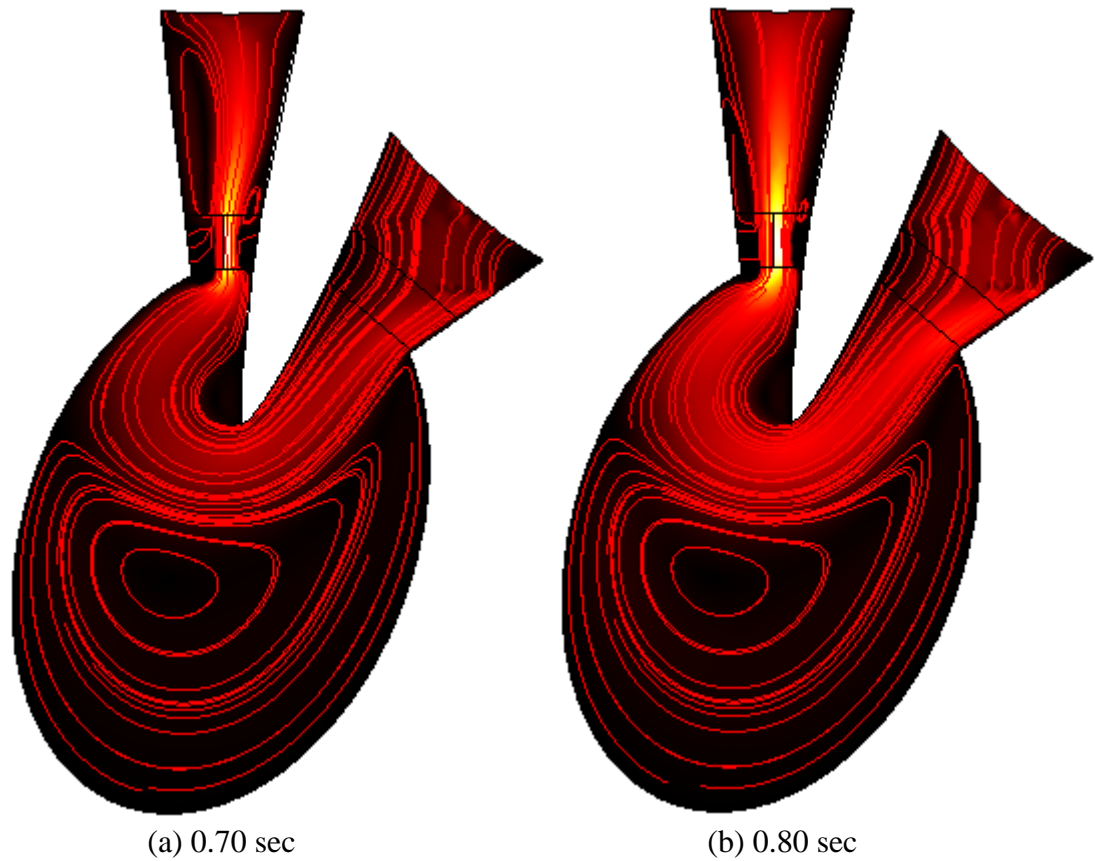


Figure 4.16: Blood Flow through the Left Ventricle Chamber during Early Systolic Phase

The flow during two instants of the early filling phase are shown above to show the behavior of the fixed mitral valve corresponding to those in both Figure 4.16(a) and Figure 4.16(b). During the accelerating stage, the conical chamber of the ventricle is bounded by a circular vortex which then rolls up into a vortex structure. In this phase the entering velocity inflow is seen with a central, approximately irrotational core surrounded by the vorticity layer. Despite the strong idealization of the model, the picture shows correct major features illustrating flow in the left ventricle during systole.

4.3.2 Simplified Valve

The motions of the leaflet boundaries in the valves play major role in depicting the velocity distribution in the left ventricle. Comprehensive description of the deforming mitral leaflet boundaries at early systolic phase is followed by a presentation on the deforming aortic leaflet boundaries at diastolic phase. The subsequent results are accessible for examination.

4.3.2.1 Deformation of the Mitral Leaflets

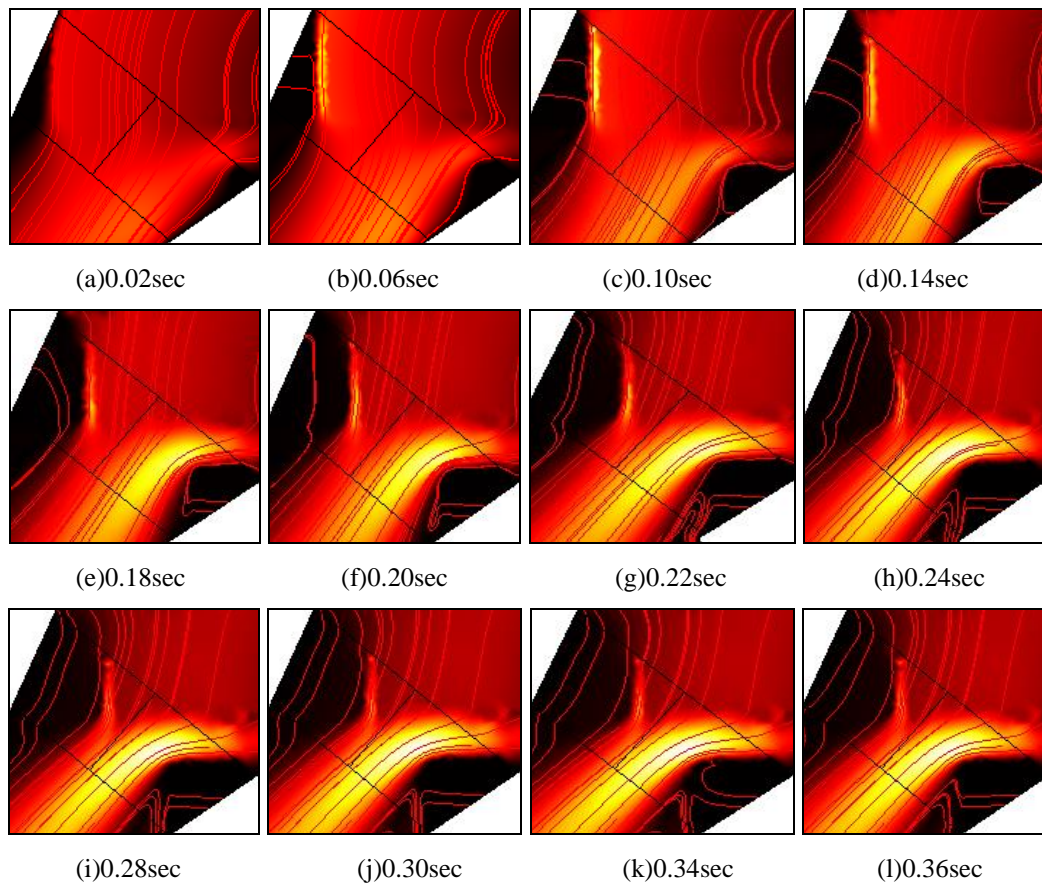


Figure 4.17: Closing Movement of the Mitral Leaflets during the Left Ventricle Contraction.

The starting results in Figure 4.17(a), Figure 4.17(b), Figure 4.17(c) and Figure 4.17(d) indicates the motion of the valve leaflets at early mitral flow. Wider inflow has been identified at this phase. In the second order of the row, Figure 4.17(e), Figure 4.17(f), Figure 4.17(g) and Figure 4.17(h) shows the movement of the leaflets at mid diastole. Here, the inflow is seen to decrease and semi closure of the mitral valve is seen. Figure 4.17(i), Figure 4.17(j), Figure 4.17(k) and Figure 4.17(l) reveals the flow pattern during the mitral valve closure.

4.3.2.2 Deformation of the Aortic Leaflets

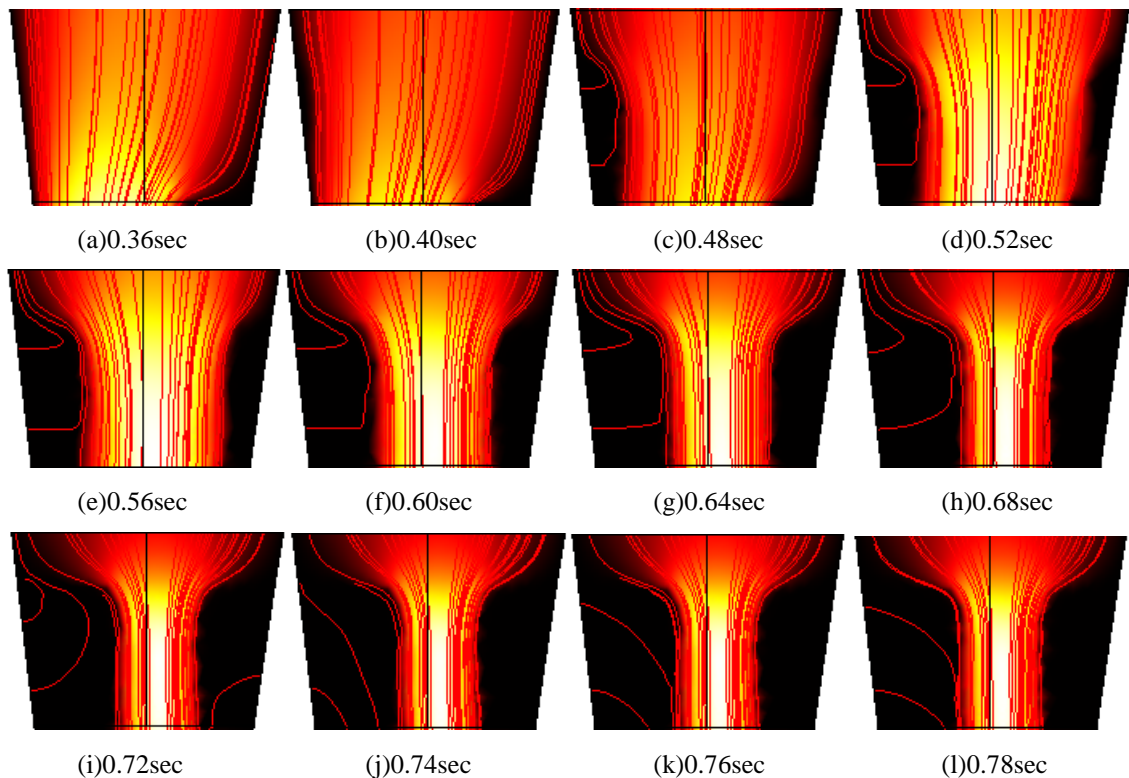


Figure 4.18: Closing Movement of the Aortic Valve Leaflets during the Left Ventricle Filling.

Figure 4.18(a), Figure 4.18(b), Figure 4.18(c) and Figure 4.18(d) denote full opening of the aortic leaflets at early ventricle contraction resulting in wider inflow of blood through the flow channel. Figure 4.18(e), Figure 4.18(f), Figure 4.18(g) and Figure 4.18(h) are the motion of the leaflets during the mid closure of the leaflets. In the last order of the row, Figure 4.18(i), Figure 4.18(j), Figure 4.18(k) and Figure 4.18(l) illustrate the motion of the leaflets during the aortic closure. In both closing motion of the valves, the lateral leaflets have been observed to gradually move towards the center of the valve resulting in thinning of the flow channels through the valve. The continuous thinning of the flow channels is identified to induce acceleration to the velocity profile of the flow. Further analysis on the velocity profile of the blood flow throughout the left ventricle chamber is presented next.

4.3.2.3 Velocity Profile in the Left Ventricle

The velocity field is visualized through a velocity vector field plot. Simplification of the plot is done by plotting only a subset of the full velocity field. In the upper left corner of each velocity field there is a plot in unit size vector corresponding to a length of 1.5 cm and a velocity of 1 m/s. In relation to flow velocity, the leaflets boundary configurations are also plotted. Figure 4.18 shows a plot of the velocity field and the aortic boundary configuration at the same twelve equidistant times as in Figure 4.17. Even though velocity vectors are seen to cross the heart boundary, this does not mean that fluid is leaking through the walls. Rather, this is a consequence of the heart boundary moving with the fluid velocity.

Using information gained from the velocity field, velocity time profiles at given positions is computed; this is the time variation of the velocity over a given line segment or at a given point focusing on velocity time profiles at the mitral valve, between the mitral leaflet boundaries, and across the aortic outflow. The mean velocity time profiles are calculated as the mean velocity over a line segment relative to the moving left ventricle boundary. It is also important to look at the velocity time profile of the centre velocity, which is simply the velocity component normal to the line segment at the centre point of the line segment. The centre velocity is reported as the velocity relative to the computational grid, i.e. in a reference frame fixed in space.

Figure 4.19 shows the velocity time profile of the mean velocity through the mitral valve and between the mitral leaflet boundaries during 2 heart cycles. Figure 4.20 shows the velocity time profile of the mean velocity across the aortic outflow during 2 heart cycles. From the velocity field flow data is obtained over a given line segment. Flow is computed by the mean velocity over the line segment multiplied by the length of the line segment. This gives a flow in the dimension of area per time, which is the natural dimension of flow in a 2D model.

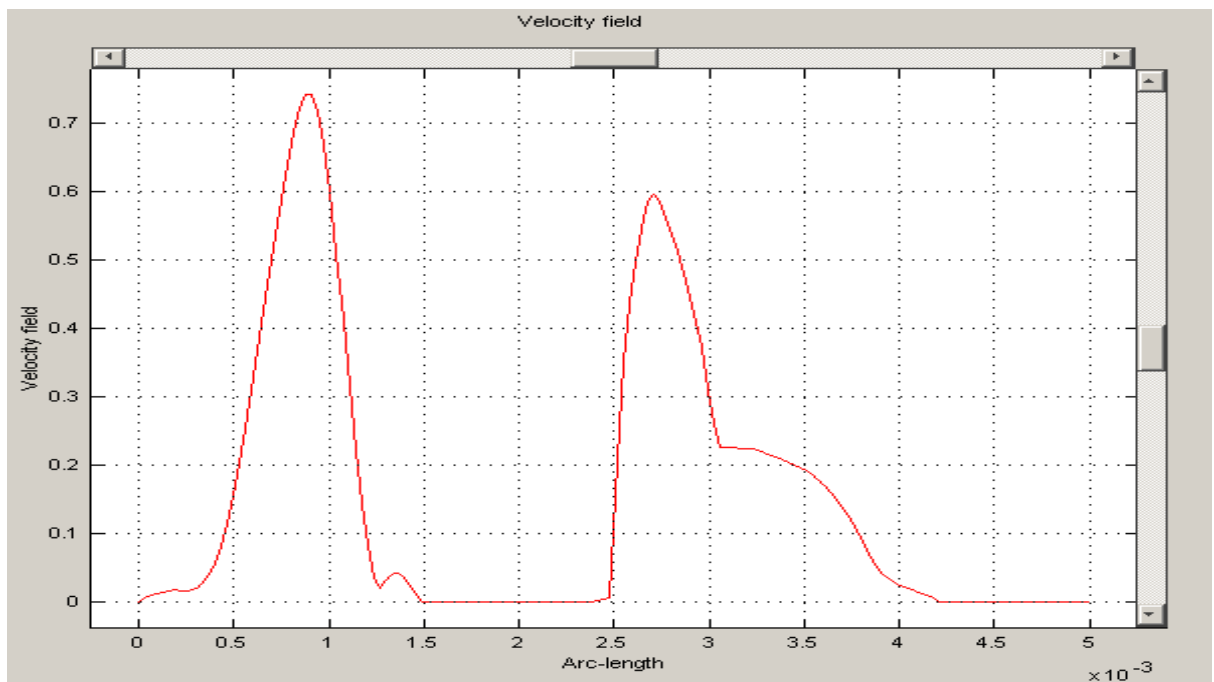


Figure 4.19: Velocity time profile of the mean velocity (cm/s) through the mitral valve and between the leaflet boundaries.

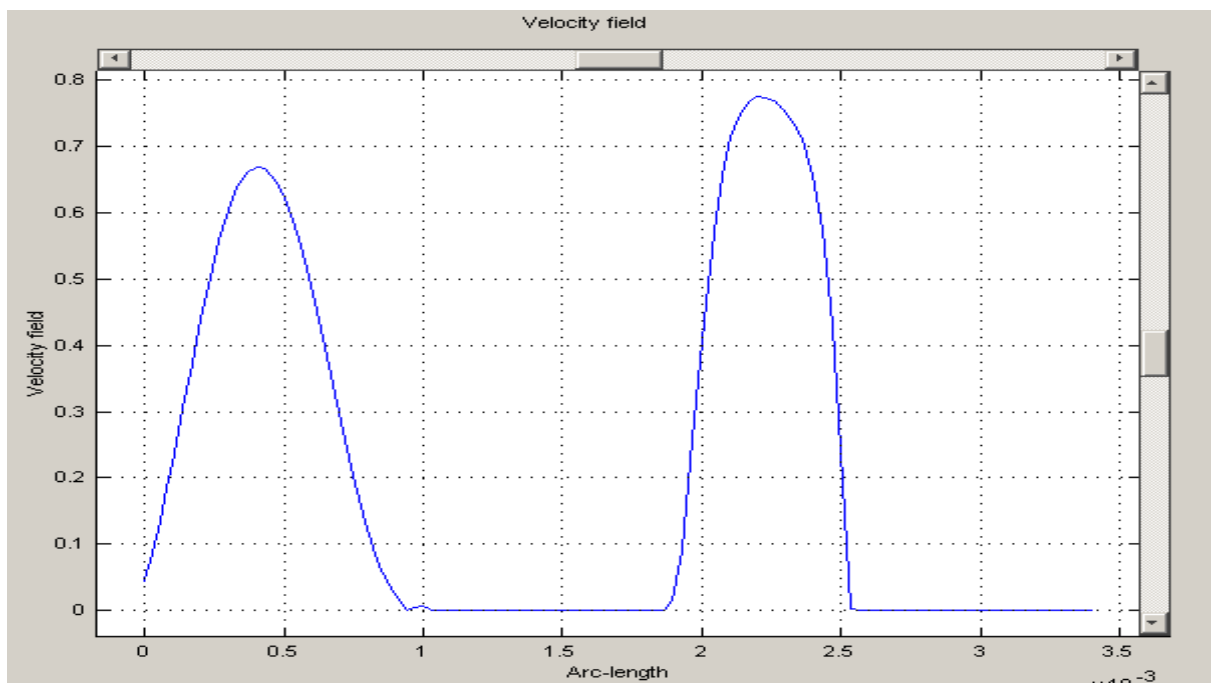


Figure 4.20: Velocity time profile of the mean velocity (cm/s) across the aortic outflow and into the aortic cylinder.

4.3.2.4 Periodic Motion of the Leaflets

The movements of the simplified valve leaflets are in general governed by the ALE modeling described in Section 3.5 but further extension to the mesh movement displacing certain boundaries is considered a necessity to account for the periodic behavior of the valves. Specifying a discontinuous function known as the Heaviside Step Function to cater for the time-stepping problem of the leaflets, emulating the step in asynchronous order is possible by manipulating the boundaries according to a sinusoidal function of time. Results from the valve simulations are laid out as follows.

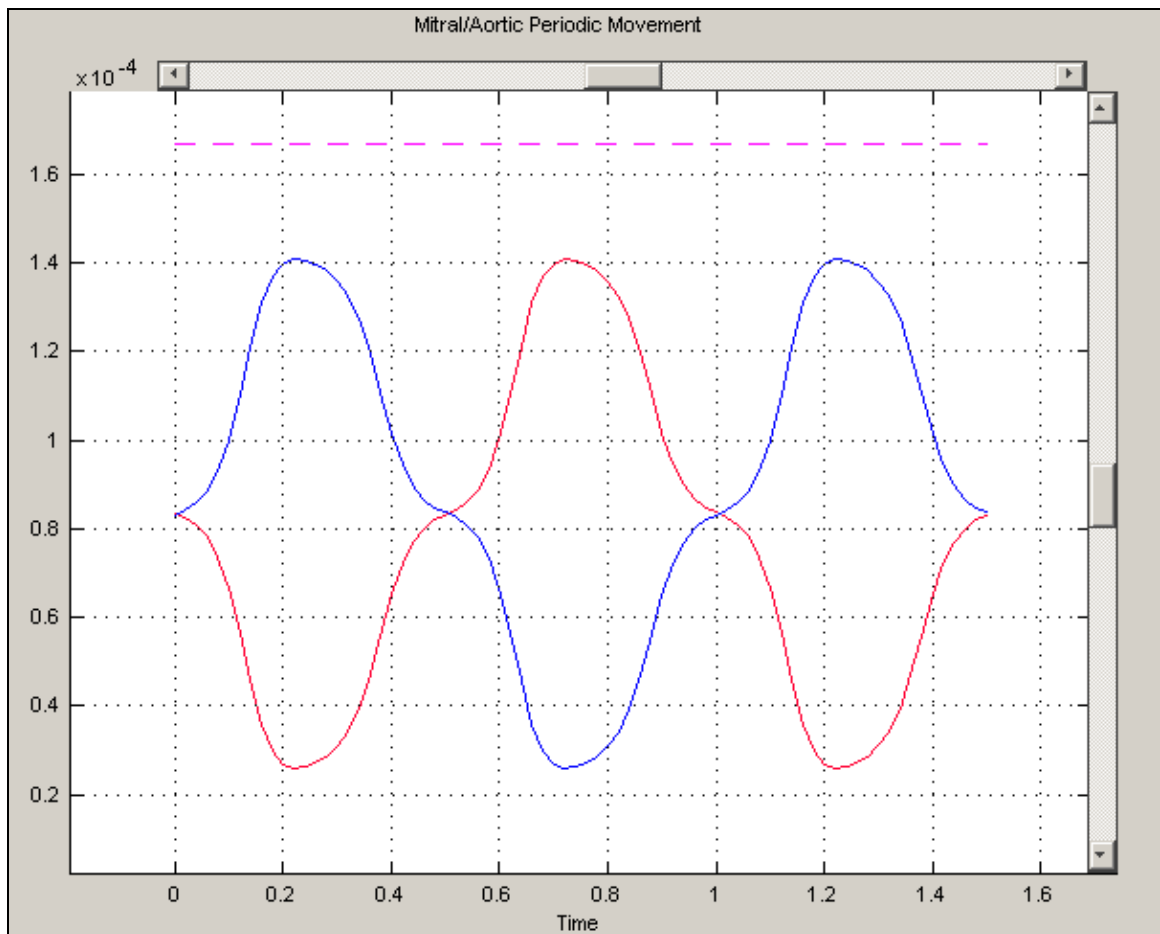


Figure 4.21: Periodic Flow due to the Periodic Motion of the Mitral and Aortic Valve Leaflets

Figure 4.21 denotes a plot of the flow rates passing through the mitral and aortic valves as well as the total flow rate over time. The blue line indicates the flow passed the mitral during systolic and the red line is the representation of the flow rate passing the aortic valve during the left ventricle dilation. The purple line (dashed) at the top of the graph is the sum of the flow in the ventricle chamber.

4.4 Conclusive Remarks

Velocity profile deriving the phenomenon involved in the blood flow of left ventricle is briefly revised. The mesh movement exercised using ALE method depicting the opening and closing movement of the mitral and aortic valves have been thoroughly investigated. Discussion on periodic behavior of the valves in relation with the corresponding fluid-structure interaction in the model is also illustrated in the chapter.

Chapter 5

Discussion

See simplicity in the complicated.

Lao Tzu

5.1 Overview

A basic framework research to study the dynamics of blood flow in the left ventricle has been covered in detail in Chapter 3 and Chapter 4. Arbitrary Lagrangian–Eulerian method is the manner employed to incorporate the leaflet motion in the simulation. Forces exerted by the fluid on the leaflets are computed and applied to the leaflet equation of motion to predict the leaflet position or displacement. Relative large velocities are computed in the valve flow region during the ventricle filling and the resulting large wall stresses controlled using stress tensor techniques can be seen during the ventricle filling duration. Results stemming from these implementations are thoroughly investigated following description on several related issues and techniques in the visualization of the mathematical model.

This chapter highlights the model assumptions concerning to the physiological aspects of the left ventricle architecture. Accuracy and convergence matter of the finite element model is also weighted with interest along discussions on the mesh generation used in the ALE model, utilization of weak constraints in the mesh movement design and the stabilization technique opted to stabilize the blood flow streams in the simulation. The hardware limitations are given a section with contribution highlights and suggestions for future direction of the project concludes the chapter.

5.2 The Left Ventricle Architecture Limitation

A presentation of framework analyzing point-sampled geometry on a discrete surface data stemming from 3D acquisition devices has been presented. A finite number of possibly noisy samples have been identified to provide incomplete information about the underlying surface captured for the reconstruction of the left ventricle. Using adaptive re-sampling method to optimize the scanned data in the presence of noise has help to capture a plausible geometrical configuration of the left ventricle from unstructured cloud of samples points, where each point is a discrete sample of certain shape attributes such as positions, surface normal, color or material properties.

High level information about the scanned left ventricle is retrieved by creating a rendition that is meaningful, particularly in terms of physiological view. Specific geometrical processing algorithms have been utilized in the rendering to obtain a continuous 3D surface defined by triangle meshes and collections of spline-patches computed from the given point data. Having obtained such a distinct surface model all subsequent processing then directly operates on this representation without any reference to the origin of the data.

5.3 Discussion on the ALE Modeling

Prior to the 3D surface reconstruction of the left ventricle, it has been possible to acquire sufficient information on the left ventricle based on comparison with various works, (de Hart et al. 2000 and Hughes et al. 1981). In regards to this matter, the information gathered has been identified as satisfactory and can be considered as useful to understand the ventricle's fundamental morphology, general and ultra structure of anatomy and its geometric configuration. Originally it is hoped that the 3D model could be used as a strong base for the left ventricle simulation but it was later recognized that the 3D model is computationally too demanding to cater for the many processing algorithm for the ALE modeling, particularly in a finite element environment. A 2D solid model has been derived from the 3D surface model and used in the project as a preliminary prototype which will later be extended to three-dimension. This will be possible if there is enough computational power.

5.3.1 Analyzing the Finite Element Convergence and Accuracy

The beauty of utilizing the finite element as a platform for the ALE modeling is the accessibility to analyze the model convergence and accuracy. Mesh movement methods comprising techniques to track the motion of the fluid and boundary in Lagrangian and Eulerian fashion, technically, are considered with high level of difficulty. The characteristics of the partial differential equations (PDEs) form the shape of the mesh movement modeling and selection of suitable PDEs in the methodology can improve model convergence and help reach an accurate solution.

5.3.2 The Mesh Generation

Attachment of boundary conditions, load conditions, and material properties to element and nodes is an essential part of generating a mesh. Analyzing the stress quality to determine displacement constraints is a simpler matter if assignment of boundary conditions is done on a solid geometry rather than to individual elements and nodes. For this reason, selection of vertices, edges and faces instead of elements and nodes to designate locations of boundary conditions is a better option instead of using elements and nodes. The elements and the nodes are too fine grain of entities to handle in large scale mesh model. Assumptions made in accordance to the observation of the valve motion during the ventricular activities are weighted heavily in the interest to select the most optimized meshing for the left ventricle model.

5.3.3 Usage of Weak Constraints

In this project, it is important that the finite element model accurately capture local variations in the solution such as the stress concentrations, pressure distributions, volume forces and parabolic profile of the flow velocity. Each property has been tested using several specific experimental works and the results obtained have been compared to values from several reliable sources of data. A handful of equations and extended parameters have been attempted in modeling the physical attribute of the non-linear problem and it is always wise in the development to start the solution process in accordance to these patterns:

- Utilize the general or the weak solution form to handle coupling of variables as they provide exact Jacobians and are considered best suited for nonlinear PDEs.
- Supply the model with the best possible initial value.
- Ensure that the boundary conditions are consistent. In doing solid modeling, boundaries adjacent to each other must be of similar attribute and values. Failure to do so would include problem in solving the physics of the boundaries as their matrix dimension does not agree to each other.
- Use the time-dependent solver and set appropriate time span so that the solution reaches a steady state which generally results in a smoother convergence.

5.3.4 Coupling of Variables

The coupling of variables is the key design behind the periodic conditions of the valve leaflets motions unfortunately the Jacobian elements introduced in the weak form equations as matrix in the computational domain, is usually large but sparse. Further observation indicates that the Jacobian solution at each node in the mesh is directly affected by the degree of freedom from the neighboring mesh elements. Introducing coupling variables help create non-local dependencies which release the sparsity of the Jacobian matrix and benefit the memory use and CPU time consumptions.

5.3.5 Artificial Stabilization Techniques

An artificial stabilization technique is a necessary supplement to the ALE modeling particularly in the fluid mechanics problem where diffusive terms are introduced through the viscosity of the blood properties. This is the same information contained in the dimensionless Reynolds number used to predict occurrence of turbulence in the flow

model. For the Navier Stokes equation employed in the ALE system, the use of streamline diffusion has helped to stabilize the streamlines plot in the model for better quality postprocessing and visualization of the left ventricle simulation.

5.4 Hardware Limitations

The model simulated in this project has been used for comparison with physiological experiments and for this matter it is important to determine at which point the model becomes periodic. Expansion of simulation time is considered beneficial to study the periodic behavior of the left ventricle cycles. In order to predict the appropriate cycle number for the simulation, the length of computation time is a factor to consider. In reference to the development process, completion of two cycles of the left ventricle takes approximately 4½ hours to compute on a 1GB Pentium IV Processor. Due to the complexity of the numerical model, many simulations are needed before the correct setting of the model is achieved. This explains the requirement for a short computation time.

5.5 Assumptions on the Left Ventricle Model

It can be deduced that the study of several principles governing the blood flow; velocity of flow, pressure and resistance relationships, are with strong benefit to modeling the physics of the ALE, also in selecting appropriate PDEs for the flow and moving boundaries. Thus, the following assumptions have been derived for the left ventricle model:

- Velocity of blood flow is proportional to the rate of volume flow and inversely proportional to the cross-sectional area of the inlet boundary. Having the larger cross-sectional inlet boundary between the two valves, velocity is depicted to be

lower in wider flow channel such as the mitral valve and higher in narrower flow channel such as the aortic.

- Blood flow is proportional to the size of the pressure gradient and is inversely proportional to the resistance of the blood vessels, vessels identified in the project as the valve cylinders and the ventricle chamber.
- Resistance to blood flow is assumed to be proportional to the viscosity of blood and the inlet length and inversely proportional to the inlet radius.

Pursuing these assumptions, the velocity profiles at the mitral valve and aortic outflow tracked from the ALE simulation is discovered to match reasonably well in comparison to fundamental physiology measurements. The timing of the velocity profiles is seen to be in good agreement, whereas the shape and maximum values of the velocity curves show some difference. The best agreement for the mitral velocity profile is at the beginning of the heart cycle, while the best agreement for the aortic profile is from the beginning until maximum outflow velocity.

5.6 Evaluating the blood flow in the left ventricle model

Obtaining a mathematical evaluation of the flow model requires further investigations to the available physiological data. In the project, flow properties of the blood has been thoroughly investigated using results from the ALE model and the assumptions in presentation have been derived based on comparison with agreeing physiological data. The work of Yellin (1995) on pressure, flow and volume events during the cardiac cycle has

been used to evaluate the pattern of blood flow particularly during the mitral inflow and the aortic outflow in this research.

Using information from the completed left ventricle simulation, two graphs have been specifically derived to show the pattern of the aortic outflow (seen in Figure 5.1(a)) and the pattern of the mitral inflow (refer to Figure 5.1(b)). Using 15 streamlines to plot the blood flow pattern in each plot, both graphs are compared to the graph obtained from that work (Yellin).

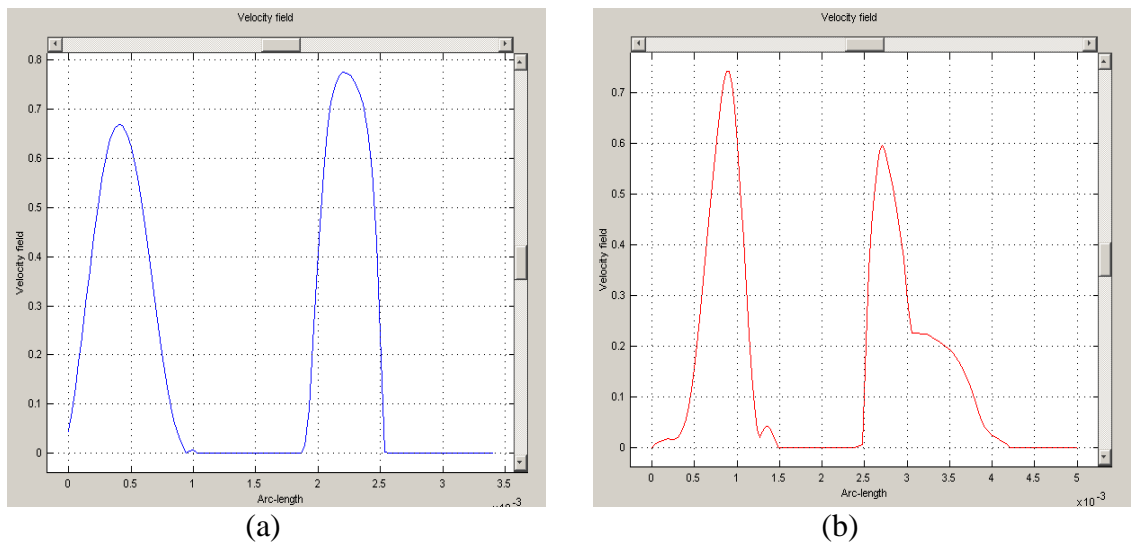


Figure 5.1: Blood flow pattern in (a) the Aortic Outflow and (b) the Mitral Inflow

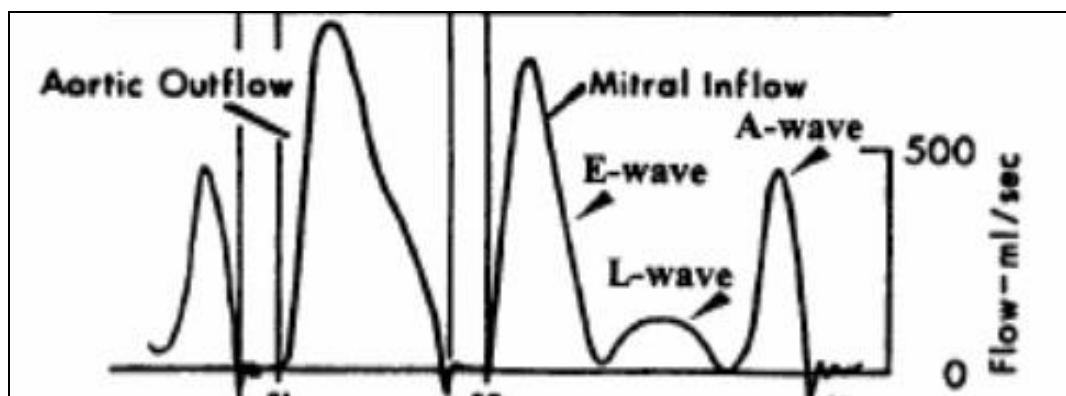


Figure 5.2: Flow Events in the Cardiac Cycle from Yellin (1995)

The data depicted in Yellin's work is a result stemming from an electrocardiogram (ECG) monitoring of the electrical pulses in the left ventricle. Further explanation on the work on cardiac mechanics has been discussed in Section 2.2.2. The ECG has been used in that research to reflect the total or summated timing within the event of the ventricular activities during the cardiac cycle and is reported to coincide with experimental data on a normal heart.

5.6.1 Evaluating the Aortic Outflow

Figure 5.1(a) depicts the velocity pattern of the aortic outflow for the left ventricle model. Based on the graph in Figure 5.2, direct comparison can be made between both aortic patterns. Reading the graph from left to right, the aortic outflow in the physiological experiment is seen to have two velocity peaks and is separated with a gap in between. This pattern explains the differing velocity peaks which pass through the aortic from the ventricle and out to the arteries. The first peak on the left indicates the velocity of the flow during the early ventricular filling, which means that the aortic valve leaflets are closing and that the flow passing through the aortic is decreasing. The gap in between represents the pattern at the time the valve is fully closed. The flat pattern in the graph indicates that there is no flow passing through the aorta during the ventricular diastole. Towards the end of the ventricular filling, i.e. the last phase of the diastole, pressure accumulated in the ventricle chamber forces the aortic leaflets to open and ejects the blood out into the aorta. This high velocity profile outflow is shown in the graph after the gap and is also seen in the graph from the simulated results.

The problem with the aortic outflow in the simulated result (i.e. Figure 5.1(a)) is at the closing stage of the aortic leaflets due to the ventricular filling. It has been identified in the simulation that the above-mentioned problem may arise due to insufficient convergence of the aortic leaflets. In the development, the Heavyside step function has been applied on the mesh displacement in the leaflets domain. However the step function was unable to unite the cross-link between the simplified leaflets of the valve, resulting in a delay in the closing stage of the aortic valve during ventricle dilation. For this reason, the blood is allowed to be ejected out through the aortic valve in longer period, consequently deriving a higher peak velocity in the simulation in comparison to the available physiological experiment.

5.6.2 Evaluating the Mitral Inflow

Figure 5.1(b) shows the velocity pattern of the mitral inflow for the left ventricle model. Based on the graph in Figure 5.2, direct comparison can be obtained between the mitral inflow pattern from the simulation and the mitral inflow pattern from the physiological experiment. Three stages of the mitral activities can be seen in Figure 5.2; the E-wave that depicts the rapid or early filling phase, the L-wave that shows the diastasis and the A-wave which represents the flow pattern during the atrial contraction. When the pressure in the left ventricle falls lower of that in the left atrium, the mitral valve is forced to open and the blood is allowed to fill the ventricle chamber. In this early filling phase, the inflow from the left atrium is considered with high pressure resulting in high velocity profile of the inflow through the mitral's orifice. Similar pattern is identified from the charted graph derived from the simulation work. The gap in between the two velocity peaks in the graph identical

to the gap for the aortic outflow discussed in Section 5.5.1 carries similar information. It depicts the closing stage of the mitral valves during the end-ventricular filling. The only different is the work by Yellin (1995) accounts for the small amount of filling from the pulmonary vein flow, i.e. the L-wave or the diastasis. In this work, the L-wave was not considered and does not fall within the scope of the research. However, in future work, it would be an added advantage to the result, if the diastasis analysis is included. At the end of the ventricle contraction, the mitral valve is again opened to allow inflow for the ventricle filling. Similar to the pattern in the aortic outflow, this high velocity profile inflow is shown in the graph after the gap and it has been encouraging to see comparable results in the graph from the simulated results.

5.7 Contribution Highlights

The 2D ALE model presented in this thesis supports the study to investigate the blood flow in the left ventricle and its interaction with the structure and function of the valves provided that the limits of the model are kept in mind. The detailed flow of the blood inside the left ventricle ALE model should not be used for investigations before the model is further improved particularly with respect to the vortex pattern in the ventricle chamber. Based on the comparison between the mitral velocity profiles, it is justified to use the ALE model to investigate the early filling in the ventricle chamber in relation to the influence of flow from the mitral valve. It is also a fair justification that investigations involving the aortic outflow profiles are beneficial in the studies pertaining to responses of the left ventricle to different physiological cases such as reaction to an increased pressure and resistance in the outflow, or, responses of flow to stiffer boundaries that depicts the ventricular and valve walls. Assessment to these problems limits the expectation to obtain complete simulation of

the flow field in the left ventricle but properties such as the form of the velocity profile and the motion of the valve leaflets during a cycle can be obtained from the simulated model.

5.8 Suggestions for future work

It is supposed that the 2D ALE model presented in this thesis is fairly reasonable in understanding the blood flow in the left ventricle of the heart. In consequence to the limitations discussed in the previous section, suggestions for future work for the developed model should include investigations and simulations similar to the following scenarios:

- Diastolic function. The investigations presented in this thesis could be extended by simulating a higher stiffness property at certain part of the ventricular wall due to an infarction.
- Aortic valve stenosis. This narrowing of the aortic valve can be better simulated by introducing one or several cross links in between the three aortic valve leaflets which would allow for better closure during the ventricle dilation.
- Mitral valve regurgitation. This is backflow of blood from the ventricle to the atrium (through the mitral domain) due to mitral valve deficiency and has the potential to be simulated by introducing bending resistance in the mitral leaflets, which would cause them not to close. Bending resistance can be introduced by the procedure described in Peskin and McQueen (1989) on modeling prosthetic heart valves.

- Blood as micro-polar fluid. A more realistic way to depict the motion of blood flow is to model blood as micro-polar fluid. The entire pathway of the bloodstream in the left ventricle; which starts from the mitral valve, through the ventricle chamber and out of the aortic valve, can be set with periodic conditions and modified Navier-Stokes equations to account for rotational effects of blood cells. The main challenge here would be to control the blood micro-rotation using specific fluid pressure and vorticity.

The results presented in this thesis support the idea of computational models as a tool for understanding the blood flow or hemodynamics in the left ventricle of the heart. However, since the intra-ventricular flow pattern is in real time, a three dimensional, future works should eventually be performed with a 3D virtual model. It is understood that this would not have to be a computationally demanding model of the entire heart, like the model of Peskin and McQueen (1980). Instead, a simpler 3D model of the left side of the heart would be enough to meet the demands of a hemodynamic tool. The work presented here has shown that an anatomically simplified 2D ALE model can, within limits, has the ability to predict physiologically correct flow patterns. Thus a simplified 3D ALE model in vision should also be able to comprehend such task and perhaps furthermore. Detailed evaluation and validation on such virtual 3D model can be well examined with comparison to dependable sources of data for example the MR (magnetic resonance) velocity data. Upon completion of such implementation, the model could be utilized for investigations incorporating similar cases presented in this thesis and those suggested above in reference to the future work.

Chapter 6

Conclusion

The Noblest Pleasure is The Joy of Understanding.

Leonardo Da Vinci

6.1 Assessment

This thesis has reviewed the basic framework used to derive a model of blood flow in the left ventricle by means of a two-dimensional ALE modeling. In addition, simplification of the valves to represent the mitral and the aorta in the left part of the heart has been considered a major priority in the construction process. Emphasizing blood regulation through the left ventricle, the flow is assumed to be incompressible, non-Newtonian, and is depicted to have parabolic velocity profile. The valves, albeit with much simplifications, played very important role in determining the pattern of flow in the ventricle chamber. In accordance to these parametric demands the working valves have been designed with a periodic behavior similar to physiological data obtained from various sources.

It is clear that the interaction between theory and experiments must be iterative. In successive investigations, there is hope for each process to converge and with that an understanding of the problem is expected to achieve both qualitatively and quantitatively. With such understanding, prediction of changes in the flow pattern in the left ventricle can be derived with conviction pertaining to changes to various anomalies such as difference to boundary conditions or the material properties. In the early phase of the development acquiring information about the constitutive equation best suited for the model is a tiring but weighted as most important for without the constitutive laws, no reliable analysis can be done.

On the other hand, without the solution of boundary valued problems the constitutive laws cannot be determined. For these very reasoning, resulting experiments are recognized with high degree of difficulty and often the case of nonlinearities as with the work in this

project. With each modeling case, the results are optimized to yield to the desired agreements else new analyses based on a different starting point would have become a necessity.

REFERENCES

- Aluri, S. and Chandran, K. B. 2001. Numerical simulation of mechanical mitral heart valve closure. *Journal of Biomedical Engineering* 29:665–676.
- Aluri, S., and Chandran, K. B. 2001. Numerical Simulation of Mechanical Mitral Heart Valve Closure. *Ann. Biomed. Eng.* 29:665–676.
- Arts, T., Prinzen, F. and Reneman, R. 1993. Mechanics of the wall of the left ventricle. *Institute of Physics Publishing* pp.153-173.
- Atlas of Echocardiography. 14 January 1999.
http://info.med.yale.edu/intmed/cardio/echo_atlas/references/heart_anatomy.html
(accessed May 9 2006).
- Baaijens, F. P. T. 2001. A fictitious domain/mortar element method for fluid-structure interaction. *Int. J. Num. Meth. Fluids* 35:743–761.
- Batchelor, G. 1967. An introduction to fluid dynamics. Cambridge University Press, London.
- Bellhouse, B. 1972. Fluid mechanics of a model mitral valve in the left ventricle. *Cardiovascular Res* 6: 199-210.
- Beneken, J. and Wit, B. 1967. A physical approach to hemodynamic aspects of the human cardiovascular system. Saunders pp.1-46.
- Berne R. M. and Levy, M. N. 1967. Cardiovascular Physiology. St. Louis pp.312.
- Bertrand, F., Tanguy, P. A. and Thibault, F. 1997. A three-dimensional fictitious domain method for incompressible flow problems. *International Journal Num. Meth. Fluids* 25:719–736.
- Bluestein, D., Einav, S. and Hwang, N. H. 1994. A squeeze flow phenomenon at the closing of a bileaflet mechanical heart valve prosthesis. *Journal of Biomechanical Engineering* 27:1369–1378.
- Brezzi, F. and Fortin, M. 1981. Mixed and Hybrid Finite Element Methods. Springer-Verlag pp.350.
- Brutsaert, D., U. Stanislas, and T. Gillebert. 1993. Diastolic failure: pathophysiology and therapeutic implications. *American Journal Cardiology* 22: 318-325.
- Brutsaert, D., and S. Sys. 1989. Relaxation and diastole of the heart. *Physiol Rev* 69: 1228-1234.

- Cebeci, T. and Bradshaw, P. 1977. Momentum transfer in boundary layers. McGraw-Hill pp.22
- Chandran, K. B. 1992. Cardiovascular Biomechanics, New York University.
- Cheng, R., Lai, Y. G. and Chandran, K. B. 2003. Two-dimensional fluid-structure interaction simulation of bi-leaflet mechanical heart valve flow dynamics. *Heart Valve Dis.* 12:772–780.
- Cheng, R., Lai, Y. G. and Chandran, K. B. 2004. Three-dimensional fluid-structure interaction simulation of bi-leaflet mechanical heart valve flow dynamics. *Annals of Biomedical Engineering* 32:1471-1483
- Chorin, A. J. 1968. Numerical Solution of the Navier Stokes equations. *Journal of Mathematical Computation* 22:745-762.
- Costanzo L. S. 1998. Physiology. Saunders pp.99-111.
- de Hart, J. 2002. Fluid-Structure Interaction in the Aortic Heart Valve: A Three-Dimensional Computational Analysis. Ph.D. diss., Eindhoven University of Technology.
- de Hart, J., Peters, G. W. M., Schreurs, P. J. G., and Baaijens, F. P. T. (2000) A two-dimensional fluid-structure interaction model of the aortic valve. *Journal of Biomech.*, 33(9):1079–1088.
- Donea, J., Giuliani, S. and Halleux, J. P. 1982. An arbitrary Lagrangian-Eulerian finite-element method for transientdynamic fluid structure interactions. *Comp. Meth. Appl. Mech. Engng.* 33:689–723.
- Ethier, C. R. and Steinman, D. A. 1994. Exact fully 3D Navier-Stokes solutions for benchmarking. *Int. J. Num. Meth.Fluids* 19:369–375.
- Fung, Y. C. 1981. Biomechanics Mechanical Properties of Living Tissues. Spring-Verlag, New York.
- Gijsen, F. J. H., Allanic, E., Vosse, F. N. and Janssen, J. D. 1999. The influence of the non-Newtonian properties of blood on the flow in large arteries: steady flow in a carotid bifurcation model. *Journal of Biomechanics* 32:601–608.
- Gijsen, F. J. H., Allanic, E., Vosse, F. N. and Janssen, J. D. 1999. The influence of the non-Newtonian properties of blood on the flow in large arteries: unsteady flow in a 90° curved tube. *Journal of Biomechanics* 32:705–713.
- Glowinski, R., Pan, T. W. and Periaux, J. 1998. Distributed Lagrange multiplier methods for incompressible viscous flow around moving rigid bodies. *Comp. Meth. Appl. Mech. Engng.* 151:181–194.
- Gray, H. 2003. Gray's Anatomy. PRC Publishing Ltd. pp.635

- Gresho, P. M. and Sani, R. L. 2000. *Incompressible Flow and the Finite Element Method (Volume 1 & 2)*. John Wiley & Sons, New York.
- Guadagni, G., Fiore, G. B., Martino, E. D., Redaelli, A., Fumero, A., Dubini, G., Inzoli, F. 2001. A fluid-structure analysis of the structural and the fluid dynamic behavior of a new disposable pulsatile pump for cardiopulmonary bypass. *Bioengineering Conference ASME volume 50*.
- Hose, D. R., Lawford, P. V., Narracott, A. J., Penrose, J. M. T., Staples, C. J., Jones, I. P., Nuesser, P., Choub, L., Quinn, D. (1998) *BloodSim: Coupled Solid-Fluid Simulation of Cardiovascular Systems*
- Huang, Z. J., Merkle, C. L., Abdallah, S., and Tarbell, J. M. 1994. Numerical Simulation of Unsteady Laminar Flow Through a Tilting Disk Heart Valve: Prediction of Vortex Shedding. *Journal of Biomechanics* 27(4):391–402.
- Hughes, T. 2000. *The Finite Element Method: Linear Static and Dynamic Finite Element Analysis*. New York, Dover Publications.
- Hughes, T., Liu, W., Zimmermann, T. 1981. Lagrangian-Eulerian Finite Element Formulation for Incompressible Viscous Flows. *Computer Methods in Applied Mechanics and Engineering*, vol. 29, no. 3, 329-349.
- Johnson, A. A. and Tezduyar, T. E. 1994. Mesh update strategies in parallel finite element computations of flow problems with moving boundaries and interfaces. *Comp. Meth. Appl. Mech. Engng.* 119:73–94.
- Kim, S., Cho, Y. I., Jeon, A. H., Hogenauer, B. and Kensey, K.R. 2000. A new method for blood viscosity measurement. *Journal of Non-Newtonian Fluid Mechanics*, 94:47-56.
- King, M. J., Corden, J., David, T., and Fisher, J. 1996. A Three-Dimensional, Time-Dependent Analysis of Flow Through a Bileaflet Mechanical Heart Valve: Comparison of Experimental and Numerical Results. *Journal of Biomechanics* 29(5):609–618.
- King, M. J., David, T. and Fisher, J. 1994. An Initial Parametric Study on Fluid Flow Through Bileaflet Mechanical Heart Valves using Computational Fluid Dynamics. *J. Eng. Med.*, 208:63–72.
- King, M. J., David, T., and Fisher, J. 1997. Three-Dimensional Study of the Effect of Two Leaflet Opening Angles on the Time-Dependent Flow Through a Bileaflet Mechanical Heart Valve. *Med. Eng. Phys.*, 19(5):235–241.
- Kiris, C., Kwak, D., Rogers, S., and Chang, I. D. 1997. Computational Approach for Probing the Flow Through Artificial Heart Devices *ASME J. Biomech. Eng.* 119:452–460.
- Knobbe, Edwin M. 2004. Mesh Movement Governed By Entropy Production. *Proceedings 13th International Meshing Roundtable*, pp.265-276.

- Krafczyk, M., Cerrolaza, M., Schulz, M., and Rank, E. 1998. Analysis of 3D Transient Blood Flow Passing Through and Artificial Aortic Valve by Lattice–Boltzmann Methods. *Journal of Biomechanics* 31:453–62.
- Kyeleswarapu K. K. 1996. Evaluation of Continuum Models for Characterizing the Constitutive Behavior of Blood. Ph.D. diss., Department of Mechanical Engineering, University of Pittsburgh.
- Lai, Y. G. 2000. Unstructured grid arbitrarily shaped element method for fluid flow simulation. *AIAA J.* 38:2246–2252.
- Lai, Y. G., Chandran, K. B. and Lemmon, J. 2002. A numerical simulation of mechanical heart valve closure fluid dynamics. *Journal of Biomechanics*, 35:881–892.
- Lai, Y. G., Chandran, K. B., and Lemmon, J. 2002. A Numerical Simulation of Mechanical Heart Valve Closure Fluid Dynamics. *J. Biomech.* 35:881–892.
- Lee, C., and L. Talbot. 1979. A fluid mechanical study of the closure of heart valves. *Journal of Fluid Mechanics* 91: 41-63.
- McQueen, D., C. Peskin, and E. Yellin. 1982. Fluid dynamics of the mitral valve: physiological aspects of a mathematical model. *American Journal of Physiology* 242: H1095-H1110.
- Pedrizetti, G. 1998. Fluid flow in a tube with an elastic membrane insertion. *Journal of Fluid Mechanics* 375: 39-64.
- Pedrizetti, G., Domenichini, F., Tortoriello, A., and Zovatto, L. 2002. Pulsatile flow inside moderately elastic arteries, its modeling and effects of elasticity. *Computational Methods in Biomechanics and Biomedical Engineering* (in press)
- Pedrizetti, G. 1996. Unsteady tube flow over an expansion, *Journal of Fluid Mechanics*, 310: 89-111.
- Perktold, K and Rappitsch, G. 1995. Computer simulation of local blood flow and vessel mechanics in a compliant carotid artery bifurcation model. *Journal of Biomechanics.* 28:845–856.
- Peskin, C. S. 1972. Flow Patterns Around Heart Valves: A Numerical Method. *Journal of Computational Physics* 10:252–271.
- Peskin, C. S. 1977. Numerical analysis of blood flow in the heart. *Journal of Computational Physics* 25:220-252.
- Peskin, C., and D. McQueen. 1989. A three-dimensional computational method for blood flow in the heart immersed elastic fibers in a viscous incompressible fluid. *Journal of Computer Physics* 81: 372-405.

- Price, S. and Wilson, L. 1992. Pathophysiology, clinical concepts of disease processes. Mosby - Year Book Inc, Philadelphia.
- Rosenfeld, M., Avrahami, I., and Einav, S. 2002 Unsteady Effects on the Flow Across Tilting Disk Valves. *ASME J. Biomech. Eng.*, 124:21–29.
- Rutten, M. C. M. 1998. Fluid Solid Interaction in Large Arteries. Ph.D. diss., Eindhoven University of Technology.
- Schreurs, P. J. G. 1983. Numerical Simulation of Forming Processes: the use of the Arbitrary Lagrangian-Eulerian (ALE) Formulation and the Finite Element Method. Ph.D. diss., Eindhoven University of Technology.
- Shim, E.-B., and Chang, K.-S. 1997. Numerical Analysis of Three-Dimensional Björk–Shiley Valvular Flow in an Aorta. *ASME J. Biomech. Eng.*, 119:45–51.
- Yellin, E. 1995. The momentum of mass, the momentum of ideas, and diastolic function of the heart. IOI Press.
- Yellin, E. L., Nikolic, S. D. and Frater, R. W. 1994. Left ventricular diastolic function and mitral valve flow. *Journal of Heart Valve* 3: 41-4.
- Yoganathan, A., Hopmeyer, J. and Heinrich, R. 1995. Mechanics of heart valves in biomedical engineering handbook. (in CRC press)

APPENDIX A

3D rendition of the left ventricle model:

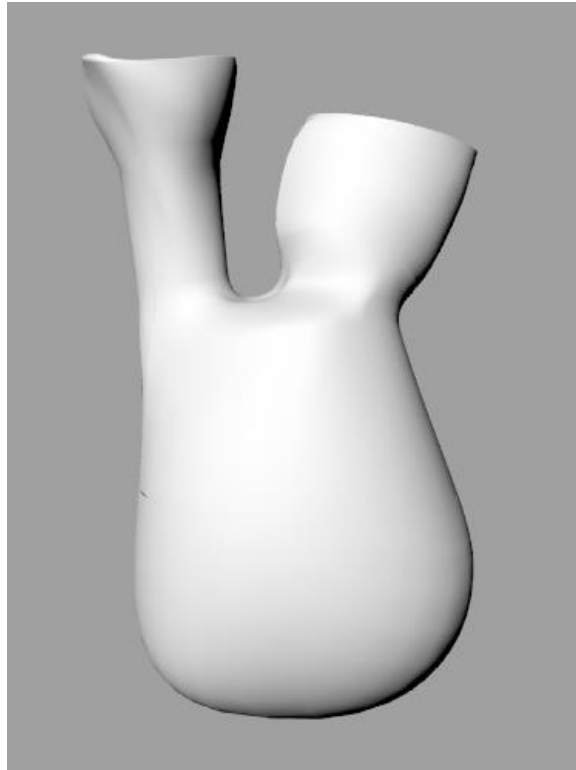
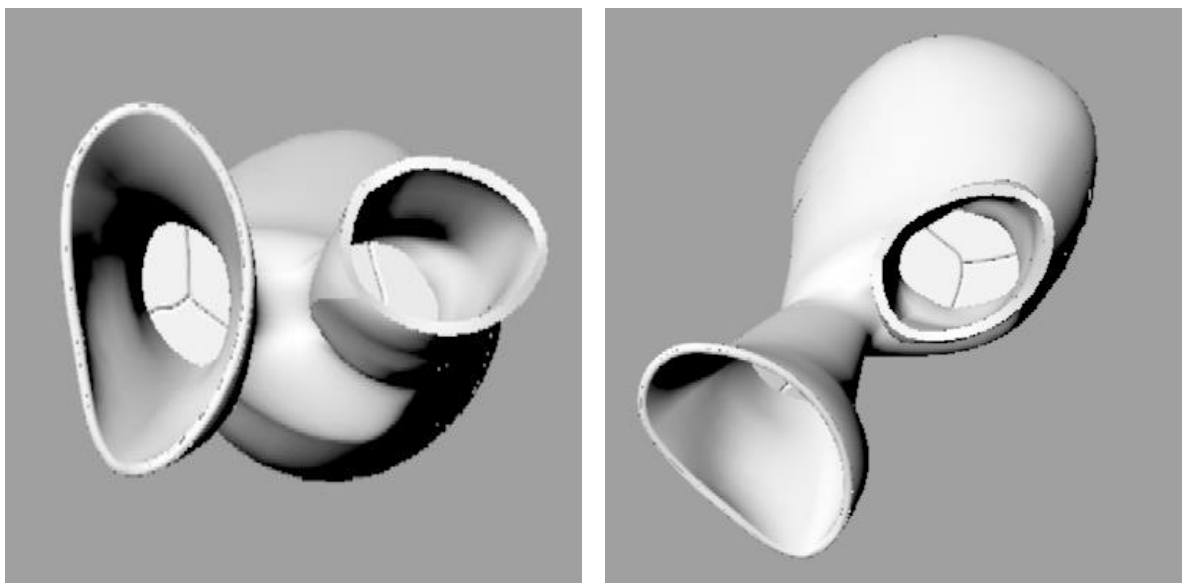


Figure A.1: 3D Rendition of the Left Ventricle (Front View)



(a)

(b)

FigureA.2: The rendered Left Ventricle showing (a) the aortic tricuspid leaflets and (b) the mitral tricuspid leaflets

APPENDIX B

Data measurements on the major boundaries from the reconstruction of 3D left ventricle surface model which have been used in modeling the solid geometry of the left part of the heart.

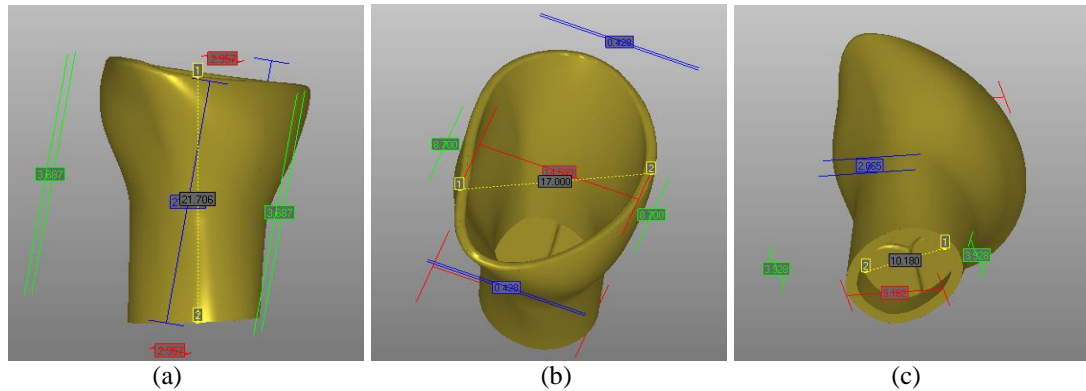


Figure B.1: The measurement studies the length of the aortic cylinder, diameter of the cylindrical opening and diameter of the semilunar valve at the orifice. (a) Length of the aortic cylinder is computed to be 21.706mm. (b) Diameter of the cylindrical opening is computed to be 17.000mm. (c) At the base, the diameter of the semilunar valve is computed as 10.180mm.

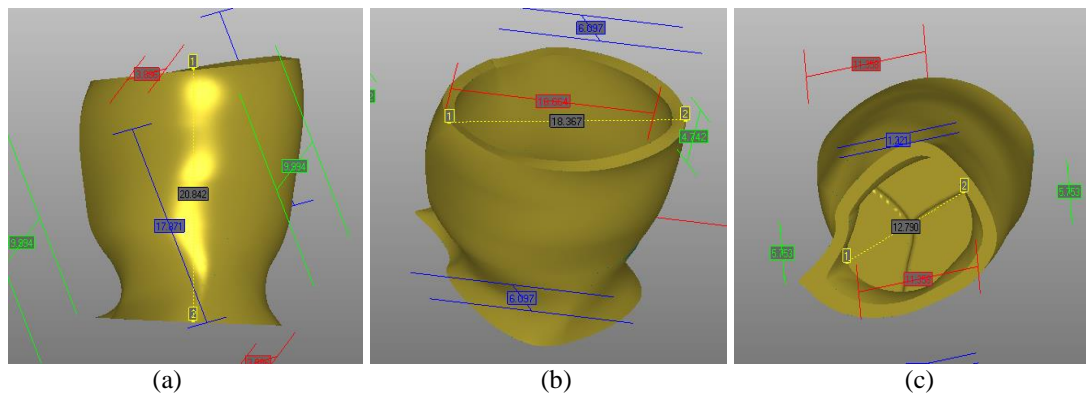


Figure B.2: The measurement studies the length of the mitral cylinder, diameter of the cylindrical opening and diameter of the mitral valve at the orifice. (a) Length of the mitral cylinder is computed to be 20.842mm. (b) Diameter of the cylindrical opening is calculated to be 18.367mm. (c) Diameter of the mitral valve at the orifice is calculated to be 14.845mm.

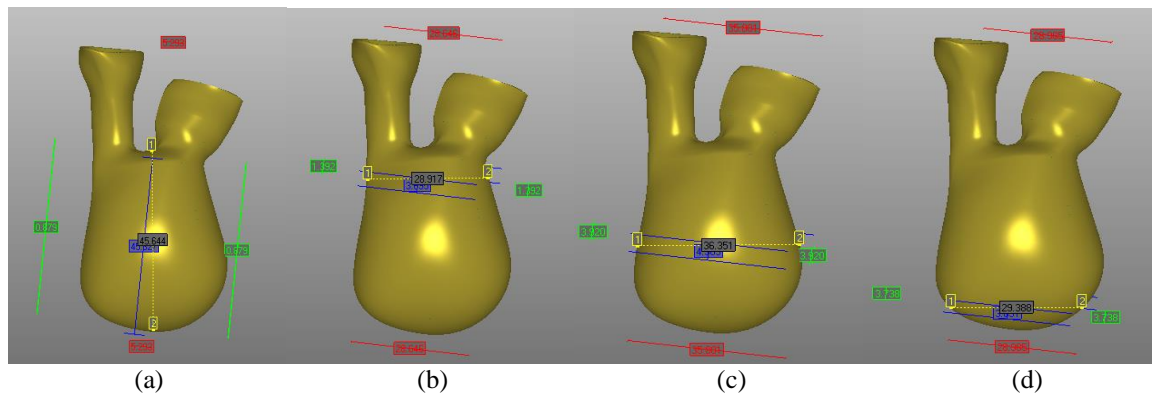


Figure B.3: The measurement studies the vertical length of the chamber and three curvature diameters that are significant to the shape of the body. (a) The length of the body from the base to the ventricle's apex is computed to be 45.644mm. (b) Diameter of the body near the base of the valves is calculated to be 38.917mm. (c) Diameter of the body in the middle part of the chamber is computed to be 36.351mm. (d) Diameter of the body near the ventricle's apex is calculated to be 29.388mm.